NAVAL POSTGRADUATE SCHOOL

MONTEREY, CALIFORNIA

DISSERTATION

FIELD AND NUMERICAL STUDY ON NATURAL RIVER MIXING

by

William A. Swick

June 2011

Dissertation Supervisor: James MacMahan

Approved for public release; distribution is unlimited

THIS PAGE INTENTIONALLY LEFT BLANK

REPORT DOCUMENTATION PAGE		*Form Approved OMB No. 0704-0188*

1. AGENCY USE ONLY (*Leave blank*)	2. REPORT DATE June 2011	3. REPORT TYPE AND DATES COVERED Dissertation	
4. TITLE AND SUBTITLE: Field and Numerical Study on Natural River Mixing		**5. FUNDING NUMBERS**	
6. AUTHOR(S) William A. Swick			
7. PERFORMING ORGANIZATION NAME(S) AND ADDRESS(ES) Naval Postgraduate School Monterey, CA 93943-5000		**8. PERFORMING ORGANIZATION REPORT NUMBER**	
9. SPONSORING / MONITORING AGENCY NAME(S) AND ADDRESS(ES) N/A		**10. SPONSORING / MONITORING AGENCY REPORT NUMBER**	

11. SUPPLEMENTARY NOTES The views expressed in this thesis are those of the author and do not reflect the official policy or position of the Department of Defense or the U.S. Government. IRB Protocol number N/A.

12a. DISTRIBUTION / AVAILABILITY STATEMENT Approved for public release; distribution is unlimited	12b. DISTRIBUTION CODE

13. ABSTRACT (maximum 200 words)

Mixing in several natural rivers is investigated using comprehensive point-source dye experiments, Lagrangian GPS-equipped drifter observations and a validated three-dimensional hydrodynamic model. The high spatial and temporal observations provide estimates of mixing that were previously unobtainable. The presence of river irregularities are shown to greatly enhance the local streamwise and transverse diffusivity due to large-scale horizontal coherent flow structures. Tracer study transverse diffusivity was initially small and increased following channel features. Model simulations compared well with field observations. Idealized bathymetric features reveal transport is dominated by the mean flow and combined channel feature influence is nonlinear. Lagrangian analysis of continuous drifter observations describe fine-scale natural river processes and provides quantitative estimates of the mean flow field, pathways, and spatial variability of mixing in natural rivers. Near-field diffusivity estimates are shown to be independent of drifter deployment location and the effect of river bends on streamwise and transverse diffusivity is quantified. Single-particle streamwise diffusivity increased linearly associated with turbulence and velocity shear. Two-particle streamwise diffusivity scales as Richardson-like. Reaches with numerous bends resulted in anomalously small two particle diffusivities scaling with river bends owing to surface flow convergence. Transverse length scales >20m are predominantly random.

14. SUBJECT TERMS Dispersion, Diffusivity, Transport, Mixing, Delft3D, River, Lagrangian, Drifters, Coherent Velocity Structures, Single Particle, Two Particle, One Particle, Tracer, Hydrodynamic Modeling, Integrated Tracer Statistics			15. NUMBER OF PAGES 129
			16. PRICE CODE
17. SECURITY CLASSIFICATION OF REPORT Unclassified	18. SECURITY CLASSIFICATION OF THIS PAGE Unclassified	19. SECURITY CLASSIFICATION OF ABSTRACT Unclassified	20. LIMITATION OF ABSTRACT UU

i

THIS PAGE INTENTIONALLY LEFT BLANK

FIELD AND NUMERICAL STUDY ON NATURAL RIVER MIXING

William A. Swick
Lieutenant Commander, United States Navy
B.A., Villanova University, 1996
M.S., Naval Postgraduate School, 2004

Submitted in partial fulfillment of the
requirements for the degree of

DOCTOR OF PHILOSOPHY IN PHYSICAL OCEANOGRAPHY

from the

NAVAL POSTGRADUATE SCHOOL
June 2011

Author: _____
                           William A. Swick

Approved by:

_____   _____
Jamie H. MacMahan   Thomas H. C. Herbers
Professor of Oceanography   Professor of Oceanography
Dissertation Supervisor
Dissertation Committee Chair

_____   _____
Edward B. Thornton   Timothy P. Stanton
Professor of Oceanography (Emer.)   Professor of Oceanography

_____   _____
Adrianus J. H. M. Reniers   Qing Wang
Professor of Oceanography   Professor of Meteorology

Approved by: _____
                  Jeffery D. Paduan, Chair, Department of Oceanography

Approved by: _____
                  Douglas Moses, Vice Provost for Academic Affairs

THIS PAGE INTENTIONALLY LEFT BLANK

ABSTRACT

Mixing in several natural rivers is investigated using comprehensive point-source dye experiments, Lagrangian GPS-equipped drifter observations and a validated three-dimensional hydrodynamic model. The high spatial and temporal observations provide estimates of mixing that were previously unobtainable. The presence of river irregularities are shown to greatly enhance the local streamwise and transverse diffusivity due to large-scale horizontal coherent flow structures. Tracer study transverse diffusivity was initially small and increased following channel features. Model simulations compared well with field observations. Idealized bathymetric features reveal transport is dominated by the mean flow and combined channel feature influence is non-linear. Lagrangian analysis of continuous drifter observations describe fine-scale natural river processes and provides quantitative estimates of the mean flow field, pathways, and spatial variability of mixing in natural rivers. Near-field diffusivity estimates are shown to be independent of drifter deployment location and the effect of river bends on streamwise and transverse diffusivity is quantified. Single-particle streamwise diffusivity increased linearly associated with turbulence and velocity shear. Two-particle streamwise diffusivity scales as Richardson-like. Reaches with numerous bends resulted in anomalously small two particle diffusivities scaling with river bends owing to surface flow convergence. Transverse length scales >20m are predominantly random.

THIS PAGE INTENTIONALLY LEFT BLANK

TABLE OF CONTENTS

viii

LIST OF FIGURES

THIS PAGE INTENTIONALLY LEFT BLANK

LIST OF TABLES

THIS PAGE INTENTIONALLY LEFT BLANK

LIST OF ACRONYMS AND ABBREVIATIONS

1D	One-dimensional
2D	Two-dimensional
2DH	Two-dimensional-horizontal; depth-averaged
3D	Three-dimensional
ADCP	Acoustic Doppler Current Profiler
ADV	Acoustic Doppler Velocimeter
DOF	Degrees of Freedom
GPS	Global Positioning System
HLES	Horizontal Large Eddy Simulation
hr	Hour
Hz	Hertz
km	Kilometers
LES	Large Eddy Simulation
m	Meters
mm	Millimeters
NPS	Naval Postgraduate School
O( )	Of the Order of ... (used to denote approximate magnitude)
RANS	Reynolds Averaged Navier-Stokes
s	Seconds
USGS	U.S. Geological Survey

THIS PAGE INTENTIONALLY LEFT BLANK

ACKNOWLEDGMENTS

I would like to express my gratitude to my supervisor Dr. Jamie MacMahan whose expertise, understanding, and drive shaped my graduate experience. His innovation, knowledge, and skill made my dissertation possible. No rain days.

It was a great privilege to have Dr. Ed Thornton as a continued presence and mentor in my academic career. I am grateful to him for taking time out of his schedule to accompany me on experiments and for his "holistic" approach to research.

A special thanks goes to Dr. Ad Reniers and his family for opening their home to me. Dr. Reniers provided invaluable insight on numerical modeling during my stay.

I would like to thank Professor Stanton for his sound advice and direction.

Dr. Herbers and Dr. Wang your academic support, input and counsel were greatly appreciated.

To Dr. Jon Nelson your knowledge and coordination made this research possible.

I would like to thank Dr. Garwood, my Master's Thesis Advisor, whose encouragement and guidance inspired me to reach higher.

Thank you to Ron Cowen and Keith Wyckoff for your ingenuity, outstanding boatsman skills, and hard work. To my fellow graduate students "the Varsity" Jenna, Will, Patrick and Chris who lugged, dragged, swam, dove, tanned (Patrick) and hustled in pursuit of the data. I enjoyed many hours of good conversion with all of you. I was especially happy to share my grasp of primal sports with you. "Do you see a man skilled in his work? He will stand before kings."

I especially thank my Dad and Mom; your example and prayers have formed me.

Most importantly, to Laura, my wife of 13 years, your love and support has been unwavering. You have carried the family the past few months; I owe you a fancy dinner somewhere with cloth napkins! To my children Maeve, Liam, Moira, and Shannon you are my joy, my light, and my happiness.

THIS PAGE INTENTIONALLY LEFT BLANK

I.   INTRODUCTION

Natural rivers are dynamically complex environments. Here, small and large-scale mixing processes act to produce highly localized mixing rates and spatially inhomogeneous concentration distributions. Previous mixing studies noted local influences, such as eddy structure, "dead zones," and curvature that cause large departure from theoretical dispersion behavior (Fischer et al. 1979, Rutherford 1994). However, natural river analyses could not separate scales of transport and mixing owing to cost, logistical and technical limitations. Therefore, mixing was described by bulk parameterizations of flow character, based on mean channel dimensions, which led to highly variable streamwise spreading rates, diffusivity K $(O(10^{-1}-10^3)$ m^2/s) estimates (Rutherford 1994). Today, advances in instrumentation and the availability of accurate processed-based, three-dimensional (3D) numerical models allow for an unparalleled study that resolves small and large-scale processes of transport and mixing in natural rivers. The combined observational and numerical modeling approach provides greater understanding of local flow field effects and overall behavior of natural river mixing.

This dissertation investigates transport and mixing in several natural rivers through a series of comprehensive in situ transport and mixing experiments. These experiments utilized new high spatial and temporal resolution sensing techniques to provide unique insight into flow structure, and scales of mixing processes. Additionally, extensive fieldwork allows for the validation of a 3D numerical model that is used to examine the influence of river geometry on mixing. For the first time, Lagrangian statistical analysis of high-resolution Global Positioning System (GPS)-Equipped drifter positions allows for new perspective into the flow structure of the individual reaches and an overall sense of the effect of river shape and speed on statistical dispersion behavior while providing distinctions in the governing mechanisms to mixing.

Chapter II introduces the small, inexpensive GPS-equipped drifters designed for use in natural rivers and streams. These provide near-continuous estimates of mixing previously unobtainable with the river dye efforts. Observations from twenty river drifters on the Skagit River, WA, USA highlight the ease of use and the broad range of

information the river drifters afford scientists and engineers. Lagrangian statistical analysis of the drifter observations describe fine-scale natural river processes and provides quantitative estimates of the mean flow field, pathways, and dispersion in natural river environments. Lastly, deployment methods and limitations of GPS-drifters are discussed. The material contained in this chapter was presented at Oceans 09 MTS/IEEE, Biloxi, MS and is published in the Conference proceedings *OCEANS 2009, MTS/IEEE Biloxi - Marine Technology for Our Future: Global and Local Challenges* (Swick and MacMahan 2009).

Chapter III investigates the spatial variability of mixing in natural rivers using Lagrangian statistics computed from GPS-equipped surface drifter observations on four hydraulically unique reaches in Skagit River, WA and Kootenai River, ID, USA. Near-field diffusivity estimates are shown to be independent of initial drifter deployment location and the effect of river bend's influence on the streamwise and transverse diffusivity is quantified. Single-particle, streamwise diffusivity increased linearly ($R^2>0.92$) with associated turbulent and shear velocity variances of $0.04 - 0.82$ m^2/s^2. An order of magnitude difference was found between single–particle (flow translation) and two-particle (relative spreading) dispersion, suggesting that mixing is due to randomness of particle movement in a flow field with background shear. For all streamwise separation lengths, l_s, diffusivity scales as Richardson ($l_s^{4/3}$). Reaches with numerous bends resulted in anomalously small two particle diffusivities associated with the streamwise distances of river bends owing to surface flow convergence. Transverse length scales (l_n) are predominantly random, expect when $l_n<20$ m. For the first time, the spatial variability of mixing is quantified, which highlights the significance of channel features in a natural river setting. The material in this chapter will be submitted for publication to the journal *Earth Surface Processes and Landforms*.

Chapter IV utilizes two comprehensive point-source dye experiments performed in a 1.6 m deep, 30 m wide channel, and 550 m reach of the Kootenai River, Idaho, USA to describe natural river transport and mixing dynamics. The channel is relatively straight and uniform with significant bathymetric features (shallow- water riffle, a channel constriction, and an embayment) located toward the middle of the study reach. Eulerian

and Lagrangian flow characteristics and steady state plume behavior were obtained through a combination of stationary and moving observational platforms consisting of dye sensors, GPS-equipped drifters, acoustic Doppler current profilers, and acoustic velocimeters. In the straight sections, the transverse diffusivity, k_n, was ~0.02 m^2/s. The flow variability associated with bathymetric features increase k_n (0.06m^2/s) by a factor of three. Dye concentration maximum, $C_{max}(s)$, followed a 3D mixing decay as a function of downstream distance, s, as $C_{max}(s) \sim s^{-3/2}$ and then, for s >125m, $C_{max}(s) \sim s^{-1}$, indicating 2D mixing behavior. Lagrangian drifter pathways highlight separation eddies along the channel bank. Simulated results from a three-dimensional hydrodynamic model compared well with field observations for velocity (m=0.81, R^2=0.87), water level (m=0.99, R^2=0.97), and dye concentration (m=1.04, R^2=0.86), where m is the slope and R^2 is the correlation coefficient of a linear regression. Numerical estimates of dye patterns, dispersion, integrated mean particle pathways and mean vorticity patterns for idealized, individual prominent bathymetry features reveal transport is dominated by the mean flow. The effect of combined channel features is highly nonlinear, increasing mixing by 200%. Coherent flow structures associated with persistent eddies generated by channel features are important in transporting dye across the channel. The material contained in this chapter will be submitted for publication to the journal *Water Resources Research* (Swick, MacMahan, Reniers and Thornton 2011).

THIS PAGE INTENTIONALLY LEFT BLANK

II. THE USE OF POSITION-TRACKING DRIFTERS IN RIVERINE ENVIRONMENTS

Position tracking drifters offer a new perspective in describing flow characteristics in riverine environments that have been overlooked in previous studies. To date, most riverine observations are based on fixed Eulerian observations, which have limitations in completely describing material transport. Mean flow field and dispersion estimates are typically the two most common observations obtained with Eulerian observations in riverine environments. Due to cost and logistical constraints, Eulerian observations are limited to a small number of fixed measurements reducing their spatial description. Acoustic Doppler Current Profilers (ADCPs) have increased flow observations into the vertical and generally across a channel, improving discharge estimates. ADCPs can be used to spatially map the flow field over larger distances. However, Eulerian observations cannot accurately describe the particle pathways and assumptions must be made concerning river kinematics between observations points.

For estimating dispersion, river field studies have used radioactive or fluorescent tracers by recording concentrations at fixed locations downstream of an injection point (Glover 1964, Wilson and Forrest 1964, Fischer 1968, Godfrey and Frederick 1970, Nordin and Sabol 1974, Beltaos 1980, Atkinson and Davis 2000, Ho et al 2002). A number of theoretical and empirical dispersion models were developed from these types of observations (McQuivey and Keefer 1974, Atkinson and Davis 2000, Boxall and Guymer 2006). Deploying additional tracer concentration sensors is cost prohibitive; therefore cross-channel (transverse) mixing and vertical estimates are often inferred or limited. In most rivers, the ratio of width to depth is large causing the tracer to rapidly mix in the vertical before becoming mixed in the transverse. In order to predict the far field longitudinal dispersion, assuming that vertical mixing is short, an accurate estimate of transverse mixing is still required. When the tracer is completely mixed in the vertical and transverse dimensions, the three dimensional advection dispersion equation can be simplified to one-dimension.

5

The use of Global Positioning System (GPS)-equipped drifters provides high temporal and spatial resolution data unattainable by tracer concentration methods or Eulerian velocity observations. The riverine community has typically not used drifters in their studies. Previous drifters required direct line of sight making it difficult to track their positions with accuracy over long distances, which are required for dispersion estimates (Davis 1985, Rutherford 1994). Tracer studies were advantageous in this respect. Recent advances in GPS technology have decreased the cost and size of GPS handheld units, while position accuracy has increased. It is now possible to build a large number of inexpensive (~$300), small GPS-equipped drifters for O(km)-O(hrs) applications, such as riverine environments (Stockdale et al. 2008). GPS-equipped drifters allow for a near-continuous observation of their relative expansion and a better estimate of advection and mixing in both the transverse and longitudinal directions as a function of time and space. Lagrangian drifter observations provide information of the particle pathways and material transport for sediment, biotic, abiotic and pollutants. Moreover, drifter position data can be spatially averaged to obtain a gridded velocity flow field.

Twenty river drifters were released on the Skagit River, WA, and neighboring marsh channels in later September, 2008. The use of GPS-equipped drifters in a riverine environment and associated statistical methods, cost estimates, and results are described below.

A.   RIVER DRIFTER

1.   River Drifter

MacMahan et al. (2008) demonstrated the feasibility of mounting a handheld GPS receiver onto an inexpensive PVC float to describe flow behavior within the surf zone. The handheld GPS was the size and weight of a cell phone and had internal logging and power capabilities. The GPS internal memory supports 5400 positions, in post-processing mode, can sample at intervals ranging from 2 to 240 seconds and allows for 8

hours of continuous sampling. The GPS absolute position and speed errors are 0.4 m and 0.01 m s^{-1}. Survey-grade post-processing software is also required to achieve the stated position accuracies, which costs ~$2000.

For this type of GPS, the largest source of positioning error is related to signal multi-pathing associated with their inexpensive patch antennas (Saeki and Hori 2006). To reduce multi-pathing, the GPS patch antenna was placed on a 0.07 m diameter circle of aluminum sheeting. This reduced the position errors by an order of magnitude. In a wavy surfzone environment, the GPS-equipped drifters closely followed a simultaneously released patch of dye, verifying that the drifter observations are valid Lagrangian tracer estimates (MacMahan et al. 2008). The same GPS receiver is used for the river drifter.

The river drifter body is also a modification of the surfzone drifter (MacMahan et al. 2008). The river drifter consists of a ballasted, subaqueous 0.46 m long by 0.10 m diameter PVC central tube connected to a 0.33 m long antenna mast of 0.03 m diameter PVC (Figure 1). The drifters are ballasted with a low center of gravity to reduce potential pitch and roll effects. The handheld GPS is housed in a waterproof plastic box attached to the drifter near the waterline. The compact design of the drifter allows for a number of drifters to easily be transported to the field site, placed on a vessel, or manually carried to shallow streams. The complete drifter weighs only 3.6 kg and costs ~$300. Note that twenty drifters cost ~$6,000, which is approximately the same cost of one tracer-dye concentration sensor, or one-fourth the cost of an ADCP.

2.   Drifter Deployment Overview

Seven drifter deployments were performed between September 25 through 27, 2008 for three different reaches (Upper Skagit, North Fork and Marsh Channel) of the Skagit River (Figure 2). The flow speed, reach length, and channel width varied between each reach (Table 1). Two different deployment schemes were used. The first deployment scheme, drifters were simultaneously released near the center of the channel in a large group, referred to as a cluster. For the second deployment scheme drifters were released across the channel at relatively constant separation interval, referred to as line abreast.

The Skagit River originates in southwestern British Columbia, Canada and flows Southeasterly through Washington, U.S.A before draining into the Puget Sound. The Upper Skagit River is composed of a sinuous channel containing 3 to 4 bends in alternating directions, and varying in width from 125 to 158 m (Figure 2a). The mean river speed was 1.10 m/s. The river divides approximately 14 km downstream. The northern branch of the divide is known as the Northfork Skagit River. The Northfork is weakly sinuous with slightly narrower, 93-154 m, channel (Figure 2b). The mean river speed on the Northfork was 0.55 m/s, half the speed of the Upper Skagit flow. Lastly, a short deployment was made in a small, 2 m wide, sinuous marsh channel which contained one complete meander (Figure 2c). At the time of deployment, the measured mean speed of the channel was 0.16 m/s.

The Upper Skagit and Northfork drifter releases were conducted from a small boat. The marsh channel release point was inaccessible by boat and the drifters were carried to the deployment location. Two people carried eight drifters through the marsh and hand-released them from the channel bank 40 m upstream. The deployment was conducted during an ebbing tide in an effort to capture the strongest current in this small channel.

3.   Quality Control and River Coordinate Frame Transform

The time series of drifter positions were quality-controlled by removing erroneous points that exceeded three velocity standard deviations. Time gaps in the data were interpolated with a spline algorithm for gaps less than 10 seconds and a linear algorithm for gaps greater than 10 seconds. A 62 second moving average was applied to smooth the river data and a 5 second moving average was applied to the marsh channel. Velocity estimates were computed using a forward-differencing scheme.

A few drifters were snagged on riverbank obstructions such as: trees, logs, boat docks, and rocks. Due to a limited number of drifters, one snagged drifter can cause rapid unnatural growth in the dispersion. To address this problem, the data from snagged drifters were removed by visual inspection.

A geographic coordinate frame is not ideal for describing the statistical behavior of the flow, owing to the sinuosity of the channels. Therefore the geographic coordinate system was transformed to a local orthogonal curvilinear coordinate system, where the longitudinal axis (s) is along the river centerline, and the transverse axis (n) is normal to the river centerline. Legleiter and Kyriadkidis (2007) generously provided the MATLAB code to transform the coordinate frame of each deployment reach to a local river coordinate frame (s,n). The accuracy and precision of the coordinate transform is primarily a function of curvature and discretization of the centerline. Errors associated with the transformation are O(cm) (Legleiter and Kyriadkidis 2007). Additional quality controls, as described above, were performed to remove erroneous points after the transformation. An example of the transformation is shown in Figure (3) for the Upper Skagit reach, where 14 individual drifter tracks and speeds are plotted in geographic (Figure 3a) and local coordinates (Figure 3b). The speeds compare well between each coordinate frame. In the local coordinate frame, the magnitude of the transverse drifter convergence and divergence is clearly seen, but the geographic coordinate frame is required to show flow fluctuations associated with river meanders. The cluster's separation is controlled by the river meanders, ranging from 3 m to 100 m. The drifter's relative distribution in time is illustrated by the symbols showing the drifter positions 500, 1000, 1500 and 2000 seconds after release.

B.   DRIFTER STATISTICS

1.   Eulerian Velocity Mapping Calculation

If two drifters are released at the same location, but at different times, or if they are released at slightly different locations at the same time, they will generally follow very different paths associated with coherent and random fluid motions. A measure of the spatial and temporal scales for coherent and random fluid motions is required, such that proper statistical confidence levels describing the uncertainties are obtained (LaCasce 2008).

Spatial binning the drifter observations is required to properly describe the Eulerian flow field. However, there is a compromise between the spatial resolution, bin size, and statistical confidence. Five or more independent observations are required within a bin to be statistically significant (Spydell et al. 2007). The number of independent observations, known as degrees of freedom (DOF), in a bin is determined by the total time that the drifters occupy a bin divided by the Lagrangian decorrelation time, T_L, given by:

$$DOF_{bin} = \sum_{j=1}^{N} t_i / T_L \tag{1}$$

where DOF_{bin} is degrees of freedom for each bin, j denotes each individual drifter and t_i is the time each drifter spent inside an individual bin. T_L represents fluid particle memory and describes the time scale of the longest fluctuation. Therefore, a priori knowledge of this time is required to adequately select the longitudinal and transverse bin dimensions.

T_L is directly calculated from the ensemble average of the autocovariance function, $C_{ii}(\tau)$, for each drifter concurrently deployed, and is defined as:

$$C_{ii}(\tau) = \langle v_i'(t'=0) v_i'(t'=\tau) \rangle \tag{2}$$

where v' is the anomalous drifter velocity which is calculated by removing the ensemble mean velocity from each individual drifter velocity time series, t' is a relative time step which allows displacement calculations for each drifter for all arbitrary starting positions, i denotes the respective local coordinate direction (s, n), and the angle brackets denote averaging over all drifters for each time lag, τ (Spydell et al. 2007). Autocorrelation is the autocovariance divided by the covariance, $\langle v_i'^2 \rangle = \langle v_i'(0) v_i'(0) \rangle$, which is also known as the intensity of turbulence squared.

The autocovariance magnitude and shape are similar for multiple deployments but vary between reaches (Figure 4a-f). The variance is an order of magnitude larger for the Upper Skagit (0.02 m^2/s^2 longitudinal, 0.005 m^2/s^2 transverse) than the Northfork (~0.004 m^2/s^2 longitudinal, ~0.001 m^2/s^2 transverse) and marsh channel (~0.002 m^2/s^2 longitudinal, ~0.0003 m^2/s^2 transverse) due to the larger velocities. The Upper Skagit River longitudinal autocovariance, C_{ss}, becomes negatively correlated after 1000 seconds

10

(Figure 4a). In the North Fork deployments, C_{ss} negatively decorrelate after 400 and 800 seconds (Figure 4b). The autocovariance functions do not asymptote to zero, but instead periodicity is observed owing to the velocity fluctuations associated with river shape.

There are four methods to estimate the T_L from the autocovariance function: 1) the integral temporal scale, 2) absolute diffusivity maxima, 3) zero-crossing or 4) e-folding time. The integral temporal scale is computed by integrating the autocorrelation function over all time lags. The integral of the autocovariance function is absolute diffusivity, K_{ss} (discussed below). The asymptotic diffusivity, K^{∞}, divided by the intensity of turbulence squared corresponds to T_L (Dever et al. 1998). The zero crossing is the time lag at the first zero crossing. E-folding time is the time required for the autocovariance function to decrease by a factor of $1/e$.

The integral method tends to be the standard method used in riverine studies. However, this method was considered an unsuitable descriptor of decorrelation time due to quasi-periodic fluctuations in the mean river speeds with river location. These large scale fluctuations are manifested as oscillating negative and positive residual energies in the autocovariance functions. This resulted in varying decorrelation times using the integral method that were considered inappropriate. The absolute diffusivity maxima method is similar to the integral temporal scale, except that the first maxima of absolute diffusivity in the quasi-periodic autocovariance function is considered to be K^{∞}. The zero crossing method was not used because there are cases for which the autocovariance function asymptotes to a value slightly greater than zero for some time before becoming negative, causing T_L to be larger than expected (Figure 4a,b). Owing to the periodic oscillations and the inconsistent shape prior to the zero crossing in autocovariance anomalous velocity functions, the absolute diffusivity maxima and e-folding time methods provided the most consistent T_L estimates. Both estimates compared well with each other, but are 4 to 20 times shorter then traditional mixing theory estimates (Table 2). Without the ability to directly calculate the autocovariance anomalous velocity function past studies have relied on mixing length theory to provide a rough estimate of T_L (Rutherford 1994). The mixing length equation is given by:

$$L_s = \alpha(Ub^2/K_n) \tag{3}$$

where L_s is the downstream distance needed for complete mixing, U is mean river velocity, b is river width, K_n is the transverse diffusivity and α is an empirical scaling constant. There are large uncertainties associated with this calculation because α and K_n are not known. T_L is computed by dividing L_s by U. Natural rivers and streams have riffles, pools, bends, side wall roughness which have large contributions to mixing which are not captured in traditional transverse diffusivity calculations. Incorporating all scales of the river flow using high temporal resolution river drifters provides a much shorter decorrelation time.

Once T_L is determined, the proper bin size is selected to ensure statistical confidence. Northfork cluster and line abreast release T_L are approximately 2 and 3 minutes respectively (Table 2).

Therefore, 15 minutes (900 seconds) of drifter data with each bin is required to obtain the minimum 5 DOF to be statistically confident. For example, a mean river velocity of 1 m/s requires 5 drifters to occupy a bin that is 180 m long or 10 drifters to occupy a bin that is 90 m long to have a statistically significant result. This is highly dependent upon the fluctuations in the rivers, number of drifters deployed, and mean river velocity. An evenly distributed release of drifters is believed to provide the best scenario of measuring the transverse flow field, whereas, a cluster release in the center of the channel would provide the highest longitudinal resolution, with the added benefit of allowing relative dispersion estimates (see "Dispersion and Diffusivity" discussion below). However, this is not necessarily the case. Transverse movement and distribution of the drifters is strongly controlled by river meanders. For that reason, despite deploying in the optimal line abreast configuration, uneven transverse coverage would still remain. In the apex of bends the drifters tend to converge to the outer edge of the channel, limiting the transverse coverage, such as was observed during the line abreast release in the Northfork (Figure 5b, d). Longitudinal bin size of 250 m was needed to attain four to five transverse bins, spanning ~60 m, with greater than 5 DOF. In contrast, the cluster release (Figure 5a, c) had two transverse bins, separated by the centerline, using a finer

12

longitudinal bin of 70 m. Although the cluster release provides large DOF for each bin (as high as 13), the transverse resolution could not be increased. In the line abreast case, increasing the longitudinal resolution did not ensure transverse coverage throughout the deployment. Once the drifters converged into the sweeping bend the mean speed calculations ultimately became confined to only the outer bin (Figure 5d).

2.   Dispersion and Diffusivity

The movement and spreading of a tracer cloud can be quantified by a group of drifters. The ensemble average centroid position of the drifter group provides the overall advection. Spreading about the centroid position in time is measured by the variance, or "relative dispersion". The rate of spreading in time is known as the relative diffusivity, K_i, where i is the respective river frame coordinate direction (s, n). The values of K_s are calculated from the slope of a regression line in the later stages of the deployment, when t $>T_L$, and the values of K_n are calculated as the average slope of increasing dispersion (divergence) and decreasing dispersion (convergence) (Table 3). Figure 6 shows the time evolution of the longitudinal variance of the drifter's positions for the releases on Upper Skagit (a,d), Northfork (b,e) and Marsh Channel (c,f).

Two longitudinal dispersion (Figure 6a,b) regimes are identified in two larger reaches for the cluster deployments. There is an early stage, when the drifters are in close proximity, and a later stage after the drifter cluster has spread enough to sample the velocity shear in the transverse river profile. In the early stage, the proximity of the drifters suggests they are not experiencing significant velocity shear differences and the spreading is slow. The later stage begins when the drifters have separated enough to experience the transverse profile velocity shear. In this stage, dispersion noticeably increases. The transition from the early to the later regime is seen as sharp increases in variance. At the transition, the diffusivity values increase from small values, <1.0 m2/s, to values >2.0 m^2/s (Table 3). Note the line abreast deployment (Figure 6b dashed line) exhibits no slow growth stage because immediately upon release the drifter cloud is experiencing large transverse velocity shear.

Another method to estimate spreading and mixing characteristics of a river is from the single-particle statistic. Single-particle statistics consider the ensemble average pathway of a single drifter over many independent releases originating from a common release location. Over many observations a probability density function (PDF) can be created to map the original release position to the probability the drifter will arrive at a position at a later time. The variance is the second moment of the PDF, known as "absolute dispersion." Absolute dispersion estimates differ from the relative dispersion estimates in that both the spread about the center of mass and the advection from the starting position are considered. Absolute diffusivity, k, is calculated as the rate of change of absolute dispersion in time. At long time periods, $t \gg T_L$, relative diffusivity, K, and absolute diffusivity, K, are comparable (Spydell et al. 2007).

Longitudinal single particle diffusivities, K_{ss}, for Upper Skagit, Northfork cluster and line abreast, and Marsh Channel deployments show that the diffusivity increases for 1016, 396, 665 and 36 seconds, respectively, before K_{ss} values drop off (Figure 4g-i). This drop off in diffusivity values is caused by periodicity in the river shape discussed above. By taking the maxima of K_{ss} as K^{∞}, we can obtain an estimate of the average absolute diffusivity, because of the effects of river periodicity. The time of these maxima corresponds to the decorrelation time of the zero crossing method. In the larger river deployments K_{ss} compares well; estimates are about half that of the relative diffusivity calculation. The Marsh Channel diffusivity differs by an order of magnitude.

C.   DISCUSSION – LIMITATIONS AND BENEFITS OF GPS

Though the use of GPS-equipped drifters in riverine environments has many advantages over traditional Eulerian current observations and dye studies, there are methodological and practical limitations that require consideration. One clear limitation is that drifters only provide surface estimates, which may not fully represent tracer dispersion, as dye can mix vertically. Though complete vertical mixing occurs much sooner than transverse mixing, vertical circulations remain important to river kinematics.

14

Surface only observations may result in biased river mixings estimates. Further studies are needed to compare dye and drifter methods in a natural and controlled riverine environment.

The relatively large bin size required for statistical confident mean flow is a limitation, but it is not unique to Lagrangian drifters. Regardless of the measurement method, the largest coherent motions must be observed to ensure statistical confidence. Our results suggest that in rivers with bends increasing the number of drifters or modifying the deployment schemes would not necessarily increase the transverse coverage. However, carefully paired longitudinal and transverse bin dimensions may provide desired resolutions. For example, the longitudinal bin can be stretched over longer distances, which may allow for a higher transverse bin resolution. Additionally, increased spatial coverage can be obtained by multiple releases in specific areas or possibly, but not necessarily, through the use of more drifters. The spatial coverage for flow field mapping cannot be precisely controlled. As shown in Figure 3, drifters may disperse in one section only to converge in another section resulting in a reduction of transverse coverage. Lastly, current handheld GPS-equipped drifters are not ideal for long-term studies because of limited internal battery life (8 hours). Extra batteries can be installed to lengthen the observational time.

D.   CONCLUSION

The application of a new Lagrangian riverine characterization technique fills the observational gaps left by traditional longitudinal tracer methods. Data obtained during an experiment utilizing twenty GPS equipped river drifters provide both Eulerian and Lagrangian observations demonstrating a wide range of riverine applications. Statistical analysis of the high temporal resolution (0.5 Hz) drifter data provides measurements to describe fine-scale riverine processes. Both divergence (positive diffusivity) and convergence (negative diffusivity) is observed in longitudinal and transverse directions. Transverse convergence occurs before the apex in bends, whereas, longitudinal convergence is observed in the exits of bends due to flow deceleration (Figures 3 and 6). River shape induced periodicities in the velocity field are shown in the oscillatory

behavior of the autocovariance function. GPS-equipped drifters represent all scales of the surface flow and T_L is directly calculated from the autocovariance function. River studies can be performed at minimal cost and logistical preparation. Prior knowledge or measurements of a field site are not required. GPS-equipped river drifters are inexpensive, easy to deploy, and provide high temporal and spatial resolution data that provide new insights into river kinematics.

III.   SPATIAL VARIABILITY OF NATURAL RIVER MIXING

A.   INTRODUCTION

The transport and mixing of a solute in a natural river is controlled by three fundamental processes: 1) molecular and turbulent diffusion, which are continuous and irreversible processes that act to reduce concentration gradients, 2) shear dispersion, which accounts for the differential advective effects of the velocity profile over the channel depth, and 3) direct transport processes, such as coherent trapping eddies formed by irregularities in the river bank. Taylor (1954) was the first to quantify the relationship between velocity shear dispersion and turbulent diffusion. He hypothesized, assuming homogeneous turbulence, vertical and transverse velocity shear dispersion is balanced by small-scale turbulent diffusion after sufficient mixing has occurred. "Sufficient mixing" is a time known as the Lagrangian decorrelation time, T_L, which represents the time it takes for fluid particle motion to become decorrelated from its initial velocity. After a time much longer than T_L, termed far field, the spreading of a tracer in stationary turbulence is linear in time and turbulent diffusion and velocity shear effects can be described by a constant coefficient known as diffusivity, K. The analysis also describes a second result that occurs immediately after release of a point source, known as the near field.   In this region, the effects of turbulence dominate transport and mixing, and assuming turbulence is constant, dispersion follows a quadratic relation to t. In practice, this region extends to a distance where the differential advection due to transverse velocity deviations becomes important (Fischer et al. 1979).

Taylor's analysis is limited in natural settings because it only applies after long time periods and stipulates stationary homogenous turbulence. It is well known rivers are spatially inhomogeneous and complex. Previous mixing studies noted local influences, such as eddy structure, "dead zones", and curvature that cause large departure from theoretical dispersion behavior (Fischer et al. 1979, Rutherford 1994). Studies conducted in natural rivers have been based on fixed Eulerian observations, which measured the temporal evolution of tracer concentration curves at several downstream locations

(Glover 1964, Fischer 1968, Godfrey and Frederick 1970, Nordin and Sabol 1974, Beltaos 1980, Atkinson and Davis 2000, Ho et al. 2002). Owing to the cost and logistical difficultly of deploying a large number of tracer concentration sensors, tracer experiments have been limited by the number of downstream measurements. Additionally, due to the cumulative nature of tracer spreading, analyses could not separate local scale mixing effects. The distribution and time evolution of a dye release is coupled to both the overall transport of the velocity field and the dye gradients, and additionally, the dye measurements are made at fixed locations and assumptions must be made concerning river kinematics between observations points. For these reasons, mixing is often described by bulk parameterizations of flow character, based on mean channel dimensions, which led to highly variable streamwise K ($O(10^{-1}$-10^{3})) estimates (Rutherford 1994).

The Lagrangian reference frame provides a direct connection to the dynamics of transport and mixing that reveals physical insight. However, until recently, positions from surface drifters in natural environments were not possible owing to the difficulty of visually tracking drifter positions with accuracy over long distances (Rutherford 1994). Advances in GPS technology have decreased the cost and size of GPS handheld units, while position accuracy has increased, and it is now possible to build a large number of inexpensive (~$300), small GPS-equipped drifters for O(km)-O(hrs) applications, such as riverine environments (Stockdale et. al. 2008, Swick and MacMahan 2009, Lee et. al. 2011, Swick et al. 2011). GPS-equipped drifters allow for near-continuous observations in time and space, and provide high resolution estimates of advection and mixing in both the transverse and streamwise directions.

High resolution (0.5 Hz) GPS drifter observations collected from 13 deployments on four hydraulically unique river reaches in the Northwestern United States are used to examine the processes of transport and mixing in natural rivers. The high spatial and temporal resolutions of drifter observations are used to investigate dispersion from both small-scale local effects to reach-scale influences. This large dataset is used to calculate two Lagrangian statistical descriptors, single particle, or "absolute dispersion", which describes the advection and turbulent properties of a flow and two particle drifter pairs, or

"relative dispersion", which provide insight into the physics at different scales. This combined approach provides greater understanding of local flow field effects and overall behavior of natural river mixing.

B.   RIVER SITES AND DRIFTER METHODS

1.   River Drifter Design

Two different GPS-equipped surface floats were used to obtain trajectory data. The first design was used in experiments conducted in 2009 and a second shallower draft design was used in 2010. The river drifter body used for releases in 2009 was a modification of a surfzone drifter used by MacMahan et al. (2009) and consisted of a subaqueous 0.46 m long by 0.10 m diameter PVC central tube, ballasted with a low center of gravity to minimize pitch and roll, connected to a 0.33 m long antenna mast of 0.03 m diameter PVC. The 2010 design is a 0.5 m square float constructed from 0.04 m diameter PVC tubing and drafting only 0.03 m, which has extended battery life (2010 drifter~27 hrs compared to 2009 drifter~6 hrs). Both drifter designs employed the same handheld GPS unit that yielded post-processed position accuracies of less than 0.4m in absolute position and less than 0.01 m/s in velocity, described in detail in MacMahan et al. (2009). The GPS units are housed in a waterproof plastic box attached to the drifter near the waterline; an additional external battery is included in the 2010 drifter. Multi-pathing was reduced in both drifter designs by shielding the GPS internal antenna and adding an external GPS patch antenna placed on a 0.07 m diameter circle of aluminum sheeting. Dye release comparisons with the drifters in 2009 (MacMahan et al. 2009) and in 2010 (Swick el. al. 2011) found good agreement.

2.   Field Site Description and Quality Control

Drifter deployments were performed on four distinct reaches of the Skagit River, WA and Kootenai, ID, chosen based on differences in mean velocity, width, depth, and shape (Table 1). The rivers and individual reaches are described below.

a. *Skagit River, WA*

The Skagit River originates in southwestern British Columbia, Canada and flows southeasterly through WA, U.S.A. (Figure 2). Two subsections, Northfork (NOF), (River kilometers 3-5) (Figure 2a) and Upper Skagit (UPS), (River kilometers 26-31) (Figure 2b) were selected for drifter deployments. The NOF reach is a single sweeping bend, varying in width from 93 to 154m and has as mean river speed of 0.6 m/s (Figure 2a). The UPS reach is mildly sinuous, sinuosity=1.09, containing 4 curves in alternating directions and varying in width from 125 to 158m (Figure 2a). The mean river speeds (1.1 m/s) were similar for all deployments.

b. *Kootenai River, ID*

The Kootenai River flows west through Idaho before turning northwest into British Columbia, Canada (Figure 7). Two reaches, Braided (BRK) (River kilometer 250-252) (Figure 7a) and Meander (MEK) (River kilometer 233-247) (Figure 7b) were selected for drifter deployments. BRK is a relatively straight section varying in width from 70to 127 m ending in a sweeping curve, with mean drifter speed of 1.4 m/s. MEK is a sinuous reach, sinuosity=1.40, containing 3 curves and varying in width from 125 to 200m with mean drifter speed of 0.4 m/s.

3. Release Methods

Drifters were released in three configurations: 1) single large cluster, R_C, 2) transverse line abreast, R_L, and 3) small clusters spaced across the river, R_{Sc}. R_C were performed by hand-releasing up to 20 drifters simultaneously in a tight group from a boat approximately centered in the river. This pattern is employed to simulate a point source slug discharge so that drifters are deployed with minimal separation. R_L was performed by hand-releasing drifters evenly across the river, spanning the river, so that the drifters immediately experience the differential advection of the transverse surface velocity profile. A combination of the two configurations, R_{Sc}, is performed by releasing six clusters of six drifters spanning the river. Once released the drifters were untouched until final retrieval.

On the Skagit River, drifters sampling at 0.5Hz were released in the two configurations R_C and R_L, yielding a total of six deployments from September 25 - 27, 2008. Three deployments, (two R_C, of 16 drifters, and one R_L of 20 drifters) were conducted on NOF, on September 26, 2008 and September 27, 2008 respectively. Three R_C of 20 drifters were conducted on September 25 and 26, 2008 on the UPS reach (Table 1).

Three release configurations were used on the Kootenai River resulting in a total of seven deployments in 2009 and 2010. Six deployments with drifter sampling at 0.5Hz were conducted on August 26 and 27, 2009 and August 18, 2010. One deployment with drifter sampling at 0.2 Hz was conducted on August 17, 2010. Hydraulic conditions were similar over both years and the drifter speed comparisons for the MEK deployments were within 0.04 m/s.

Three R_{Sc}, each with 18 drifters sampling at 0.5Hz, were conducted on BRK on August 18, 2010 (Table 1). Four deployments were conducted on MEK, two R_C and one R_L each with 20 drifters sampling at 0.5Hz on August 26 and 27, 2009 and one R_{Sc} of 36 drifters sampling at 0.2Hz on August 17, 2010.

4.   Quality Control

Since drifters have a tendency to get snagged on the riverbank or obstacles (trees, rocks, docks), 10% (1-2 drifters) of all released drifters were removed per deployment and not included in the dataset. The GPS drifter geographic position trajectories were transformed to a local system to describe the flow patterns relative to the river centerline. The local coordinate system is defined by a streamwise axis (s), along the river centerline, and a transverse axis (n), normal to the river centerline and described in detail in Legleiter and Kyriadkidis (2007) (Figure 3). Velocities were computed using a forward-differencing scheme and all data were quality-controlled by removing points that exceed three velocity standard deviations. Time gaps were filled with a spline interpolation for gaps less than 10 seconds and linear interpolation for gaps greater than 10 seconds (Spydell et al. 2007).

C. DRIFTER TRAJECTORIES AND LAGRANGIAN STATISTICS

As is well known, the transport and distortion of a patch of marked fluid released into a natural river undergoes a complex, highly variable mixing behavior. However, previous natural river investigations could not capture the small-scale processes owing to low-resolution observations and the cumulative nature of dye. GPS drifter observations fill the gaps left by traditional tracer methods and allow new insights into the local variations in in the natural river flow field. For example, drifter pathways and speeds reveal strong modulations of flow acceleration and convergence entering a river bend followed by flow deceleration and divergence upon exiting bends (Figure 8). Additionally, "dead zones" are highlighted by pockets of decreased velocities along channel banks. Instantaneous drifter positions, 15mins (+), 30mins (circle), 1 hr (square), and 3 hrs (diamond) allow for insight into the resulting increased spreading and streamwise skewness caused by dead zones. Slow water along the channel banks in BRK cause the drifter distribution (Figure 8, third panel, s=800m) to be stretched in the streamwise direction with the tail of the drifter group located along the channel bank. UPS illustrates a single drifter within a dead zone for the length of the deployment (Figure 8, second panel, s=1000m). This drifter was floating undisturbed in a region of still water, not hung up on the bottom or an obstruction. Flow field convergence into a bend, contracting the drifter group, and divergence exiting a bend, expanding the drifter group is illustrated in the meandering reaches (Figure 8, second panel and bottom panel). Additionally, coherent flow structures cause large streamwise dispersion and skewness in the tracer distribution. A large eddy located at 3320m in the MEK deployment (Figure 9 - 70m in the streamwise direction and 30m in the transverse direction) has drawn five drifters into it and, in all cases, they circle the eddy before being released. The time to circle the full extent of the eddy is 5 min. One drifter rotates within the eddy for two full rotations and is release after more than 15 mins. Though such velocity structures and slow water along channel banks have been known to exist, previous investigators could only measure their signatures by dispersion. The dispersion was termed "dead zone dispersion" and additional dead zone parameterizations were required to fit observations (Davis et al. 2000). The high resolution drifter observations, coupled with a Lagrangian

22

statistical description of transport and mixing properties, provide the ability to directly assess the impact of the local flow field that results in valuable new insights into natural river dispersion.

1.   Absolute Dispersion: Single-Particle Statistics

The ensemble average of many individual drifter's mean square particle displacements, r(t), originating from a common location provides an estimate of transport and mixing, as a result of the cumulative history of the flow known as "absolute dispersion,"   For each drifter released $r_i(t) = x_i(t) - x_i(t_0)$, where i denotes local coordinate direction (s, n), $x_i(t)$ is the local coordinate position at each time, $x_i(t_0)$ is a common streamwise release position and t_0 is the time each drifter was located at $x_i(t_0)$. Initial drifter releases were conducted simultaneously in the same streamwise locations and $x_i(t_0 = 0)$.   However, in the investigations of the local influences of river shape on mixing $r_i(t)$ are calculated by measuring each drifter's mean square particle displacements from selected $x_i(t_0)$. In these cases, t_0 varies between drifters. Absolute dispersion, $\sigma_i^2(t)$, is the variance of $r_i(t)$ and one-half of the time derivative of σ_i^2 is "absolute diffusivity," K_i.

a.   Single Particle Results

Theoretically K_s will increase linearly in time for the near field indicating a constant velocity variance $\langle U^2 \rangle$, and σ_s^2 will evolve as,

$$2\kappa/t = \sigma_s^2(t)/t^2 \sim \langle U^2 \rangle. \tag{4}$$

In the far field, $\sigma_s^2(t \gg T_L)$, will proceed linearly in time and K_s will be constant.

All results that follow present the two straight reaches of the Skagit and Kootenai Rivers, NOF and BRK, together first followed by the meandering reaches of the two rivers, UPS and MEK. All deployments on each reach initially show a nearly linear behavior of K_s in time (Figure 10). Linear regression values for 80% of the total record

length are R^2=0.97, 0.99, 0.97, and 0.92 and the corresponding $\langle U'^2 \rangle$ in EQUATION 4 is estimated as two times the slope of the regression fit line, 0.04, 0.82, 0.30, and 0.04 m^2/s^2 for NOF (Figure 10a) , BRK (Figure 10b), UPS (Figure 10c)and MEK (Figure 10d)respectively. $\sqrt{\langle U'^2 \rangle}$ is ~50% of the mean speed. The linear behavior of K_S indicates $\langle U'^2 \rangle$ must be approximately constant. However, the near linear increase in K_S persist for 10 mins to 2 hrs after release (Figures 10 and 11), which is much longer than characteristic near field distances, typically 50 times the water depth (Rutherford 1994). Also, transverse velocity shear is contributing to observed diffusivity (Figure 8). The linear behavior of K_S suggests turbulence and a constant background velocity shear are the mechanisms for observed K_S; implying the drifters are sampling transverse velocity shear evenly.

Comparisons between K_S and K_n illustrate coupling between transverse and streamwise dispersion. UPS displays immediately rapid expansion $K_n > 0$ (Figure 10c bottom panel) associated with channel features and K_S linearly increases in time. Exiting the first bend (Figure 2b, #1) the drifter group is contracted, $K_n < 0$; indicating reduced transverse velocity shear and K_S decreases. In all reaches K_n is oscillating about zero, which averages the velocity shear influences to a constant value over time and results in geometry controlled oscillations about a linearly increasing K_S (Figure 10).

The influence of release location was assessed by calculating K_S from starting locations that were associated with rapid spreading for UPS, (Figure 10c, t~1800s, Figure 2b white line and 11a dash dot line), and the convergence for MEK, (Figure 10d. t~7500s, Figure 7b white line and 11b dash dot line). In both cases, the initial rate of increase in $K_S(\langle U'^2 \rangle)$ with time does not resemble the rapid divergence (UPS) and convergence (MEK) in the same location from the total record (Figure 10, dash dot lines). Variability in diffusivity occurs but it is far downstream. UPS diverges from initial behavior ~4 mins after release and MEK differs ~40 mins after "release".

This supports a nearly constant background turbulence and transverse shear contribution but highlights the importance of the relative streamwise separations of the drifters as they encounter the respective features.

Single particle statistics indicate dispersion is a function of the quasi-stationary velocity shear with local changes due to river features, however, the single particle statistic cannot quantify the dominate length scales of separation and their relative influence on diffusivity. Insight into the flow structure and relationships of diffusivity to length scales can be assessed with multiple drifter statistics, known as "relative statistics".

2.   Relative Dispersion: Two-Particle Statistics

Assessing the relative motion of two drifters allows for insight into spreading as a function of the joint motion of the drifter pair. The mean square separation of drifter pairs, known as relative dispersion, $D_{pi}^2(t)$, is calculated as,

$$D_{pi}^2(t) = \frac{1}{N_{pairs}} \sum \left(x_{ik}(t) - x_{ib}(t) \right)^2, \qquad (5)$$

where N is the total number of drifter pair combinations and $k \neq b$ specify unique drifter pair combinations (Batchelor, 1952; LaCasce and Bower, 2000). Relative diffusivity, K_{pi}, is defined as 1/2 the time derivative of $D_{pi}^2(t)$ and has two components: 1) the small scale turbulence acting on the individual drifters, which is the same term in the single particle statistic, and an additional term 2) correlating the motion between the drifter pairs (LaCasce 2008).

Owing to second term, the behavior of K_{pi} is a function of pair separation length, l_i, where i denotes separations in the respective coordinate direction; note streamwise separations, l_s, are unbounded, and transverse separations, l_n, are bounded by channel width. For small l_i, i.e. where the relative pair velocity differences are small, $K_{pi}(t)$ will behave like K_i. Likewise, when pairs are separated at scales larger than the largest structures of the flow, the velocity differences between pairs will be uncorrelated and K_{pi} will asymptote to a value, which is two times the far field absolute diffusivity value. At

25

the intermediate scales, between near field and far field, the pair separations are dominated by turbulent eddies of the same separation scale and K_{pi} will increase with separation as $K_{pi}=l_i^{4/3}$, known as the Richardson Law (LaCasce 2008). Therefore, K_{pi} and separation relationships can shed light on the smallest scales of the flow, by observing the relative dispersion as a function of initial separation, l_0, and the largest scales of the flow, by noting the scales at which separations become uncorrelated. Additionally, uncorrelated K_{pi} to l_i can indicate spatially inhomogeneous velocity features that are influencing K_{pi} at length scales associated with prominent river features. $K_{pi}>l_i^{4/3}$ indicates anomalously high separations rates and suggests "dead zone" influence.

a.   Two Particle Results

$K_{ps}(t)$ and K_s magnitudes are similar and the timing of anomalous spreading events coincide with oscillations in $K_{pn}(t)$ due to river features. However, trends between K_{ps} and K_s are very different. $K_s(t)$ is linearly increasing, whereas $K_{ps}(t)$ is variable with no relationship to time, signifying that pair separation velocities are correlated and the single particle spreading is due to nonisotropic motions, i.e. velocity shear and larger scale eddies. $K_{ps}(t)$ is small initially for R_C deployments (Figure 12 c and d blue and green line), while R_L and R_{SC} deployments (Figure 12a green line b. all lines and d. red and magenta line) exhibit larger $K_{ps}(t)$ immediately after release due to the influence of transverse velocity shear. Reach average K_{ps} are 4, 59, 59 and 7 m^2/s with a standard deviation of 5, 17, 36 and 20 m^2/s for NOF, BRK, UPS and MEK. The reach mean $K_{ps}(t)$ correspond with variations in $\langle U \rangle$ in that small values correspond to reaches with slower mean speeds and large values correspond to reaches with faster mean speeds. However, no reach characteristics, i.e. reach shape, speed or deployment methods directly explain the observed variability between reaches. This highlights the complex coupling of mixing and river features.

A separation dependence analysis (Figures 13-16) is conducted by binning the individual drifter pair's initial separation magnitude, $|l_0|$. $|l_0|$ were selected for small separations, $|l_0|<5n$ (Figures 13-16 blue dots), separations scaling with 1/4, 1/2, and

26

>1/2 river width, $5<|l_0|<25m$ (Figures 13-16, green dots), $25<|l_0|<50m$ (Figures 13-16, red dots), $50<|l_0|<100m$ (Figures 13-16, magenta dots), and separations scaling with river meanders, $100<|l_0|<500m$ (Figures 13-16, black dots) and $|l_0|>1000m$ (Figures 13-16, yellow dots). Relatively straight reaches NOF and BRK K_{ps} exhibit a strong agreement to a Richardson-like relationship, $l_s^{4/3}$, indicating the observed scales of motion are predominantly within the inertial subrange. Though differences from $K_{ps}=l_s^{4/3}$ are present (Figure 16 BRK $l_s>300m$), which are mostly likely due to drifters caught in slower water on opposite channel banks (Figure 8, third panel), overall straight reaches exhibit little influence from "dead zones". In all reaches, there are minimal differences due to $|l_0|$ indicating that drifter separations are too large to observe viscous subrange behavior. NOF and BRK K_{ps} do not decorrelate at long length scales (500m for NOF, Figure 13 and 700m for BRK, Figure 16), which implies the observed streamwise separations remain within the inertial subrange in the river.

K_{ps} in meandering reaches display similarities to straight reaches. However, bend influences, manifested as non-Richardson K_{ps} length scale dependence occurs at separations on the order of the convergent flow regions (Figure 8) induced by centrifugal acceleration into bend apexes. For example, UPS K_{ps} (Figure 17) increase as $l_s^{4/3}$ for $l_s<150m$ followed by uncorrelated low values of K_{ps} for $150<l_s<300m$ and $400<l_s<500m$. MEK K_{ps} illustrates similar behavior, $l_s<100m$ has a Richardson length scale dependence but for $l_s>100m$ there are many small values of K_{ps} which do not fit $l_s^{4/3}$ (Figure 16). These anomalously low K_{ps} values are more pronounced in the meandering reaches compared with the relatively straight reaches indicating the river shape is regulating this behavior.

Recalling the two particle statistic is a measure of the joint motion of particle pairs, it is hypothesized the low K_{ps} values are due to a convergent flow moving drifters close together into the thalweg, thereby reducing separation velocities between pairs. Comparing drifter trajectories and speeds for the meanders reaches, UPS (Figure 8,

second panel s=2000s and Figure 17) and MEK (Figure 8, bottom panel s=3700 and Figure 16) support this, depicting areas of strong convergence that bring drifters close together.

All reaches indicate turbulent transverse fluctuations are approximately 20 m, ~1/5th river width. K_{pn} increases as $l_n^{4/3}$ for $l_n < 20m$ and is random for separations greater than 30 m (Figures 13-16 a. – d. bottom panels).

Overall, the two-particle statistic describes a flow where transverse velocity shear is the dominant dispersion mechanism, which is modulated by transverse spreading due to flow convergence and divergence due to river features. Additionally trapping events are highlighted by high K_{ps} values, which show no separation scale dependence, i.e. UPS (Figure 15).

D.   SUMMARY AND CONCLUSION

The physical perspectives provided by single and two particle statistics allows insight into the flow structure of the individual reaches and an overall sense of how differences in river shape and speed modify statistical dispersion behavior while providing distinctions in the governing mechanisms to mixing. The single particle statistic captures a theoretical near field behavior of dispersion proceeding quadratically in time scaled with a nearly constant background "velocity variance" $\langle U^2 \rangle$. Persistent linear increase in K_s, $R^2 > 0.92$, indicate the drifters are randomly sampling transverse velocity shear evenly. The linearity allows for the combined effects of turbulence and shear to be calculated directly from the slope of the regression line. This slope, $\langle U^2 \rangle$ (m^2/s^2), scales with mean river speed, as shown by NOF and MEK having smaller values, 0.04 m^2/s^2, and the fast flow reaches, BRK and UPS, having larger values, 0.30 and 0.82 m^2/s^2, $\sqrt{\langle U^2 \rangle}$ accounts for 50% of the mean speed. Differences between straight and meandering reaches quantify the influence of river shape on mixing. The straight reaches have higher R^2 values than the meanders reaches, additionally, oscillations in K_n are directly reflected in K_s, reinforcing local variability due to bends.

28

Interestingly, single particle comparisons using varying starting locations produce the same K_s behavior in time; the spreading is nearly constant for an initial period lasting several minutes (UPS~5mins and MEK~40mins). This indicates the small-scale mixing and velocity shear effects are not very different spatially and the large scale mixing coupled with the spatial separation of the drifters cause nonlinear diffusivity behavior in time.

Relative dispersion results support this by revealing markedly different overall dispersion behavior, one order of magnitude, indicating the mechanism for K_t behavior is not isotropic turbulence but rather a nearly constant transverse velocity shear. K_{ps} is highly variable with standard deviation of K_{ps} ranging from 29% to 125% of the mean. While the mean K_{ps} magnitude patterns were similar to magnitude patterns of $\langle U^2 \rangle$ among reaches, no common link was found that relates the observed variably of K_{ps}. K_{ps} is correlated and proceeds as $K_{ps} \sim l^{4/3}$ for all length scales. The K_{ps} to separation scale relationship describes reduced diffusivity at approximately bend apex length scales due to the flow convergence, which minimize relative pair separation velocity. These flow convergence structures are observed directly with trajectories and speed observation from drifters (Figure 8, second panel and bottom panel). These features accelerate and transversely contract the drifters into bend apexes and decelerate and transversely expand the drifters exiting bends thereby controlling differential advective influences of the transverse velocity profile. Until now, river field studies have used tracers or hydraulic river characteristics to estimate dispersion. However, tracer methods have several shortfalls that include behavior between sample locations and particle pathways are unknown, tracer methods are costly, are logistically difficult and time consuming to carry out. Additionally, natural river turbulence is neither stationary nor homogenous, and theoretical assumptions are limited in their application. The application of a new Lagrangian drifter river characterization technique fills the observational gaps inherent in traditional tracer methods.

Local and reach average processes of streamwise and transverse dispersion have been quantified utilizing GPS-equipped, high temporal and spatial resolution, drifter observations. Lagrangian data from GPS-equipped drifters allows the combined

influence of turbulence and transverse velocity shear to be quantified and additional insight into how the relative contribution of local geometry contributes to mixing.

IV.   NUMERICAL MODEL COMPARISONS OF TRANSVERSE MIXING IN A NATURAL RIVER

A.   INTRODUCTION

The ability to predict the transport, dispersal, and accumulation properties of a natural river is essential to all facets of water quality management. Whether the aim is to promote the productivity components, such as fostering the transport of larvae from spawning to rearing habitats, or to mitigate potentially harmful human and environmental effects from wastewater discharges or unintentional spills, a detailed understanding of the chemical and biological properties of the substance coupled with the temporal and spatial characterization of the river is required. Channel geometric irregularities create a dynamic velocity field, which is critical in defining the distribution and local severity of the spill. The combination of the larger scale motions, which increase pollutant gradients by stretching and folding the plume, and the smaller scale Fickian diffusion processes, which act to smooth pollutant gradients, define the pollutant distribution. Therefore, mixing cannot simply be estimated using mean hydraulic and average geometric channel parameters (Rutherford 1994, Dow et al. 2009). Increases in computational power and the availability of processed-based, three-dimensional (3D) numerical models, now allow investigators to move away from empirically fitted bulk mixing descriptors and focus on simulating the spatial and temporal transport and mixing processes.

To date, most numerical models have been compared with laboratory experiments owing to the comprehensiveness of the datasets and their inherent control (Demuren and Rodi 1986, Simoes and Wang 1997, Gualtieri 2010, Wilson et al. 2003, Wilson et al. 2007). The results of numerical models accurately represent the observed transport and mixing processes. However, laboratory settings tend to underestimate natural channel mixing. For example in natural straight channels with relatively constant depth and width profiles, transverse spreading rates (diffusivity, k_n) are a factor of two larger than measured in the laboratory, where subscript n represents the direction normal to the centerline, (Fischer et al. 1979, Rutherford 1994).

Comprehensive field studies are needed to directly investigate the complexities of natural channel mixing and to further validate 3D numerical transport and mixing models. However, there have been few field studies with sufficient spatial and temporal resolution needed to describe the flow and resulting dye transport and mixing processes. Dow et al. (2009) evaluated transverse mixing characteristics of a wastewater treatment plant using a steady-state dye approach. Bathymetric and velocity observations were used to calibrate a 2D hydrodynamic model and estimate transverse diffusivity. Recently, dye visualizations of a mixing experiment in a natural channel with a groin field qualitatively agreed with a detailed large eddy simulation (LES) numerical investigation (Constantinescu et al., 2009).

This thesis describes comprehensive field observations of dye transport and mixing obtained on the Kootenai River in August 2010, executed specifically to provide quantitative comparisons with a Reynolds Averaged Navier-Stokes (RANS) model with horizontal large eddy simulation (HLES) (Delft3D-FLOW). A detailed dispersion experiment is performed using a combination of Lagrangian and Eulerian methods. Fixed and moving platforms captured the local evolution of a passive concentration plume and Global Positioning System (GPS) drifters provided high temporal and spatial resolution particle pathways, which are used to assess the numerical model mixing and transport performance. Measured bathymetric surveys, in situ water elevations, and stream discharge are inputs for the model boundary conditions. The numerical flow field is compared to spatial maps of 20-min time-averaged velocity profiles that were obtained at 49 locations throughout the 500m river section. After successful model validation, the effects of river geometry are numerically investigated by decomposing the natural river features into idealized cases. In describing the dominant transport and mixing processes associated with these features 1 min integrated particle trajectories, vorticity and lateral momentum fluxes are computed and described and compared with modeled dye behavior and experimental observations.

B.   TRANSPORT AND MIXING FIELD EXPERIMENT

1.   Morphology

A small channel in the Kootenai River, ID was selected for being a relatively straight shallow section with existing U.S. Geological Survey (USGS) stream channel bathymetry and substrate data (Barton et al. 2004, Barton et al. 2005, Fosness and Williams 2009). The channel bathymetry is transformed to a river local coordinate frame by the method outlined in Legleiter and Kyriadkidis (2006), where the streamwise axis, s, is along the river centerline (positive in the downstream orientation), and the transverse axis, n, is normal to the river centerline originating on the river-right bank (positive to the left) (Figure 17a). The 30-m wide, 550-m-long channel is relatively straight with a sinuosity =1.01 defined as path distance divided by straight-line distance, with an average thalweg depth of 1.6 m and mean depth of 0.7 m. The channel contains a constriction and riffle located at s=160 to 223m, where s=0 is the location of dye release, and large bank irregularities with a natural embayment at s=247 to 355m (Figure 17a). The bottom consists of poorly sorted cobble and gravel. Measured particle-size at a cross section 5 km upstream of the study site ranged from 20.8 to 78.2 mm (D16 and D84), with a median particle-size (D50) of 39.9 mm (Fosness and Williams 2009). Discharge is controlled 100km upstream at the Libby Dam, which was constant throughout the experiment.

Additional bathymetric surveys were performed to supplement the USGS bathymetry and to ensure that the river morphology had not evolved. A survey-grade GPS was located directly above a 200 kHz echo sounder mounted on a motorized, electric kayak that traversed the channel with streamwise transect spacing of ~10 m. Channel bank locations and water elevations were obtained from a survey-grade GPS mounted on a person walking the water line. Vertical and horizontal control for the river survey is based on the previously established USGS control stations (Barton et al. 2004). The stationarity of hydrologic conditions were monitored using a surveyed pressure sensor located 500 m upstream of the dye release point and repeated Teledyne RD

Instrument, RiverRay (600 kHz) ADCP transects that provided discharge measurements. Both the pressure and discharge (9.7 m^3/s) were constant for the study.

2. Eulerian Velocity

Prior to the dye release, 20-minute, time-averaged velocity profiles were acquired at 49 locations throughout the channel using downward-facing 2 MHz Nortek Acoustic Doppler Current Profilers (ADCPs) mounted on three catamarans (Figure 17a "+"s). The ADCPs, sampling at 1 Hz with 0.05 m surface blanking distance and 0.20-m bin size, remained in a stationary location for a 20-minute duration. Mean velocities ($\bar{u}$) are faster in the center (0.5 m/s) and slower (0.3 m/s) near the channel banks, which is typical of open channel flow regulated by channel depth variations. Near the riffle/constriction, s=160 to 223m, the channel narrows from 30 m to 15 m and shallows from 1.6 m to 0.7 m causing the flow to increase to a maximum speed of 1.4 m/s. Vertical velocity profiles showed good agreement (R^2~0.7) with a logarithmic law of the wall profile in the center of the channel, where R^2 is the log-linear regression coefficient squared (Figure 17b).

ADCP velocities are inherently noisy and require approximately 10 minutes of averaging to reduce the noise (Muste et al. 2004, Brown et al. 2011). Additionally, ADCPs have a relatively slow sampling rate (1Hz) and low spatial resolution (84 cm at 1m distance) owing to spatial averaging across the beams. Therefore, a faster-sampling (32Hz), single-point acoustic Doppler velocimeter (ADV) was used to resolve turbulent flow at different locations in the channel. The ADV was mounted on a fixed frame at a height of 1 m off the river bed (approximate mid-water column), which was deployed for approximately 1.5 hours at four locations, s=194m, 327m, 330m and 360m (Figure 17a stars).

3. Lagrangian Drifters

Drifter observations are advantageous for river studies, because they provide high temporal and spatial resolution of the near instantaneous flow field. The Lagrangian reference frame allows for a direct connection to the dynamics of transport and mixing, revealing physical insight, which often cannot be obtained using Eulerian measurements.

GPS-equipped drifters are used to explore a wide range of phenomena in oceans, estuaries and inlets (Davis 1985, Dever et al. 1998, Spydell et al. 2007, LaCasce 2008, Brown et al. 2009, MacMahan et al. 2009) and recently in natural river environments (Stockdale et al. 2008, Swick and MacMahan 2009). Two drifter releases (D1 (Figure 18a) and D2 (Figure `8b)) of eleven GPS-equipped surface drifters were hand-deployed in a tight cluster from the same location as the dye release, see §IV B 4, August 16, 2010 between the hours of 1030 to 1430 and left untouched until final retrieval at s ~ 500m. The drifter body is constructed from 0.04 m diameter PVC tubing in a 0.50 m square and drafts 0.03 m. The GPS was housed in a waterproof plastic box attached to the drifter near the waterline and a patch antenna was placed on a 0.07 m diameter circle of aluminum sheeting to reduce multi-pathing (Saeki and Hori 2006, MacMahan et al. 2009).

The drifter's compact design allows for use in shallow rivers in order to provide a near-continuous synoptic view of particle transport, which is lost through the steady-state dye releases and the diffusive nature of the dye solute (described in §IV B 4.). For example, the distribution and time evolution of a dye release is coupled to both the overall transport of the velocity field and the dye gradients, which make it difficult to separate mixing processes. Close to the source, the velocity field will transport large patches of dye producing large concentration fronts and filaments in the concentration distribution. However, far from the source, where the dye plume is well mixed and the concentration gradients are small, changes in transverse concentrations will be small regardless of the underlying flow structure. Furthermore, although the dye plume behavior is Lagrangian, the dye measurements are made at fixed locations. While the Lagrangian behavior of the dye can be inferred by mapping the spatial plume, the measurements are Eulerian. Drifters provide true Lagrangian information and can resolve smaller spatial and temporal scale velocity field process, not possible by fixed-point concentration transects.

Although advantageous in many ways, drifters have limitations. Specifically, drifter dispersion estimates are limited by the small number of drifters deployed, which can have anomalous results based on the trajectory of an individual drifter. Secondly, the

drifter group spreads in the streamwise direction over time and is therefore encountering differing flow regions in the streamwise direction. As a result, the overall drifter dispersion calculation will contain spatial effects and is not directly comparable to dye dispersion. To account for this difference between dye and drifter dispersion measurements, the drifter transverse dispersion is computed in two ways: 1) a Lagrangian measurement where σ_{nd}^2 is calculated as the 2nd moment of the transverse drifter displacement relative to the drifter group average position in time. σ_{nd}^2 is calculated by cumulating all drifter transverse positions as they pass a fixed streamwise location and then calculate the 2nd moment of the total transverse drifter displacement relative to the drifter group average transverse position. and 2) a Eulerian measurement taken at streamwise cross-sections with implied time averaging, σ_{nb}^2, which is directly comparable to dye dispersion, σ_n^2. For direct comparison with σ_n^2, σ_{nb}^2 is calculated for D1 and D2 at the same streamwise transect locations of dye sampling for the two dye studies (T1 and T2) discussed in §IV B 4.

The transverse diffusivity, k_n, is calculated as one half of the slope of a linear regression fit of σ_{nd}^2 as,

$$k_n = \frac{1}{2}\frac{d\sigma_{nd}^2}{dt}.$$

(6)

Similarly,

$$k_n = \frac{1}{2}\frac{d\sigma_{nb}^2}{ds}V,$$

(7)

and transformed to time using $V = ds/dt$.

4. Tracer Concentration

Two dye studies (T1 and T2) were conducted August 16, 2010 prior to their respective drifter releases. Rhodamine-WT dye (2.5% by weight) was released continuously at 6 mL/s from a 18.9L container onboard a kayak fixed at the channel centerline. The fluorescent dye was released for approximately one-hour through an 8mm diameter tube located 0.05 m below the waterline through a butterfly valve that was

36

manually controlled by a human operator to provide a constant concentration discharge. Concentration, C (ppb), were acquired with 13 WETLabs ECO fluorometers that sampled at 0.9 Hz with a Rhodamine detection range of 0 to 234 ppb and a sensitivity of 0.09 ppb. The duration of each experiment was less than one hour. Owing to the short, one-hour duration, the dye is conserved and no concentration decay corrections are applied (Bright Concentrations Division, Technical Data Bulletin 2002). Fluorometers collocated with GPS units mounted on fixed and moving platforms allowed for the measurement of the temporal and spatial concentrations. The GPS units, sampling at 0.5 Hz, provided absolute post-processed positions with accuracies <0.4 m (MacMahan et al. 2009). The temporal evolution of the dye plume was acquired by deploying a total of 10 fluorometers at streamwise distances s=0m, 28m, 110m, 313m, and 550m in the channel centerline (Figure 17a, black dots). At 0m, one fluorometer was deployed at the surface. At 28m and 110m, three fluorometers were deployed at the bottom, mid-depth, and surface. At 313m, two fluorometers were deployed at bottom and the surface. At 550m, a single fluorometer was deployed at the surface.

The surface spatial distribution of the dye plume was mapped utilizing 3 GPS- and fluorometer-equipped, 1m long, catamarans. Mobile dye sampling did not commence until steady state conditions were established, which was determined *a priori* to be 25 minutes after dye was released. The sampling delay time of 25 minutes was based on dye time of travel, 925 s, to the farthest downstream sampling point, 500 m, multiplied by 1.5 to account for the largest scale temporal fluctuations of the velocity field based on channel parameters, mean velocity and width (Dow et al. 2009). Two lines were attached to each catamaran that allowed for the catamaran to be slowly pulled across the channel by two people located on opposite channel banks at 0.2 m/s, taking approximately 2.5 minutes to complete one transect of the 30 m channel. To minimize flow disturbances, care was taken to keep the lines out of the water. Transverse concentration profiles, C(s), were acquired between s=28m to 550m with an average streamwise spacing of 8 m, requiring approximately 35 minutes, which resulted in 66 and 70 individual C(s) for the two experiments. Surface concentrations measured for both deployments are superimposed on channel bathymetry (Figures 21a and b).

Concentration mass transport, M(s) (ppb m^3/s),

$$M(s) = \int_0^B h(n,s)V(s)C(n,s)\,dn,$$ (8)

is calculated to ensure that the sampling methods adequately captured the dye plume, where h(n,s) is the depth of point measurements at (n,s), $V(s) = Q/A(s)$ is the mean streamwise velocity, Q is a constant discharge, A(s) is cross sectional area at each streamwise location, and B is the sample width. Assuming the concentration is well mixed in the vertical, the transect sampling is complete and trapping of dye is negligible dye, M(s) will be constant downstream. M(s) releases T1 and T2 have standard deviations of 29% and 23% about the mean value of 120 and 122 ppb m^3/s (Figure 20). Closing the transport values in natural settings tend to be problematic (Clark et al. 2010, Geyer et al. 2008). These results are slightly better than previous dye studies in natural environments and the mean and variability of the transport measurement are consistent between deployments.

Transverse dispersion, σ_n^2, is determined by calculating the 2nd moment of C(n,s) defined as:

$$\sigma_n^2(s) = \frac{\int_0^B |n(s) - \mu(s)|^2 C(n,s)\,dn}{\int_0^B C(n,s)\,dn},$$ (9)

where $\mu(s)$ is the 1st moment of C(n,s) defined as,

$$\mu(s) = \frac{\int_0^B nC(n,s)\,dn}{\int_0^B C(n,s)\,dn}.$$ (10)

k_n, is determined in the same way as the spatial distribution of drifters given by EQUATION 7. Surface transverse integrated statistics, EQUATIONS 9 and 10 are averaged from all transects within streamwise distances of 2 m, to collapse repeated transects values. Averaging the statistics, as opposed to the transects themselves, preserves the individual transect center of mass, thereby avoiding potential meander

biases in the dispersion, which would otherwise blur the profile (Batchelor 1952, Clark et al. 2010). The total number of downstream transect locations is reduced from 66 and 70 to 41 and 50 for T1 and T2.

The experiment measurements and subsequent analysis are divided into four zones, based on plume evolution from the source and channel geometry (Figure 19). In Zone 1 (0<s<125 m) the plume is mixing in three dimensions (s, n, and vertical, z). Zone 2 (125<s<160 m) begins once complete vertical mixing has occurred, discussed below. In Zones 1 and 2, the channel is relatively straight and the depth and width are relatively constant. Zone 3 (160<s<355 m) has strong bank and bathymetric irregularities (riffle/constriction and embayment) that modify the flow and corresponding dispersion. This zone is subdivided to emphasize transport and mixing effects between distinct flow regimes induced by the channel features: 1) riffle/constriction (Zone 3rc, 160<s<260 m) and 2) embayment (Zone 3e, 260<s<355 m). At Zone 3rc, the channel contracts (25 m to 15 m) and shallows (1.7 to 0.7 m). At Zone 3e, the channel widens (15 m to 30 m) and rapidly deepens by 1 m (1.7 m) (Figure 17b). Zone 4 (355<s<500 m) begins downstream of the Zone 3e. Here the large-scale motions from Zone 3 features have been mostly dissipated and the channel, again, becomes relatively straight with small depth and width irregularities (Figure 17a).

In Zone 1, the surface plume exhibits narrow filaments of high and low concentration sheets. The surface, mid-depth and bottom dye time series, at both 28 m and 110 m (not shown), depict ramp-cliff (sawtooth) structures caused by smaller scale diffusive processes superimposed on the larger scale advective motions similar to that described by Holzer and Siggia (1994). The decay of the concentration maxima, $C_{max}(s)$, with downstream distance is in good agreement (R^2=0.86, 0.84 for T1, T2) with a 3D mixing behavior, $C_{max}(s) \sim s^{-3/2}$ (Figure 19c -red line) (Taylor et al. 1979). A Gaussian distribution has skewness equal to 0 and kurtosis equal to 3. In Zone 1, C(s) are peaky (kurtosis>3) and skewed towards river-left (positive skewness) (Table 4). Dispersion is slowly increasing (dye k_n=0.01, 0.02 m^2/s; drifter k_n=0.03, 0.03 m^2/s) and linear (dye R^2 = 0.80, 0.87; drifter R^2=0.98, 0.95) (Figure 21). Previous studies have found surface k_n to be higher than near bed k_n (Okoye 1970, Nokes 1986). Therefore the slightly higher

drifter k_n, which is a surface measurement, compared to the dye k_n, though measured on the surface incorporates depth-averaged mixing effects, is consistent (Figure 21).

In Zone 2, $C_{max}(s)$ decay with downstream distance has a 2D mixing behavior, $C_{max}(s) \sim s^{-1}$, ($R^2 = 0.82$, 0.82 for T1, T2) (Figure 19 c (black line)) (Fischer et al. 1979), indicating the plume has completely mixed in the vertical. An additional vertical mixing descriptor is the ratio of the river bed concentration to the surface concentration (Rutherford 1994). When this ratio is close to one, the dye is considered vertically well mixed. The distance of complete vertical mixing, indicated by interpolating the average dye ratios of bed to surface at s=28, 110 and 313 m, (not shown), is found to occur slightly downstream of s=110 m just before entering Zone 2, which supports the $C_{max}(s)$ 2D decay behavior. The dye plume transverse distribution becomes symmetrical, with $C(s)$ skewness values decreasing to zero at t~260 s, and slightly flatter (kurtosis<3) than a true Gaussian shape (Table 4). The dye k_n, (0.01, 0.02) remain approximately constant (Table 4, Figure 21). However, in Zone 2 the drifter behavior differs from that of the dye. Drifter σ_{nt}^2 shift from expanding to contracting, resulting in negative diffusivity (k_n =-0.02, -0.02 m^2/s) (Figure 21, color line). This contraction can be explained by the tendency to have faster transverse velocities near the surface then near the bed due to bottom friction (Rutherford 1994). This velocity difference results in a surface drifter convergence while the depth average dye spreading is not influenced. In addition to differences between dye dispersion, the two drifter dispersion measures, σ_{nt}^2 and σ_{nb}^2, begin to diverge in Zone 2 due to time averaging effects and the drifter group streamwise spread. For example, the beginning of Zone 2, D1 and D2 have 24 m and 32 m streamwise spatial footprints that induce spatial averaging in the σ_{nt}^2 quantity (Figure 21, color line) and 30 s observational time spans for both D1 and D2 that induce temporal averaging in the σ_{nb}^2 quantity (Figure 21, '+' symbol).

As the dye plume enters Zone 3rc, dispersion remains slow and linear (k_n=0.01 m^2/s for T1). Note that there were sparse data available for T2 in Zone 3rc. However, individual drifter trajectories produce large variations in drifter dispersion. For example, turbulence generated by a bank feature protruding into the channel at s=200 m causes two

40

drifters during D1 to move quickly towards the right bank (Figure 18 a), which causes an anomalous spike in σ_{hut}^2 and σ_{hus}^2 (Figure 21, color line and + at t=400 s). At the transition between Zone 3rc and 3e, a mixing interface is present between the jet-like flow in the center of the channel and stagnant water near the banks. The dye plume shifts towards the slower water within the embayment on river-right, which alters the previously symmetrical C(s) in Zone 3rc to negatively skewed distribution in Zone 3e (Table 4, Figure 19a). T2 σ_h^2 increases linearly (R^2=0.82) by a factor of six (k_n=0.06 m^2/s) (Figure 21, red dots t>500 s). However, T1 σ_h^2 increase is not present (Figure 21, black dots t>500s), and the σ_h^2 spread is slow (k_n=0.01 m^2/s) with the behavior more scattered (R^2 =0.15)(therefore regression line not included). The low σ_h^2 values for T1 compared with T2 in both Zones 3e and 4 are shown in the Appendix to be the result of not sampling the full width of the plume, and therefore are included.

Drifter trajectories provide greater detail to the transport structures present in Zone 3 as they are drawn into the embayment (1 drifter for D1 and 3 drifters for D2) within separation eddies along the mixing interface (Figure 18, river-right), which highlights a possible mechanism for increased dispersion. The pathways of the four drifters describe an elongated eddy in the streamwise direction (transverse radius ~3.5 m and streamwise radius ~7 m) which extends downstream (~50 m) of the riffle/constriction exit. The drifters circle the eddy (~0.2 m/s) resulting in a small oscillation in σ_{hut}^2 superimposed on a linear increasing dispersion trend (Figure 21, color line). The periodic oscillation is associated with the trapped drifters' transverse motion towards and away from the drifter centroid. Additionally, as all drifters on the periphery are not drawn into the eddy, rather, many move through Zone 3e unimpeded, a temporal entrainment behavior along the mixing interface can be inferred. σ_{hus}^2 (Figure 21, '+' symbol) and T2 $\sigma_h^2(t)$ (Figure 21, red dots) begin to spread rapidly at the start of Zone 3e, t~470 s, whereas σ_{hut}^2 (Figure 21, color lines) exhibits increased dispersion 20 and 100 s earlier for D1 and D2 due to the leading edge of the drifter group encountering the channel features ahead of the group's centroid position. At the time of the rapid increase in σ_{hut}^2,

41

D1 and D2 are spread over distances of 33 m and 56 m in the streamwise direction. This difference in streamwise spread between D1 and D2 results in a delayed onset of increased diffusivity for D1 and an earlier onset of increased diffusivity for D2. While the average k_n values from D1 and D2 between Zone 2 and Zone 3 show a similar pattern of a large increase in diffusivity (0.081, 0.079 and 0.081, 0.044 m^2/s calculated from σ_{hd}^2 and σ_{hs}^2 respectively), the evolution of σ_{hd}^2 and σ_{hs}^2 differ. σ_{hd}^2 is linear in time (R^2=0.85, 0.95) and σ_{hs}^2 is scattered (R^2=0.56, 0.24).

At the start of Zone 4, transverse dispersion asymptotes and all calculation methods, with the exception of T1, provide similar final asymptotic values (~35 m^2) (Figure 21). C(s>355) are nearly uniform (standard deviation of 1 ppb for T1 and 3 ppb for T2), kurtosis is close to three but the plume distribution remains negatively skewed (Table 4). Note, shortly downstream (s>400 m, t>750s) drifter dispersion is no longer useful due to the removal of the drifters (Figures 18 and 21), however, qualitative drifter distribution towards river-right agrees with Zone 4 C(s) skewness (Figure 18, Table 4). The river-right tendency of the dye and drifter observations is investigated in §IV D 2. by examining the coherent transport effects due to persistent flow structures induced by the channel features. The Delft3D measured model dispersion results are shown in Figure 21 for comparison with measured results. The model is described next.

C.   3D NUMERICAL MODEL, DELFT3D

The 3D mean and turbulent flow field and consequent transport and mixing are investigated using the numerical model Delft3D. As of January 1, 2011, the Delft3D flow, morphology and waves modules, developed by WL|Delft Hydraulics were made public as an open source code. The Delft3D-FLOW module is used in this study, which is a multi-dimensional hydrodynamic and transport simulation program. Delft3D-FLOW solves the RANS equations for the horizontal motion, continuity, and transport under the incompressible fluid, shallow water and Boussinesq assumptions. Vertical accelerations are neglected in the vertical momentum equation; therefore vertical velocities are computed from the continuity equation alone (WL|Delft Hydraulics 2007). Small-scale motions, not resolved by the model grid, are related to flow quantities by a choice of

vertical turbulence closure models. A *k-ε* turbulence closure method is chosen to calculate the isotropic 3D component of eddy viscosity, V_{3D}. However, turbulence is anisotropic for natural river flows, with the horizontal eddy viscosity coefficient, V_H, being larger than the vertical eddy viscosity, V_V. To account for anisotropy, an additional horizontal viscosity component is added due to sub-grid scale horizontal turbulence, V_{SGS}. Sub-grid scale turbulence is estimated by HLES, which uses a high-pass filter operation to account for energy lost due to grid scale dependent numerical dissipation and truncation (Uittenbogaard 1998).   User prescribed HLES parameter inputs for all simulations are: slope in log-log spectrum (-5/3), dimensional number (3), Schmidt number, σ_t, which is the ratio of momentum diffusivity and mass diffusivity (0.7), spatial low-pass filter coefficient (0.333), and relaxation time (0.5 min). Delft3D-FLOW also allows for user specified vertical, V_V^{back} and horizontal, V_H^{back} background viscosity terms to account for turbulent motions not captured in the overall execution of the model simulation, which are discussed below. The vertical viscosity is:

$$V_V = V_{mol} + \max(V_V^{back}, V_{3D}),$$ (11)

where V_{mol} is molecular diffusion, which is 10^{-6} m^2/s for water. The horizontal viscosity is a superposition of all three terms given by:

$$V_H = V_{3D} + V_{SGS} + V_H^{back}.$$ (12)

Table 5 provides an overview of eddy viscosity options contained in Delft3D-FLOW.

1.   Delft3D-FLOW Transport and Mixing of Passive Conservative Constituents

The three-dimensional advection/diffusion equation provides the basis to describe the transport of matter, *C*, (and heat) downstream from a discharge source, *S;*

$$\frac{dC'}{dt} + u_\xi \frac{dC'}{d\xi} + u_\eta \frac{dC'}{d\eta} + u_z \frac{dC'}{d\sigma} = \frac{d}{d\xi}\left(D_H \frac{dC'}{d\xi}\right) + \frac{d}{d\eta}\left(D_H \frac{dC'}{d\eta}\right) + \frac{d}{d\sigma}\left(D_V \frac{dC'}{d\sigma}\right) - \lambda + S$$ (13)

where D_V and D_H are the vertical and horizontal turbulent diffusion coefficients, defined as, $D_V = V_V/\sigma_c$, $D_H = V_H/\sigma_c$ from EQUATIONS 11 and 12. For a perfectly passive

43

concentration σ_c is one, however previous 3D numerical model research has shown σ_c less than one provided better results for compensating for anisotropic turbulence structure (Demuren and Rodi 1984). Delft3D-FLOW formulates σ_c as a function of stratification; however, there are no density differences in this study and σ_c is a constant 0.7. λ can be used to prescribed a first order nonconservative decay process, but since our dye is conserved, λ=0.

Delft3D-FLOW uses an Alternating Direction Implicit (ADI) method that splits one time-step, Δt, into two stages (Leendertse 1967). Each stage consists of half Δt where all the terms of the model equations are solved with a second order accuracy in space. The size of Δt is constrained by grid resolution based on the Courant number, CFL, for wave propagation:

$$ CFL = 2\Delta t \sqrt{gh\left(\frac{1}{\Delta s^2} + \frac{1}{\Delta n^2}\right)} < 4\sqrt{2}, \tag{14}$$

where Δs, Δn, are the grid spacing in the streamwise and transverse directions. For the spatial discretization of the horizontal advection terms, three options are available in Delft3D-FLOW: Cyclic, WAQUA and Flooding. Flooding is used for 2D simulations; Cyclic and WAQUA use higher-order approximations and are examined below. For the transport solution method, two options are available in Delft3D-FLOW: Cyclic and Van Leer-2. The Cyclic method for transport follows the ADI-method for the continuity equation and is implicit. While the Van Leer-2 method for transport is explicit and requires satisfying the Courant number for advection CFL_{adv},

$$ CFL_{adv} = \max\left(\frac{\Delta t |u_s|}{\Delta s}, \frac{\Delta t |u_n|}{\Delta n}\right) < 1 \tag{15}$$

Although both methods produce similar results, Cyclic, the implicit method, has the advantage of a less restrictive CFL condition, $CFL_{adv} < 2$ and is used here.

2. Delft3D-FLOW Sensitivity

The Delft3D-FLOW model domain for the field measurement channel consists of 500 2-m grid cells in the streamwise direction, 100 1-m grids cells in the transverse

direction. Model bathymetry is created from the measured bathymetry, described in § IV B 1., using Delft3D-RGFGRID Triangular interpolation method. The impermeability of the surface and the bottom is prescribed by a zero vertical velocity at the free surface and the bottom. Bottom roughness ($z_0= k_N/30$) is defined based on Nikuradse roughness length, k_N. A value of $k_N =40$mm (D50) provided the most accurate simulation results. Constant water elevation boundary conditions are specified at the upstream and downstream open boundaries from measurements of water elevation. Vertical mixing is important, therefore only 3D simulations are used in this study (WL|Delft Hydraulics 2007). A continuous surface passive dye release is simulated in the model domain from the same position as the field experiment.

The impact of varying Δt on model performance is examined next. Simulation quality is assessed by comparing slope (m) and goodness of fit (R^2) from a linear regression between model and measured water elevation and velocity magnitude. The maximum Δt is limited by the spatial CFL condition (Δt <0.9 s). Therefore the first three simulations (S1, S2 and S3) are run using Δt of 0.03, 0.3 and 0.6 s, respectively; all other model parameters and boundary conditions are the same (Table 6). Water elevations (m=0.97; R^2=0.96) and velocity magnitude (m=0.83-0.87; R^2=0.85-0.89) are comparable for all Δt simulations (Table 6), with a slight improvement with decreasing Δt. To balance model skill and computational time, Δt=0.3 seconds is selected for the remainder of the study.

Sensitivity of model transverse dispersion to the selection of advection scheme is assessed by running the same simulation setup (Δt=0.3) and varying only WAQUA or Cyclic (Table 6: S2, S4). Comparisons of S2 and S4 show Cyclic to be more accurate than WAQUA (Table 6). In Zone 1, the WAQUA advection scheme (S2) allows large horizontal excursions of dye filaments to be stretched off the edges of the dye plume, thereby over predicting diffusivity (m=1.55 R^2=0.90). However in Zone 1, Cyclic, which is more dissipative than the WAQUA advection scheme, does not allow the growth of filaments and the dispersion values are in better agreement (m=1.04 R^2=0.86). Within Zones 2 and 4, S2 over predicts mixing, whereas, S4 simulates a magnitude and trend of S4 dye spreading behavior that compares well to the C(s) measurements. At Zone 4, both

S2 and S4 becomes well mixed and model transverse concentration distribution agrees with C(s) statistics (Table 4). The Cyclic advection scheme provided the most accurate prediction of concentration dispersion for our study reach (Table 6). Based on the above sensitivity analysis, all subsequent model simulations in §IV D use: Cyclic advection scheme, Cyclic transport scheme, and no background diffusivity.

D. DISCUSSION

1. Channel Geometry's Effects on Large-Scale Velocity Structure and Transport

The drifter and dye observations suggest k_n is highly variable and channel irregularities greatly enhance mixing, which results in non-Gaussian plume distribution (Table 4). To further explain how channel geometry effects mixing, first, the most important velocity scales, magnitudes, and directions of motion are examined. Secondly, with understanding of the velocity field, the resultant dye response is examined. Spectra are calculated using a 7.5 min Hanning window with 50% overlap for 1.5 hrs of ADV velocities (Figure 17a, stars) and 30 min of fluorometer concentrations (Figure 17a, black dots) resulting in a frequency resolution of 0.002 Hz and 24 and 8 degrees of freedom. The ADV velocity spectral components, u_s, u_n, w, in all locations display isotropic motion (~-5/3 slope) at higher frequencies ($f > \sim 0.3$) (Figure 22), which scales with channel dimensions $f \approx \bar{u}/h$ (Sukhodolov and Uijttewaal 2010). At frequencies lower than $f \approx \bar{u}/h$ the flow is anisotropic. The streamwise and transverse fluctuations are generally one to two orders of magnitude larger than vertical scales. Importantly, there are significant differences in the transverse velocity components between locations. ADV spectra reveal that locations immediately downstream of the riffle (s=327 and 330m) (Figure 22 blue and black lines) contain one-order of magnitude more transverse energy in the lower frequencies, scaling with river velocity and width $f \approx \bar{u}/B$, than ADV locations upstream (s=195m) and farther downstream (s=361m) from the riffle. Drifter observations indicated that the low frequency lateral motion may be caused by separation eddies, induced by the Zone 3 geometry.

46

ADV spectra confirm river velocity is highly anisotropic, horizontally dominated, with predominate length scales larger than the river depth. For comparisons with the velocity spectra, the dye spectra are plotted with the same frequency scale in Figure 23. Dye variance decays rapidly downstream from the source and shifts towards lower frequency. At s=550m the spectra indicates a well-mixed plume with very little variance.

2. Numerical Evaluation of Channel Feature Influence on Mixing

Channel features (featureless straight (S), constriction (IC), riffle (IR) and embayment (IE)) are isolated and idealized in five separate numerical simulations to assess their relative and combined importance on mixing. Idealized bathymetries are based on natural channel geometry and their location is based on a distance from the dye source (Figure 24). All bathymetries are constructed by modifying a straight channel: 23 m wide, centerline depth of 1.6 m and a transverse depth profile based on a straight channel (Figure 24a). IC and IR span 70 m and are located in Zone 3rc. The IC case narrows the channel by 66% to its narrowest of 8 m between 197<s<243m. The IR case is a shallow, 0.5 m, section located 205<s<235 m. The IE case is a widening of the channel by 7m on river-right bank at Zone 3e, 240<s<350 m; this feature spans 110m.

Numerical estimates of dye patterns (Figure 25), dispersion (Figure 26), mean particle pathways and mean vorticity patterns (Figure 27 for the idealized cases and Figure 28 for the combined and natural cases), are computed so that the processes responsible for mixing can be isolated. The dye distribution represents the cumulative effect of all scales of the flow, which includes direct transport processes that are associated with the resolvable flow patterns and unresolved smaller scale diffusion, discussed in §IV C 1. The transverse channel profiles of concentration (Figure 25) are reduced to bulk estimates of dispersion as a function of distance (4) (Figure 26) to quantify the mixing between cases. The particle pathways show the trajectories, or streamlines of the flow, which are computed by integrating the mean velocity field over 1 min (Figures 27 and 28). The mean vorticity patterns are useful in highlighting the presence of eddies, their size, shape, and location. It will be shown that eddies are responsible for the material transport across the channel. Eddies in vorticity maps are

shown as either positive (red) or negative (blue) blobs that correspond to counter- and clockwise rotations. The "mean" particle pathways and vorticity are the focus in this discussion, because the mean flow field is found to be the dominant mixing mechanism, whereas the contributions owing to vertical shear and turbulence are small and discussed in §IV D 2. a.

Mixing within Zones 1 and 2 for all of the idealized channel features behave similarly to the S case, where the plumes are undisturbed and centered in the channel (Figures 25) and the particle trajectories are primarily streamwise parallel. The dispersion increase is small and linear (k_n=0.005 m^2/s) (Figure 26).

The dominant influence channel features have on flow structure and mixing is shown in Zone 3. Entering Zone 3rc, IC bathymetric feature causes a noticeable contraction in the dye plume (Figure 25b), reflected by a decrease in dispersion (Figure 26, blue line). However, IR bathymetric feature causes an expansion in the dye distribution as the channel shallows (Figure 25b), the dispersion increases (Figure 26, red line). Between Zones 3rc to 3e, the IR plume contracts and sharp concentration gradients develop. IR and IC both produce jet-like flows (Figure 27a and b) and corresponding lateral eddies along the channel shoreline. The IR jet generates eddies that extend between s=250 to 340m, whereas the IC jet dissipates in a shorter distance and its eddies only extend between s=250 to 300m. These eddies are drawing dye from the plume center core and transporting it laterally and upstream along channel banks resulting in a rapid increase in dispersion (k_n =0.25 and 0.17 m^2/s for IR and IC). For IE, a weak eddy is present in the lee of the transition (Figure 27c), but the mixing is small (k_n =0.07 m^2/s) and sustained downstream mixing is limited (Figure 25d, 26).

The magnitude of dispersion (Figure 26) is clearly related to the spatial extent of the coherent eddies produced by the mean flow (Figure 27). IR has the largest eddies and results in the most dispersion, which is 3 times larger than the S dispersion at s=450m. IC has eddies, but of smaller extent than IR and dispersion is 2 times larger than the S dispersion. Though a weak eddy is present for IE, the excursion of the plume into the embayment has little influence on overall dispersion resulting in the smallest dispersion, which is only 10% greater than the S dispersion (Figure 26). Within Zone 4 for all cases,

48

plumes are symmetrical and centered in the channel, trajectories return to streamwise parallel with small vorticity gradients and k_n is similar to the S case (Figures 25, 26 and 27).

Comparisons between an idealized combined bathymetry (CP), composed of all idealized channel features reveal spatial flow structures that greatly enhance mixing (Figures 25e, 26 magenta line and 28a) that are not present in the isolated cases. The isolated IE case, which had little effect on mixing, when now combined with the IR and IC geometry results in a very organized CP flow field with strong vorticity gradients (Figure 28a). CP trajectories trace a large eddy on river-right that spans ~75 m in the streamwise direction, occupies ~18m (60%) of the channel width and contains a large area of stagnant (low dye) water in the eddy center (Figure 25e and 28a). This eddy is extracting dye from the plume core and transporting it across the channel. Additionally, vortex pairs are present on river-left. One is a very fast flowing eddy near Zone 3rc exit (Figure 28a) that contracts the plume and forms sharp concentration gradients (Figure 25e). The other is a larger recirculation area that protrudes into the thalweg causing the jet to meander sharply. This recirculation area consists of a small coherent eddy and a disorganized region of stagnant water. Note there are no bathymetric features at this location (Figure 24e). This feature has developed due to the complex dynamics of the entire system. The effect of these combined velocity structures enhance mixing as dye is drawn from the jet core toward the banks (Figures 25e, 26 and 28a).

CP dispersion is compared to the total dispersion from the linear superposition of individual feature dispersion (Figure 26, black line with stars). Though there are similarities between CP and the superposition dispersion patterns, in the initial slow linear spread in Zones 1 and 2 followed by a rapid spreading, in Zone 3e significantly greater dispersion occurs for CP, which highlights the nonlinear effect of combined channel geometries. The CP spreading rate is a factor of 3 greater than superposition (CP: $k_n=2.0$ m^2/s, Superposition: $k_n=0.64$ m^2/s) and the maximum dispersion is a factor of 2 greater (Figure 26). At s=450 m the CP dispersion has achieved nearly complete transverse mixing, ~93 %, σ^2_n as the dispersion is 37 m^2 over the 22m wide plume (Figures 27e and 26 magenta circles).

Spatial dye patterns between the true natural bathymetry (Figure 25f) and the synthetic CP bathymetry are comparable (Figure 25e), but key differences are observed. The natural system has more inherent bathymetric and shoreline variability resulting in more variation in dispersion (Figure 26). The natural bathymetry model dispersion results are also shown in Figure 21 compared with measured dispersion. Note that the natural simulation includes an upstream riffle, which was not included in the idealized cases that contribute to the slightly higher mixing in Zones 1-2 owing to advected turbulence. In Zone 3, geometric controls confine both CP and natural plumes. Similar to the IR and CP cases, the natural plume is contracted by recirculating eddies on the channel banks at the exit of Zone 3rc (Figure 25f and 28b). The natural case eddies on river-left are small and weak (Figure 28b) and the eddies on river-right are much more complex than the CP channel. The roles of enhancing mixing by the eddy within the embayment are similar between cases, but the dye mixing on river-left observed in the CP case (Figure 25e) is not present in the natural case (Figure 25f). The differences between these two cases highlight the importance of quasi-steady eddies in spreading dye across the channel. The natural case combination of weak, to no, eddy activity on river-left and strong separation eddies on river-right are responsible for the pronounced skewness in modeled dye concentrations, drifter observations (Figure 18) and in situ dye concentration transects (Table 4). A more subtle, but potentially important difference in the natural case, are the existence of smaller "secondary" circulation eddies that are not in contact with the main stream and not present in the CP case (Figure 28a). Three secondary eddies are visible at approximately s=260, 285, 310m on right-river (Figure 28b). All eddies are rotating counter-clockwise, and the one located at s=310m is drawing dye into it (Figure 25f). It is hypothesized that the interaction between the multiple flow structures within the embayment and the main channel will result in a variable exchange rate resulting in a spatially and temporally complex dye distribution.

This will be examined in §IV D 2. b. The principal outcome of the above cases comparisons is that small differences in bathymetry result in significant differences in mixing behavior owing to nonlinear interactions.

a.   *Dominant Processes*

The dye simulations provide flow kinematics and confirm channel features influence transport and mixing, and the interactions enhance mixing. To examine the dynamics of the flow the depth-averaged momentum equation is used to provide insight into the effect various forcing components of mean flow, vertical shear, and turbulence have on the transport and mixing,

$$\frac{d(h\overline{u}_s^2)}{ds}+\frac{d(h\overline{u}_s\overline{u}_h)}{dn}-\frac{d(hT_{sn})}{dn}-\frac{d(hT_{ss})}{ds}=-gh\frac{dE}{ds}-c_f\overline{u}_s^2 \tag{16}$$

$$\quad(1)\qquad\quad(2)\qquad\quad(3)\qquad\quad(4)\qquad\quad(5)\qquad(6)$$

(Rhoads and Sukhodolov 2008), where $\overline{u}_s$ and $\overline{u}_h$ are the time and depth-averaged streamwise and transverse velocities, E is the water elevation, g is gravitational acceleration, T'_{sn} is the sum of the depth-averaged transverse momentum fluxes due to vertical shear of mean flow and turbulence. T'_{ss} is the sum of depth-averaged streamwise momentum flux and c_f is a quadratic-law friction coefficient (Rhoads and Sukhodolov 2008). T'_{sn} is given by,

$$T_{sn}=-\overline{(u_{sz}-\overline{u}_s)(u_{hz}-\overline{u}_h)}-\langle u_{sz}'u_{hz}'\rangle \tag{17}$$

where $u_{sz}-\overline{u}_s$ and $u_{hz}-\overline{u}_h$ are measures of time-averaged differences of the vertical profile about uniform flow. u_{sz},u_{hz}, are the local time-averaged streamwise and transverse velocities at each vertical level. u_{sz}' and u_{hz}' are the velocity fluctuations about the respective time and averaged velocities at each vertical level. The overbars denote averaging over time and the vertical. The lateral momentum components are partitioned into two processes: 1) the lateral transport of the concentration by $\overline{u}_s\overline{u}_h$ where the dye will move along mean flow streamlines and 2) plume mixing through mean differential vertical lateral shear $\overline{(u_{sz}-\overline{u}_s)(u_{hz}-\overline{u}_h)}$ and turbulence $\langle u_{sz}'u_{hz}'\rangle$. The transverse gradients of these terms provide the depth-averaged convective acceleration contribution for each process.

Lateral momentum flux is calculated for the combined bathymetry, CP, to examine the dynamics of lateral mixing. Positive momentum flux values (Figure 29b, red blobs) indicate acceleration toward river-left and negative momentum flux values (Figure 29b, blue blobs) indicate acceleration toward river-right. Note the scale differences on the line plots in Figure 29. CP momentum flux patterns highlight the dominance of the mean flow and the magnitude of geometry induced accelerations (Figure 29, compare line plots magnitudes). In straight sections, all lateral momentum gradients are relatively small with the transverse gradients of $\overline{u_s}\overline{u_n}$ being the largest by two orders of magnitude, < 0.01 cm^2/s^2 (Figure 29 line plot s=161 m). However, near channel features the transverse $\overline{u_s}\overline{u_n}$ O(10 cm^2/s^2) gradient remains dominant and all component accelerations are two to three orders of magnitude larger than the straight sections (Figure 29). In Zone 3rc, accelerations force water inward and a narrow jet core is approximately centered in the channel (Figure 29 bottom panel, zero momentum flux shown by the white strip between positive and negative momentum). Exiting Zone 3rc, large areas of positive and negative acceleration indicate an organized converging jet oriented towards river-left (Figure 29 and line plot s=251m). $\overline{(u_{sz}-\overline{u_s})(u_{nz}-\overline{u_n})}$ gradients are two orders of magnitude smaller and with opposite sign indicated weak differential movement of the mean flow over depth (Figure 29 line plot s=251 and 321m). The jet turns at s=275 m towards river-right and begins to broaden at a slower rate, indicated by the reversed accelerations. After the turn, the accelerations are reduced by half and opposite sign. At the end of the embayment the jet turns again and is forced back towards center where flow is weakly convergent (Figure 29b and line plot s=385). The linear attenuation of momentum flux gradients with distance from Zone 3rc exit supports the observed patterns of intense mixing followed by rapid dissipation. On river-left and river-right the counter rotating vortexes, discussed in §IV D 2., are visible with large areas of near zero momentum flux gradients that suggest possible dye trapping regions or "dead zones". In summary, gradients of the mean flow patterns are the primary forcing mechanism that mixes material across the channel.

b.   *Embayment Trapping*

It was been shown that coherent velocity structures are responsible for drawing dye out of the plume and transporting it laterally. The natural case illustrates a primary embayment eddy that is transporting particles into the embayment at s~340m and recirculating them upstream along the 1 m bathymetry contour (Figure 28b). It is clear, that while the dispersion shows a rapid increase at 250 m (Figure 26), the dye concentration comparisons and particle trajectories (Figures 25f and 28b) point toward a plume that is confined with little lateral mixing occurring across the shear zone near the exit of Zone 3rc. Experimental C(s=280, T1,4 transects averaged) has smaller dye concentrations on river-right and higher dye concentrations in the center channel. The sharp gradient on the river-right edge of the jet confirm lateral mixing is small near Zone 3rc exit (Figure 30).   Farther downstream the modeled dye fields and experiment C(s=310, T1, 5 transect averaged), (Figures 25f and 30) remain in agreement. C(s=310) (T1, 5 transect averaged) indicate the dye is spreading primarily towards the embayment and there is little mixing occurring on river-left. The separation eddy downstream of the bank protrusion (Figure 28b) highlights the transverse transport pathways from the main channel towards river-right.

Laboratory experiments on entrainment in groins fields, which are geometrically similar to the natural embayment feature, have shown that groins develop the same primary and secondary circulation structures observed in the natural channel (Figure 28b). It was found that the complex interaction between these eddies modulates the dye exchange rate with the main stream. The secondary eddy is thought to act as a dye trapping region, exchanging dye slower than the primary eddy, because it is cut off from the main channel (Weitbrecht et al. 2008). Two methods were used to quantify the exchange of the flow structures, using the Delft3D S4 model. First, the flushing behavior was determined by injecting separate slugs of dye into the primary (Figure 17a, red box) and secondary eddy (Figure 17a, black box) and the total concentration was examined within each box for six hours of simulation time.   Second, the filling behavior was examined with a third simulated dye release at a constant rate from the source at s=0 and the total concentration within the two eddies and a box at s=500m (Figure 17a, blue box)

over the six hour simulation time. Filling concentrations started once dye entered the box, i.e. time of travel was removed. It is important to stress that the three simulated dyes do not interact and are distinct measured quantities. For comparison, the flushing cases are normalized by the initial total concentration, and the filling cases are normalized by the maximum total concentration and subtracted from one. In this way the increasing filling trend and the concentration scale are reversed, i.e. the slope is negative where 1 indicates zero dye and 0 denotes the maximum amount of dye is within the box such that the temporal flushing and filling behavior can be directly compared together (Figure 31).

The time variation of the normalized concentrations within each box is compared to a first order exponential behavior as:

$$C'_{exchange}(t) = C'_0 e^{(-t/T_D)}, \tag{18}$$

where C_0 is the initial concentration and t is time. T_D is residence time and is a measure of the dye retention within a system. Large values of T_D indicate the system is isolated and exchange is small, whereas small values of T_D indicate the system is open and exchange is rapid. The straight dot-dashed lines in Figure 31 depict $C'_{exchange}(t)$ calculated from T_D values of 30s (fitted to the primary eddy flushing concentration) and 155s (fitted to the secondary eddy flushing concentration). The fitted T_D for filling cases were also computed but not shown. The degree to which the simulation data follows an exponential behavior expresses the variability of the exchange rate caused by interactions with other processes.

The time evolution of normalized concentration data describes the coupled interaction of the entire natural channel and provides insight into the spatially distinct transport and mixing character within different regions of the flow. The primary eddy is in contact with the main stream and the secondary eddy and therefore, the exchange response is a function of the interaction between all three regions of the flow (Figure 31, black solid and dashed lines). The secondary eddy is isolated from the main channel and is only in direct contact with the primary eddy and therefore, the exchange is controlled by the coupling between the two eddies (Figure 31, red solid and dashed lines). The

54

downstream box's concentration response is a reflection of all upstream transport and mixing processes and therefore, the exchange is controlled by the entire flow character of the natural channel (Figure 31, blue dash line).

The flushing concentration data (Figure 31, solid lines) follow an exponential decrease in time, $T_D=30$ s, until ~50% of the total dye remains, at t~20 mins. After t=20 mins the concentration behavior of the eddies differ. The primary eddy flushing remains exponential in time, $T_D=30$ s, highlighting a nearly constant exchange rate with the main stream. In contrast, after t=20 min, the secondary eddy flushing is highly variable and oscillates at a period of approximately 30 min. This behavior indicates a strong modulation of detrainment as the secondary eddy expels dye, followed by shorter periods of re-entrainment of a portion of the dye expelled, lasting approximately 4 mins. The initial oscillations, at t=20, 50 and 106 mins, indicate the secondary eddy is re-entraining a large percent of the total dye loss, 34%, 21% and 5% respectively. After t=135 min, the normalized concentration oscillations are smaller indicating and the flushing is approximately exponential with a slow $T_D=155$s. Overall the flushing trends between the two eddies are very different, the primary eddy flushes 95% of it concentration in 89 mins, whereas the secondary eddy flushes 95% in 287 mins, a factor of 3 slower than the secondary eddy.

The filling concentration (Figure 31, dashed lines) provides additional spatial insight by allowing for the examination of the cumulative effects of natural river flow structure. For t<20 min, the primary eddy and downstream box follow a similar behavior to the flushing case with an exponential decrease in time, $T_D=30$s, until ~50% of the maximum dye is entrained. Interestingly, the secondary eddy displays a slow fill until t=20min. Recalling the first re-entrainment event occurred at t=20 min, the initially slow fill indicates the primary eddy is withholding most of the dye, and like the flushing case, it enters the secondary eddy from the primary eddy, after a time lag. After t=20 min, the primary eddy and downstream location (s=500m) fill exponentially at an exchange rate slower than the initial filling, $T_D=37$ and 50s. T_D differences indicate the primary eddy is filling more rapidly than the downstream box, which highlights the strength of the primary eddy to draw dye out of the main stream. The secondary eddy is filling slightly

55

faster, T_D=140s, than it is flushing, T_D=150s. This is significant because it means these isolated structures can act as concentration trapping regions that can potentially contain anomalously large concentrations long after a discharge or spill has occurred.

E. CONCLUSION

An unparalleled comprehensive natural river study of transport and mixing was performed where dispersion was measured in two unique ways of constant discharge tracer releases and GPS drifter deployments, along with a reach scale array of Eulerian sensors. The natural reach was a relatively straight section, but contained three distinct features, a constriction, riffle and embayment, all located toward the middle of the 500m long study reach, which provided unique insight into the transport and mixing processes associated with natural channel geometry. For the first time, natural channel tracer tests were conducted consecutively with GPS drifter releases, which provide a direct comparison of their respective dispersion behavior. The high resolution drifter data (0.5 Hz sampling) and surface spatial distribution of the dye plume reveal that natural channel mixing is highly variable, where k_n is 0.02 m^2/s prior the features and increased by a factor of three following the features, k_n=0.06 m^2/s.

Numerical simulations (Delft3D-FLOW) compare well with GPS water elevation surveys (m=0.99, R^2=0.97), 49 velocity profiles (m=0.81, R^2=0.87), and reach scale spatial dye data (m=1.04, R^2=0.86). The effects of river geometry are numerically investigated by isolating and idealizing the natural river features to examine flow scales, particle pathways, and lateral momentum. Often in past literature the increased mixing in the presence of channel features, such as a riffle, is explained due to increased turbulent processes. However, in this channel, mixing is controlled by large scale coherent horizontal flow structures that dominate dispersion through lateral transport of dye due to the mean flow. The effect of the small variations of channel geometry is highly nonlinear, producing very different flow structures that increase mixing by a factor of two. The natural channel bathymetry reveals complex flow structures that cause variable dye exchange between isolated recirculation regions and the main stream, inducing

residence time differences by a factor of five. Additionally the variable exchange can explain observed streamwise skewness in many previous natural river studies (Rutherford 1994).

This work has shown inherent natural channel complexities make bulk parameterization estimators of mixing unreliable. Widely available 3D numerical models now allow water management practitioners to move away from analytical techniques and focus on simulating the spatial and temporal transport and mixing processes directly. These comparisons of model data with observed mixing provide a most promising alternative. This study has shown numerical models can capture local velocity structure and accurately predict dye transport and mixing in a natural channel.

THIS PAGE INTENTIONALLY LEFT BLANK

V. CONCLUSION

A combination of field data and modeling is used to investigate natural river mixing. Two continuous point source tracer releases and GPS-Equipped drifter data from five hydraulically unique reaches are analyzed and compared. The comparison determines and quantifies the influence of turbulence, transverse velocity shear and coherent velocity structures on transport and mixing. Additionally, water elevation and ADCP time-series data along with detailed bathymetric surveys allowed for a 3D transport model to be validated. The model was applied to identify the role of natural river features, such as a constriction, riffle and embayment, on transport and mixing processes.

A. USE OF POSITION-TRACKING DRIFTERS IN RIVERINE ENVIRONMENTS

The application of a new Lagrangian riverine characterization technique fills the observational gaps left by traditional longitudinal tracer methods. Data obtained during an experiment utilizing twenty GPS equipped river drifters provide both Eulerian and Lagrangian observations demonstrating a wide range of riverine applications. Statistical analysis of the high temporal resolution (0.5 Hz) drifter data provides measurements to describe fine-scale riverine processes. Both divergence (positive diffusivity) and convergence (negative diffusivity) is observed in longitudinal and transverse directions. Transverse convergence occurs before the apex in bends, whereas, longitudinal convergence is observed in the exits of bends due to flow deceleration. River shape induced periodicity in the velocity field was found in the oscillatory behavior of the autocovariance function. GPS-equipped drifters represent all scales of the surface flow and decorrelation time is directly calculated from the autocovariance function. River studies can be performed at minimal cost and logistical preparation. Prior knowledge or measurements of a field site are not required. GPS-equipped river drifters are inexpensive, easy to deploy, and provide high temporal and spatial resolution data which provide new insights into river kinematics.

B. SPATIALLY VARIABILITY OF NATURAL RIVER MIXING

The physical perspectives provided by single and two particle statistics allows insight into the flow structure of the individual reaches and an overall sense of how differences in river shape and speed modify statistical dispersion behavior while providing distinctions in the governing mechanisms to mixing. The single particle statistic captures a theoretical near field behavior of dispersion proceeding quadratically in time scaled with a nearly constant background "velocity variance" $\langle U^2 \rangle$. Persistent linear increase in K_s, $R^2 > 0.92$, indicate the drifters are randomly sampling transverse velocity shear evenly. The linearity allows for the combined effects of turbulence and shear to be calculated directly from the slope of the regression line. This slope, $\langle U^2 \rangle$ (m^2/s^2), scales with mean river speed, as shown by NOF and MEK having smaller values, 0.04 m^2/s^2, and the fast flow reaches, BRK and UPS, having larger values, 0.30 and 0.82 m^2/s^2, $\sqrt{\langle U^2 \rangle}$ accounts for 50% of the mean speed. Differences between straight and meandering reaches quantify the influence of river shape on mixing. The straight reaches have higher R^2 values than the meanders reaches, additionally, oscillations in K_n are directly reflected in K_s, reinforcing local variability due to bends. Interestingly, single particle comparisons using varying starting locations produce the same K_s behavior in time; the spreading is nearly constant for an initial period lasting several minutes (UPS~5mins and MEK~40mins). This indicates the small scale mixing and velocity shear effects are not very different spatially and the large scale mixing coupled with the spatial separation of the drifters cause nonlinear diffusivity behavior in time.

Relative dispersion results support this by revealing markedly different overall dispersion behavior, one order of magnitude, indicating the mechanism for K_r behavior is not isotropic turbulence but rather a nearly constant transverse velocity shear. K_{ps} is highly variable with standard deviation of K_{ps} ranging from 29% to 125% of the mean. While the mean K_{ps} magnitude patterns were similar to magnitude patterns of $\langle U^2 \rangle$ among reaches, no common link was found that relates the observed variably of K_{ps}. K_{ps}

is correlated and proceeds as $K_{ps} \sim l^{4/3}$ for all length scales. The K_{ps} to separation scale relationship describes reduced diffusivity at approximately bend apex length scales due to the flow convergence, which minimize relative pair separation velocity. These flow convergence structures are observed directly with trajectories and speed observation from drifters (Figure 8, second panel and bottom panel). These features accelerate and transversely contract the drifters into bend apexes and decelerate and transversely expand the drifters exiting bends thereby controlling differential advective influences of the transverse velocity profile. Until now, river field studies have used tracers or hydraulic river characteristics to estimate dispersion. However, tracer methods have several shortfalls that include behavior between sample locations and particle pathways are unknown, tracer methods are costly, are logistically difficult and time consuming to carry out. Additionally, natural river turbulence is not stationary nor homogenous, and theoretical assumptions are limited in their application. The application of a new Lagrangian drifter river characterization technique fills the observational gaps inherent in traditional tracer methods.

Local and reach average processes of streamwise and transverse dispersion have been quantified utilizing GPS-equipped, high temporal and spatial resolution, drifter observations. Lagrangian data from GPS-equipped drifters allows the combined influence of turbulence and transverse velocity shear to be quantified and additional insight into how the relative contribution of local geometry contributes to mixing.

C. NUMERICAL MODEL COMPARISONS OF TRANSVERSE MIXING IN A NATURAL RIVER

An unparalleled comprehensive natural river study of transport and mixing was performed where dispersion was measured in two unique ways of constant discharge tracer releases and GPS drifter deployments, along with a reach scale array of Eulerian sensors. The natural reach was a relatively straight section, but contained three distinct features, a constriction, riffle and embayment, all located toward the middle of the 500m long study reach, which provided unique insight into the transport and mixing processes associated with natural channel geometry. For the first time, natural channel tracer tests were conducted consecutively with GPS drifter releases, which provide a direct

comparison of their respective dispersion behavior. The high resolution drifter data (0.5 Hz sampling) and surface spatial distribution of the dye plume reveal that natural channel mixing is highly variable, where k_n is 0.02 m^2/s prior the features and increased by a factor of three following the features, k_n=0.06 m^2/s.

Numerical simulations (Delft3D-FLOW) compare well with GPS water elevation surveys (m=0.99, R^2=0.97), 49 velocity profiles (m=0.81, R^2=0.87), and reach scale spatial dye data (m=1.04, 641 R^2=0.86). The effects of river geometry are numerically investigated by isolating and idealizing the natural river features to examine flow scales, particle pathways, and lateral momentum. Often in past literature the increased mixing in the presence of channel features, such as a riffle, is explained due to increased turbulent processes. However, in this channel, mixing is controlled by large scale coherent horizontal flow structures that dominate dispersion through lateral transport of dye due to the mean flow. The effect of the small variations of channel geometry is highly nonlinear, producing very different flow structures that increase mixing by a factor of two. The natural channel bathymetry reveals complex flow structures that cause variable dye exchange between isolated recirculation regions and the main stream, inducing residence time differences by a factor of five. Additionally the variable exchange can explain observed streamwise skewness in many previous natural river studies (Rutherford 1994).

This work has shown inherent natural channel complexities make bulk parameterization estimators of mixing unreliable. Widely available 3D numerical models now allow water management practitioners to move away from analytical techniques and focus on simulating the spatial and temporal transport and mixing processes directly. These comparisons of model data with observed mixing provide a most promising alternative. This study has shown numerical models can capture local velocity structure and accurately predict dye transport and mixing in a natural channel.

APPENDIX. CAUSES FOR T1 AND T2 ZONE 3 DISPERSION DIFFERENCES

Zones 1 and 2 T1 and T2 dispersion estimates are in close agreement, however, within Zone 3 and 4 there are large dispersion differences (Figure 21). The reason for lower values of σ_h^2 (Figure 21) and M(s) (Figure 20) can be attributed to sampling width differences between the two dye releases (Figure 19a and b). To account for these differences, σ_h^2, are normalized by the variance of a uniform distribution, $\sigma_{uniform}^2(S)$, over the respective sampled width for each transect. $\sigma_{uniform}^2(S)$ is, $B^2/12$, recalling B is the width of the transect at each streamwise location. The normalization, $\sigma_h^2(S)/\sigma_{uniform}^2(S)$, allows concentration dispersion to be defined relative to the channel, where 0 denotes no mixing and 1 denotes complete transverse mixing (Figure 32). This illustrates the sensitivity of the dispersion estimate to sampling width, T1 (black dots) and T2 (red dots) are in agreement while the observed drifter and T2 rapid spreading behavior is preserved.

Table 1   GPS-Equipped drifter deployment configurations, and Lagrangian quantities.

Location	Northfork Skagit (NOF)	Braided Kootenai (BRK)	Upper Skagit (UPS)	Meander Kootenai (MEK)	Marsh
Deployments	2 R_c, 1 R_L,	3 R_{sc},	3 R_c	3 R_c, 1 R_{sc},	1 R_c
# of Drifters Used / group release	16	16	14-18	15-33	6
Average Distance Traveled (m)	1400	1600	3500	8000	35
Average Speed (m/s)	0.6	1.4	1.1	0.4	0.16
Channel Width (m)	93-154	80-150	125-158	125-200	2
Velocity variance $\langle U^2 \rangle$ (m²/s²)	0.04	0.82	0.30	0.04	–
Mean(K_{ps}) (m²/s)	4	59	59	7	–
Std(K_{ps}) (m²/s)	5	17	36	20	–

Table 2.   Longitudinal and Transverse Dispersion Coefficient Estimates

Location		Upper Skagit	North Fork Skagit		Marsh
Deployment		Cluster Release	Cluster Release	Line Abreast Release	Cluster Release
Longitudinal Single Particle Diffusivity (m^2/s) (K_{ss})		5.90	0.39	0.57	0.02
Longitudinal Diffusivity (m^2/s) (K_s)		10.0	0.18	1.47	0.22
Transverse Diffusivity (m^2/s) (K_n)	Divergent	1.20	0.09	0.85	0.01
	Convergent	-3.01	-0.09	-0.41	-0.02

Table 3.   Single Particle Lagrangian Decorrelation Time

LOCATION	UPPER SKAGIT	NORTH FORK SKAGIT		MARSH
DEPLOYMENT SCHEME	CLUSTER RELEASE	CLUSTER RELEASE	LINE ABREAST RELEASE	CLUSTER RELEASE
LONGITUDINAL DECORRELATION TIME (S)	222	134	188	16
TRANSVERSE DECORRELATION TIME (S)	72	58	110	14
ABSOLUTE DIFFUSIVITY MAXIMA DECORRELATION TIME (S)	258	138	162	14
MIXING TIME THEORY (S)	3266	22222	23529	80

Table 4   Zone average C(s) Statistics (T1, T2)

	Zone 1	Zone 2	Zone 3rc	Zone 3e	Zone 4
Skewness	1.50, 1.75	0.70, 0.53	0.17, 0.18	-0.21, 0.17	-0.50, -0.64
Kurtosis	4.94, 6.83	2.26, 2.05	1.62, 1.64	3.10, 1.94	2.25, 3.05
k_n	0.02, 0.01	0.01, 0.02	0.01, -0.01	0.01, 0.06	0.02, 0.01

Table 5   Overview of eddy viscosity options contained in Delft3D-FLOW.

Model Description	v_{SGS}	v_H^{bak}	v_{3D}	v_V^{bak}
2D, no HLES	-	User Input	-	-
2D, with HLES	computed by HLES	User Input	-	-
3D, no HLES	-	User Input	computed by vertical turbulence model.	User Input
3D, with HLES	computed by HLES	User Input	computed by vertical turbulence model.	User Input

Table 6   Numerical simulation and their agreement with observations.

ID	Model Description	Time Step (s)	(m,R^2) Velocity	(m,R^2) - Water Elevation	(m,R^2) – Dye Dispersion	Simulation Time (hrs)
S1.	WAQUA,HLES, $v_{V,H}^{bak}=0$	0.03	0.87,0.89	0.97,0.96	1.88,0.88	72
S2.	WAQUA,HLES, $v_{V,H}^{bak}=0$	0.30	0.84,0.85	0.97,0.96	1.55,0.90	5
S3.	WAQUA,HLES, $v_{V,H}^{bak}=0$	0.60	0.83,0.85	0.97,0.96	1.17,0.90	3
S4.	Cyclic, HLES, $v_{V,H}^{bak}=0$	0.30	0.81,0.87	0.99,0.97	1.04,0.86	5
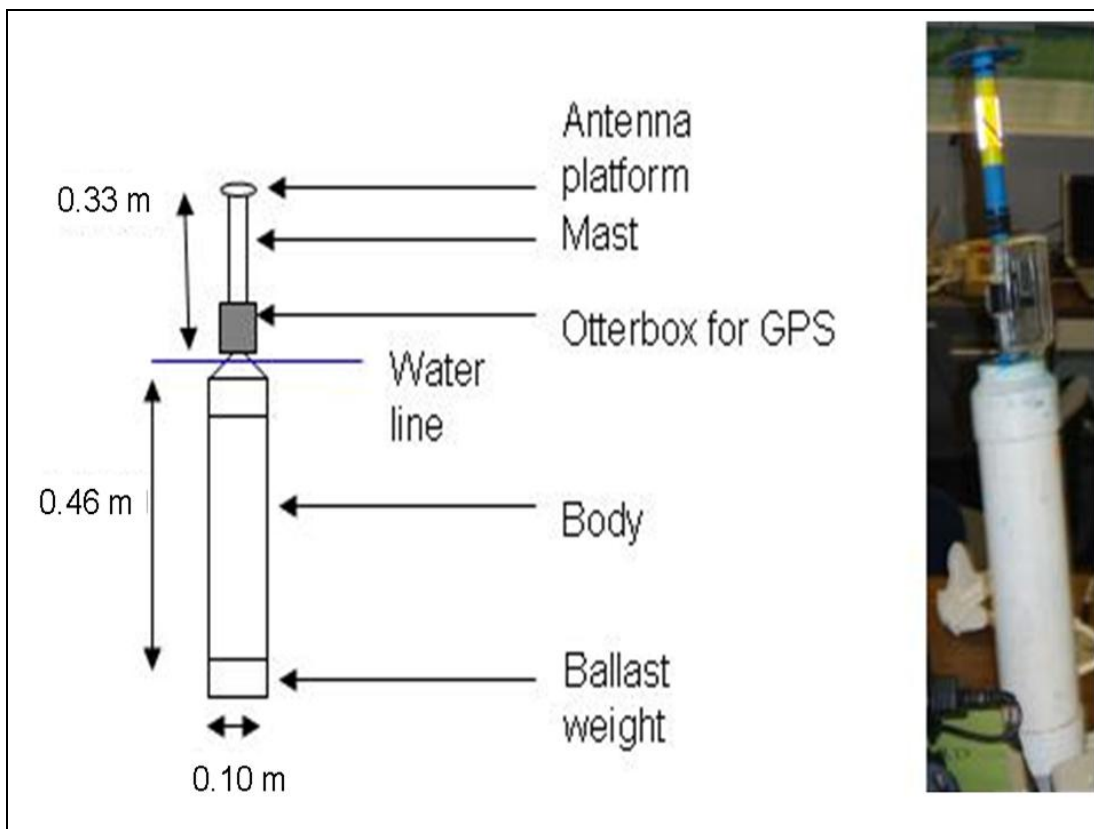
Figure 1.   Schematic of the GPS-equipped river drifter and photograph.
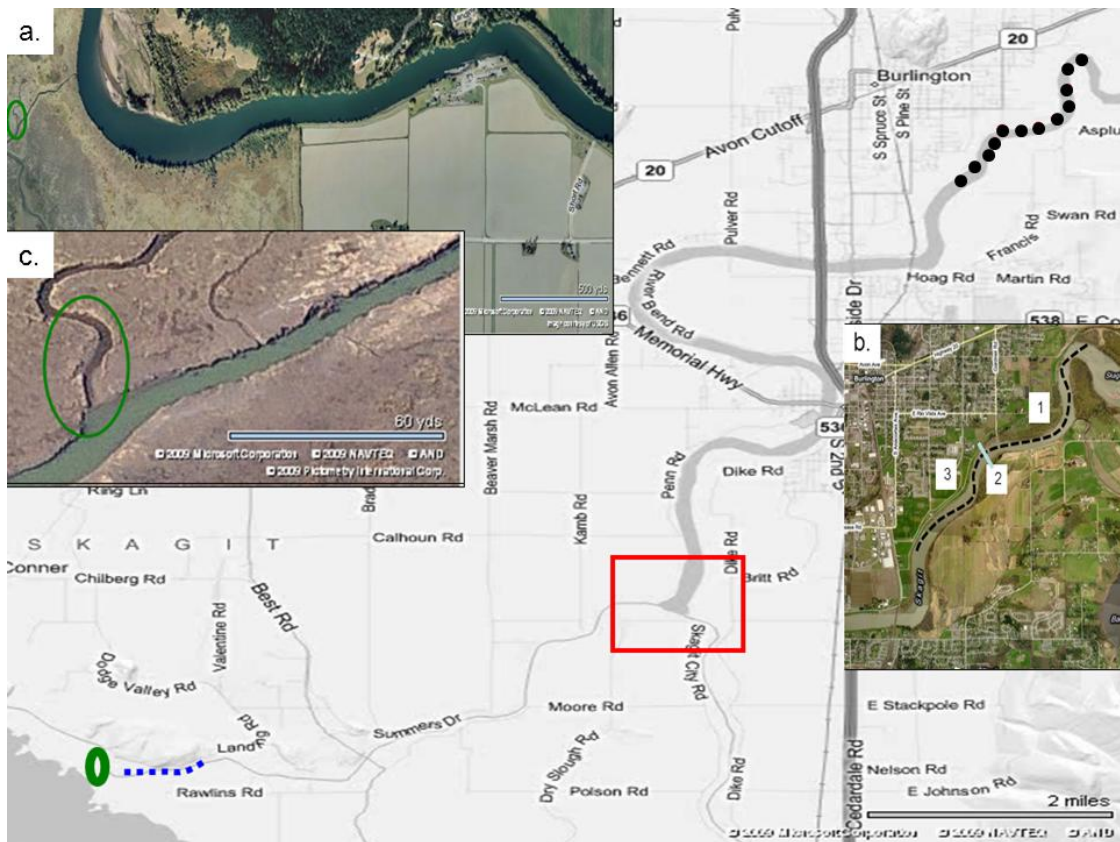
Figure 2.   Vicinity map of the Skagit River, WA, U.S.A. and drifter deployment reaches: (a) North Fork, blue dotted line, (b) Upper Skagit, black dotted line and (c) Marsh Channel, green oval. The Skagit River flows from the northeast corner of the figure to the southwest, splitting into the North and South forks (red square) before flowing into Skagit Bay. Scales of insets are shown in the bottom right corner of each inset (Microsoft Corporation 2011).
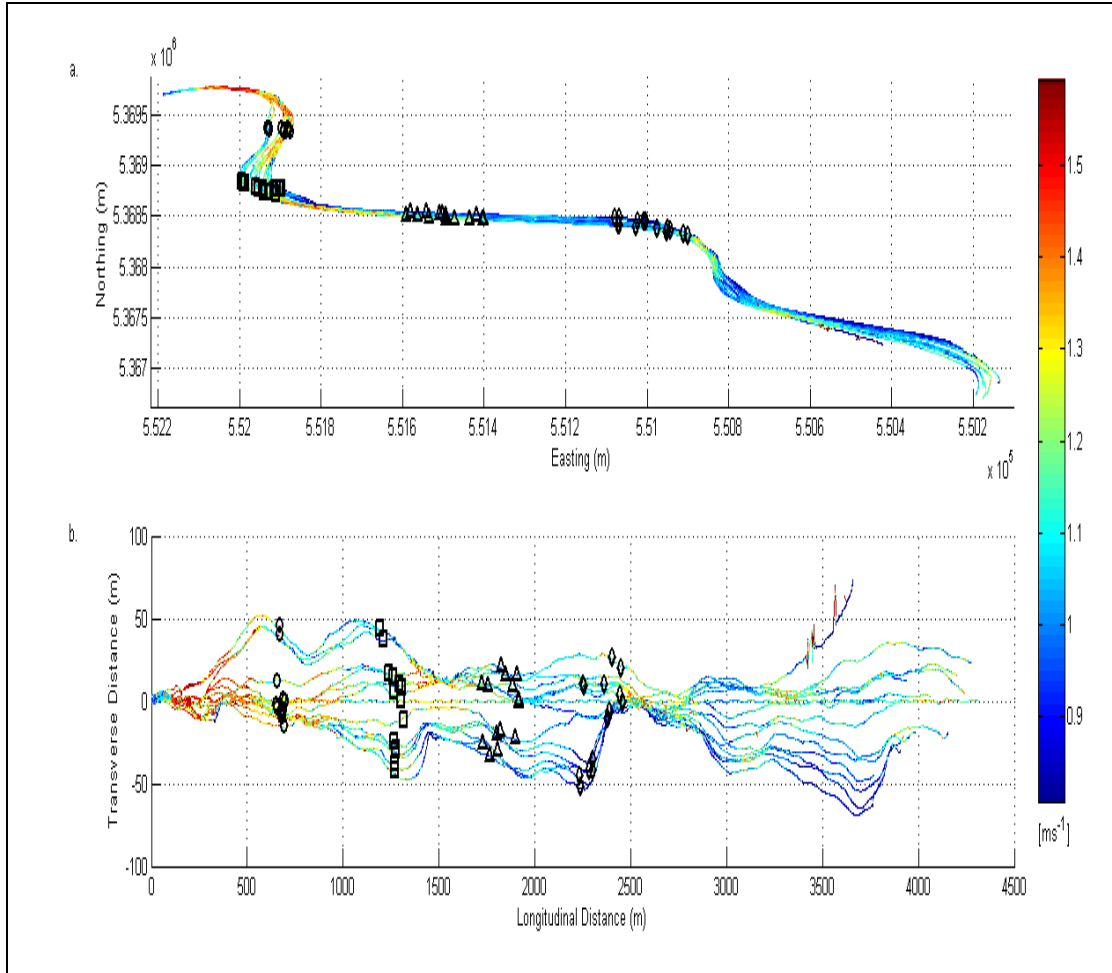
Figure 3.   Upper Skagit deployment coordinate transform: (a) geographic coordinates, (b) river-fitted local coordinate frame utilizing Legleiter and Kyriadkidis (2007) technique. Symbols represent the position of the drifters at 500 (circle), 1000 (square), 1500 ((triangle) and 2000 (diamond) seconds after release. Colorbar plotted on the right, where color represents drifter speed.
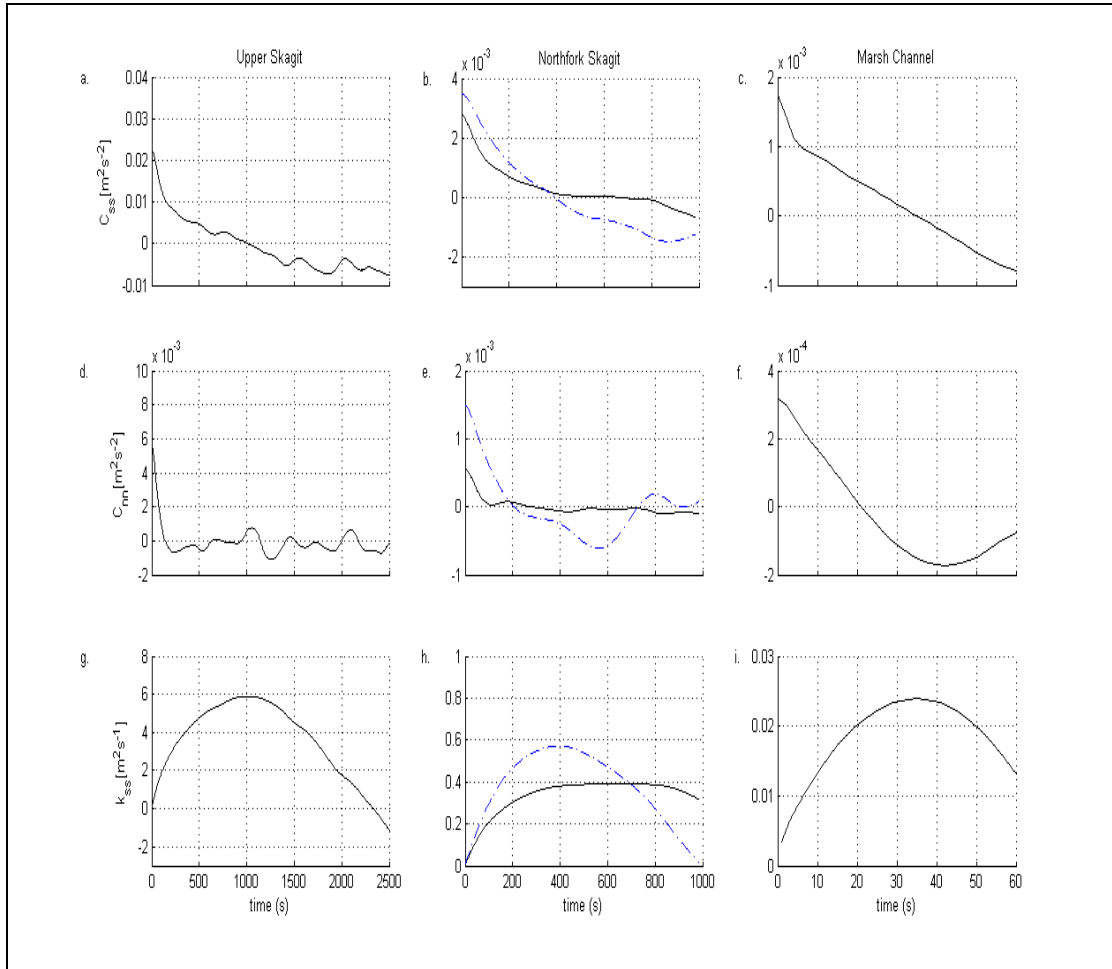
Figure 4.   Autocovariance anomalous velocity functions for the Upper Skagit (left
          column), Northfork (middle column) cluster release (solid line) and line breast
     release (dashed line) and Marsh Channel (right column). Longitudinal (C_{ss}) (a-c),
          transverse (C_{nn}) (d-f) and longitudinal single-particle diffusivities (k_{ss}) (g-i)
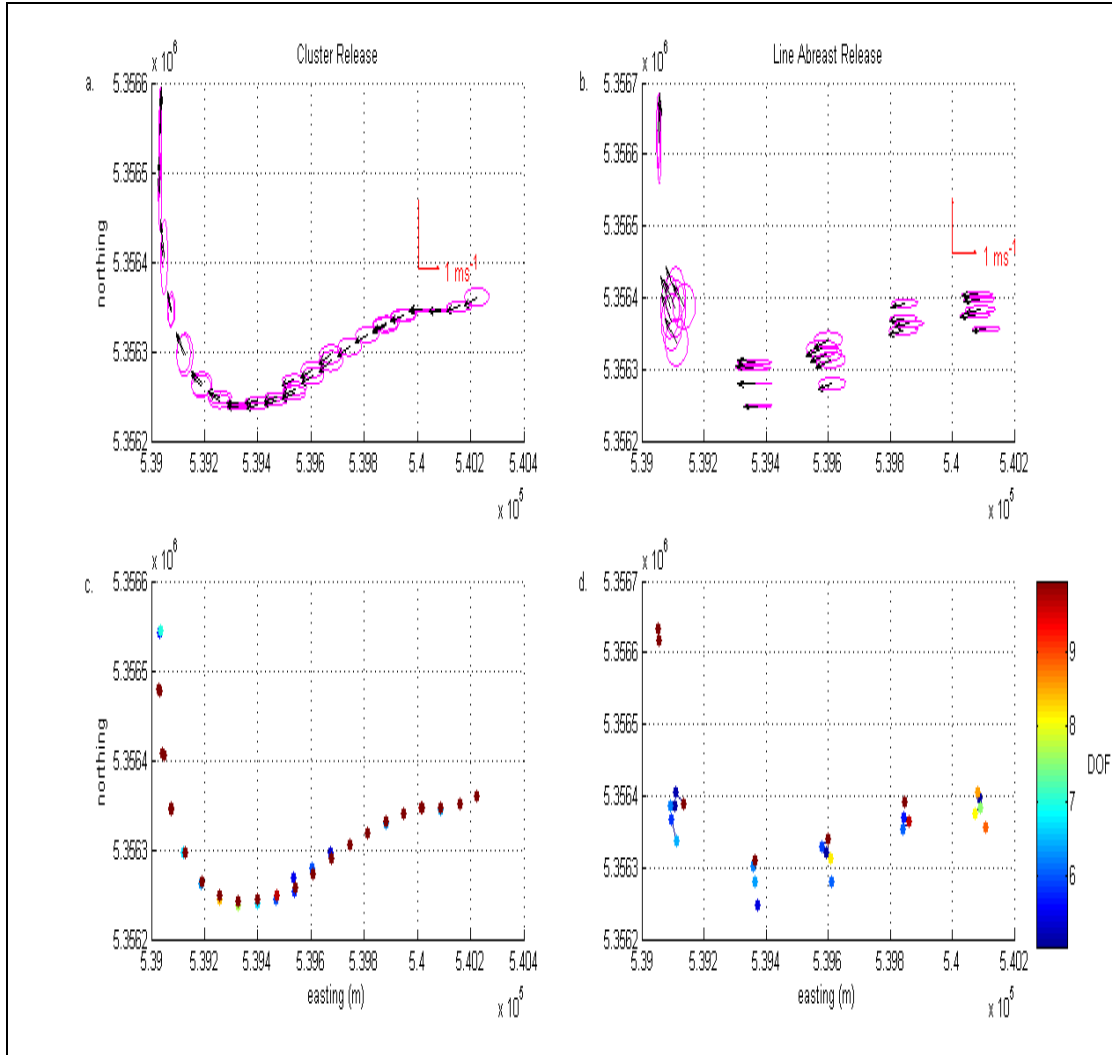
Figure 5.　　　　Plan view of spatially-binned mean velocities and fluctuation ellipses (a,b) for Northfork cluster (left) and line abreast releases (right) . The DOF in each bin are plotted in color with scale to the right (c,d); only bins with greater than 5 DOF are shown. The red vector (a,b) provides a speed scale.
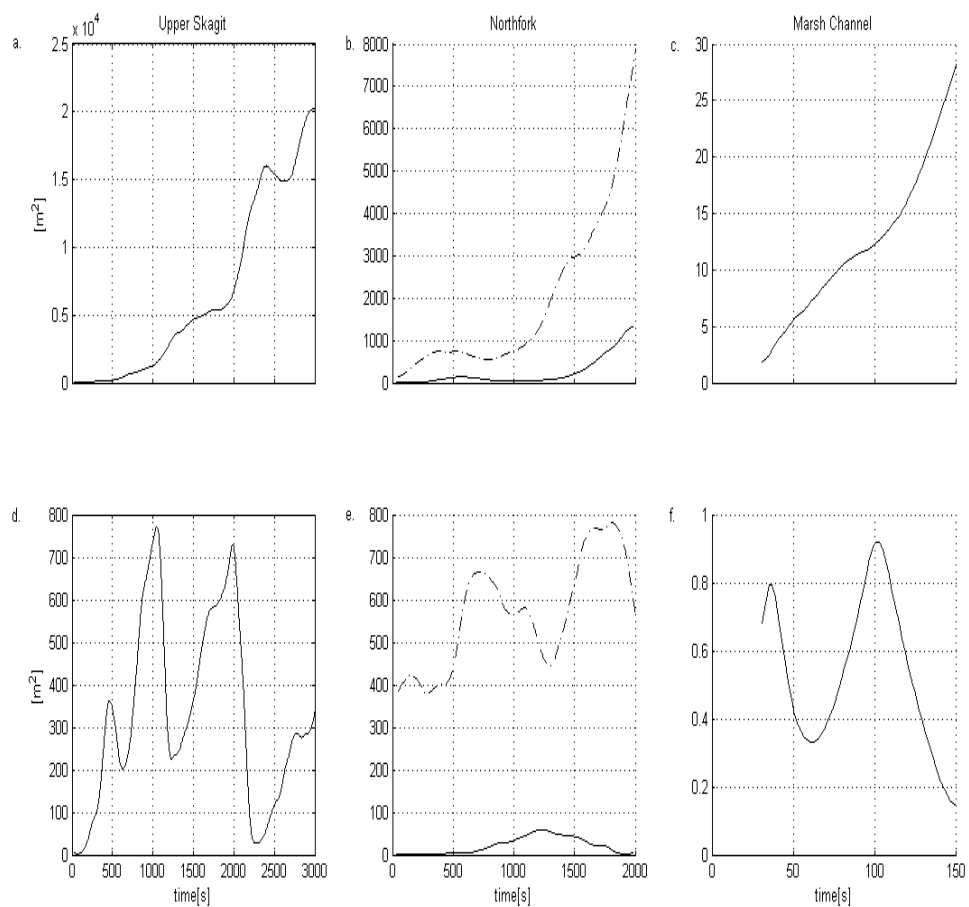
Figure 6.   Longitudinal (a-c) and transverse (d-f) variance of the drifter's positions about the center of mass vs. time for the releases on Upper Skagit (left column), Northfork (middle column) cluster release (solid line) and line abreast release (dashed line) and Marsh Channel (right column). The values of diffusivity are calculated from the slope of a regression line after $t>T_L$.
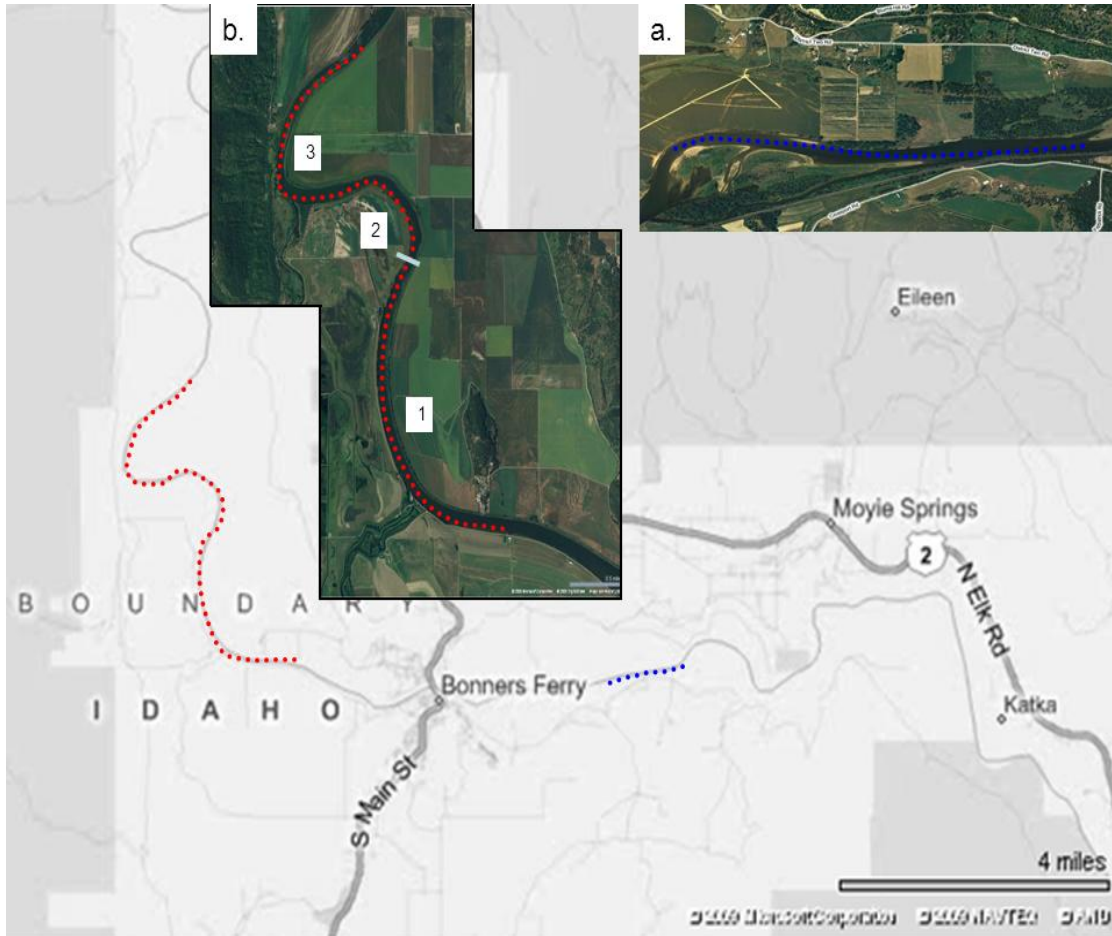
Figure 7.　　　Vicinity map of the Kootenai River, ID, U.S.A. and drifter deployment reaches: (a) Braided Reach, blue dotted line and (b) Meander Reach, red dotted line. The Kootenai River flows from East to West through Idaho before turning northwest into British Columbia (Microsoft Corporation 2011).
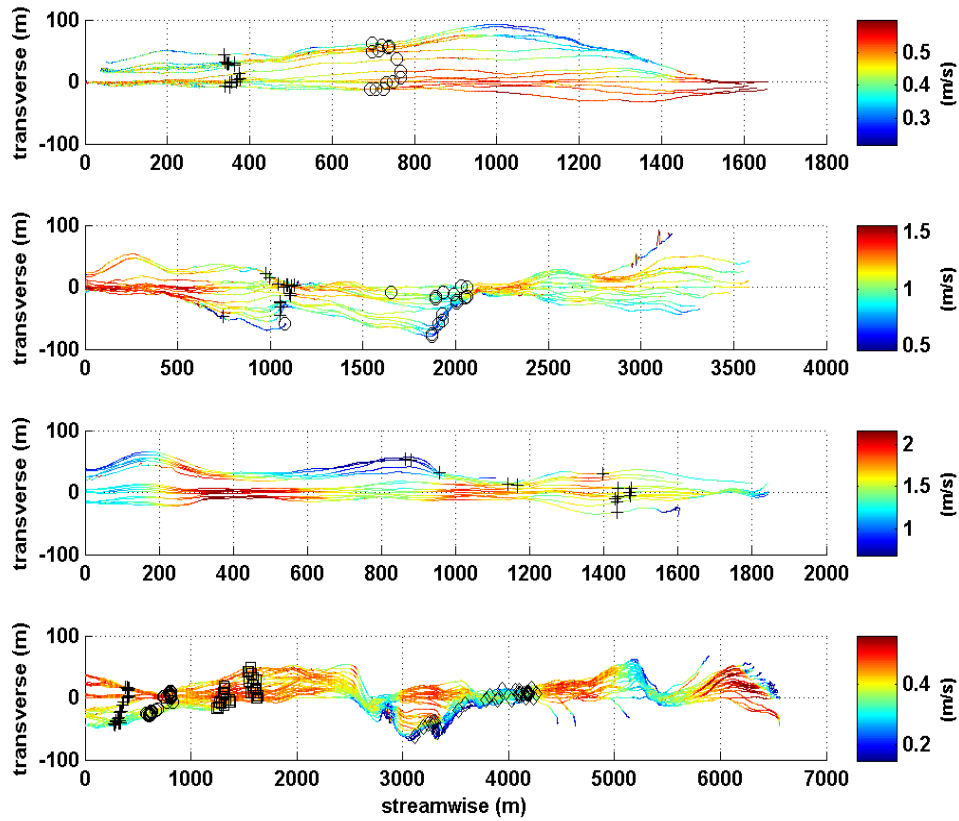
Figure 8. Drifter trajectories and velocity on all reaches in local coordinate. Skagit River reaches, Northfork (NOF)(top panel) and Upper Skagit (UPS)(second panel). Kootenai river reaches, Braided (BRK))(third panel)and Meander(MEK) (bottom panel) Symbols are instantaneous drifter positions 15mins (+), 30mins (circle), 1 hr (square), and 3 hrs (diamond) after release. Colorbars are plotted on the right, where color represents drifter speed. Note differences in speeds.
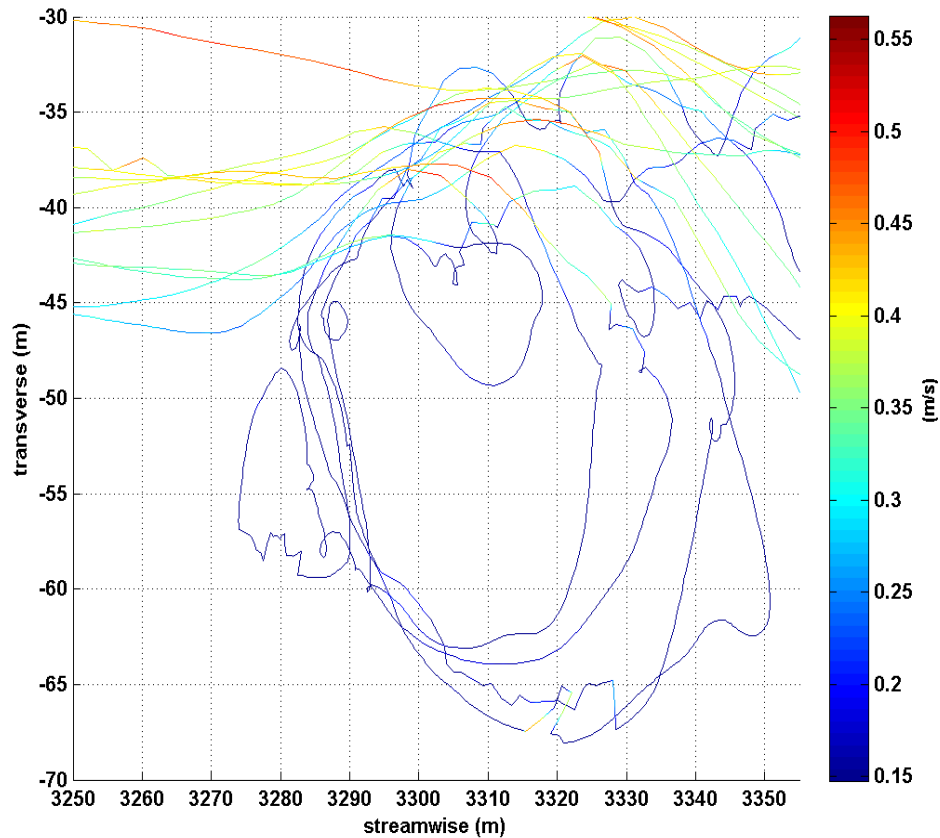
Figure 9.   Meander reach eddy (70m in the streamwise direction and 30m in the transverse direction) . Five drifters circle the eddy before being released. The time to circle the full extent of the eddy is 5 min. One drifter rotates within the eddy for two full rotations and is release after more than 15 mins.
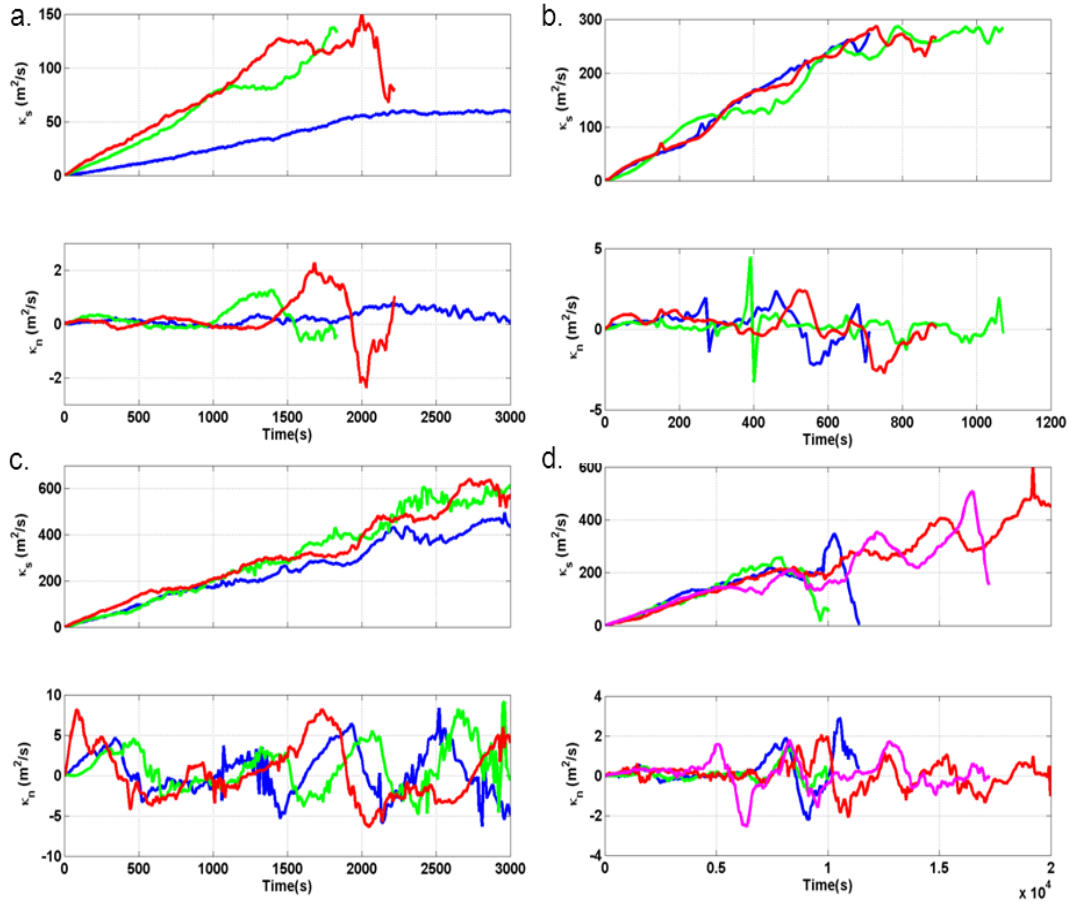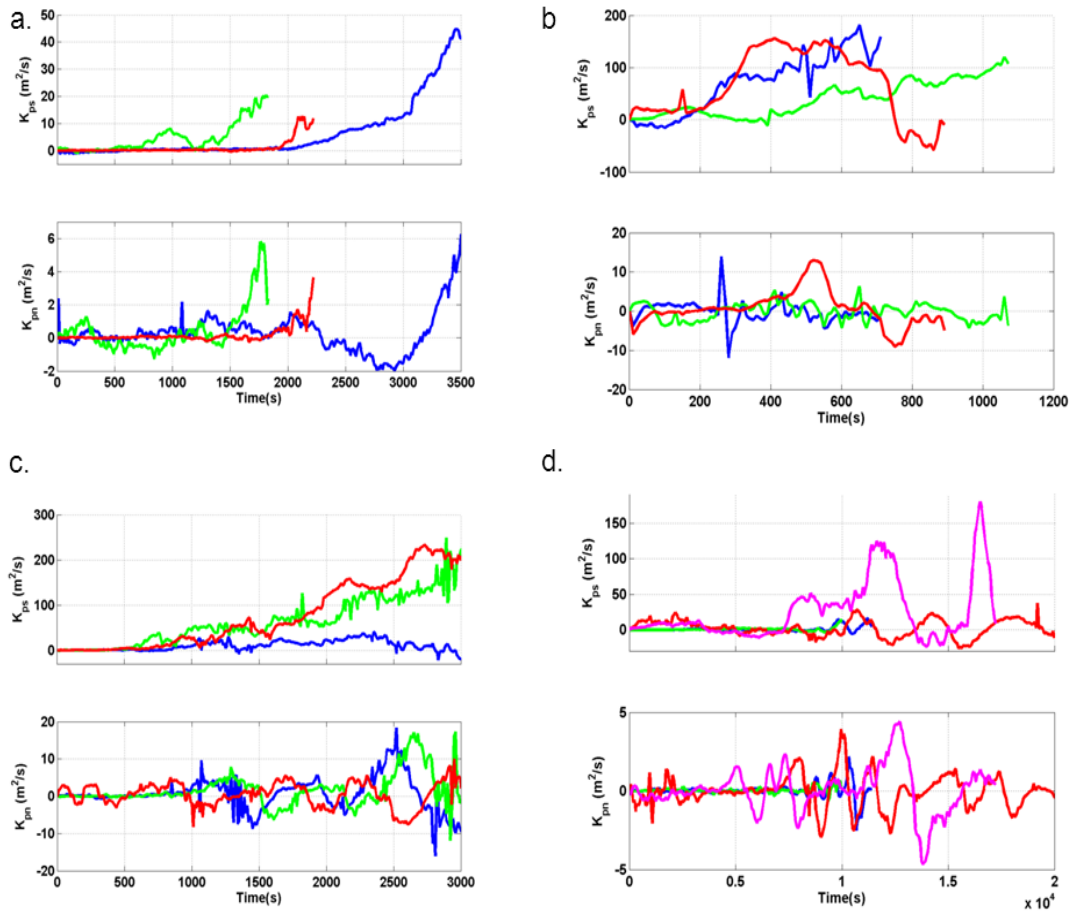
Figure 10.   Absolute Diffusivity, κ_i, quadrants are NOF (a.), BRK (b.), UPS (c.) and MEK (d.) Panels in each quadrant are streamwise, κ_s (top) and transverse, κ_n (bottom). Line colors represent individual deployments.
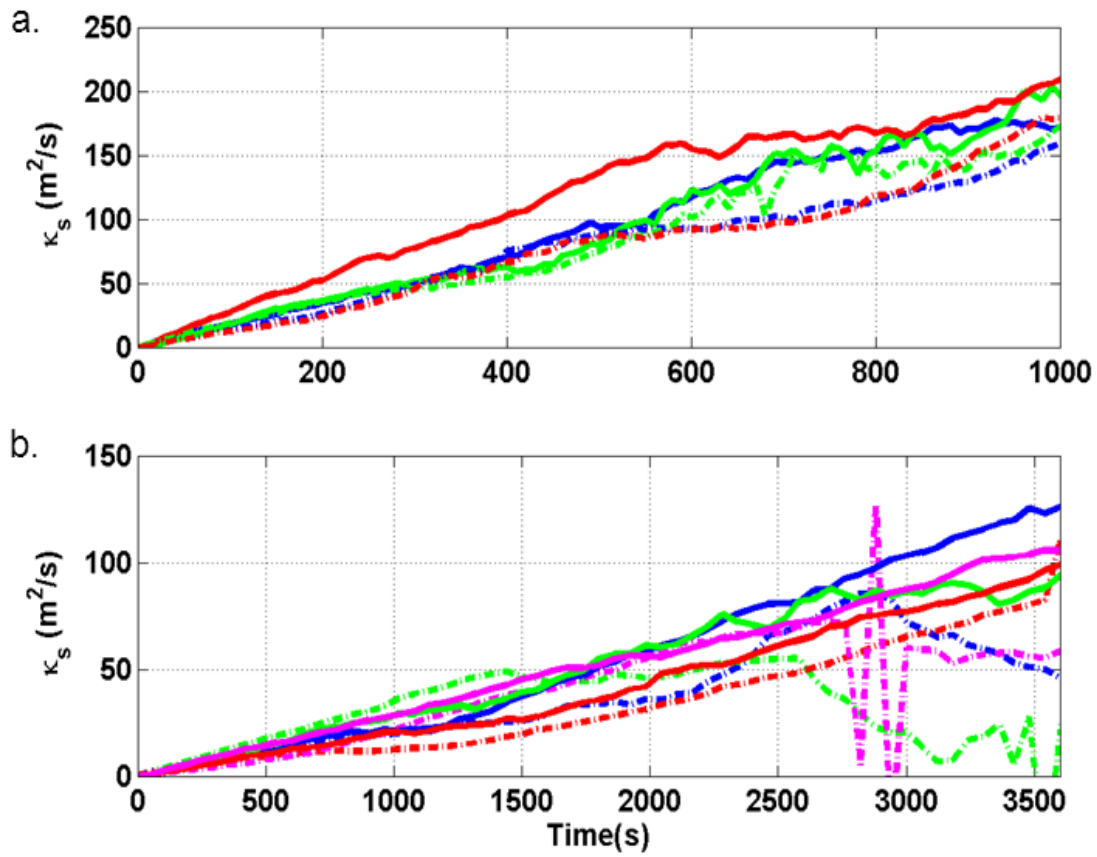
Figure 11.   Absolute Diffusivity, $\mathcal{K}_s$, from initial release (solid line) and selected starting locations (dash dot line). Rapid spread location in UPS (a.) restarted at location marked with a white line in Figures 1b and convergent location in MEK (b.) restarted at location marked with a white line in Figures 2b. Line colors represent individual deployments.

Figure 12.   Relative Diffusivity K_{pi}, Quadrants are NOF (a.), BRK (b.), UPS (c.) and
MEK (d.) Panels in each quadrant are streamwise (top) and transverse (bottom).
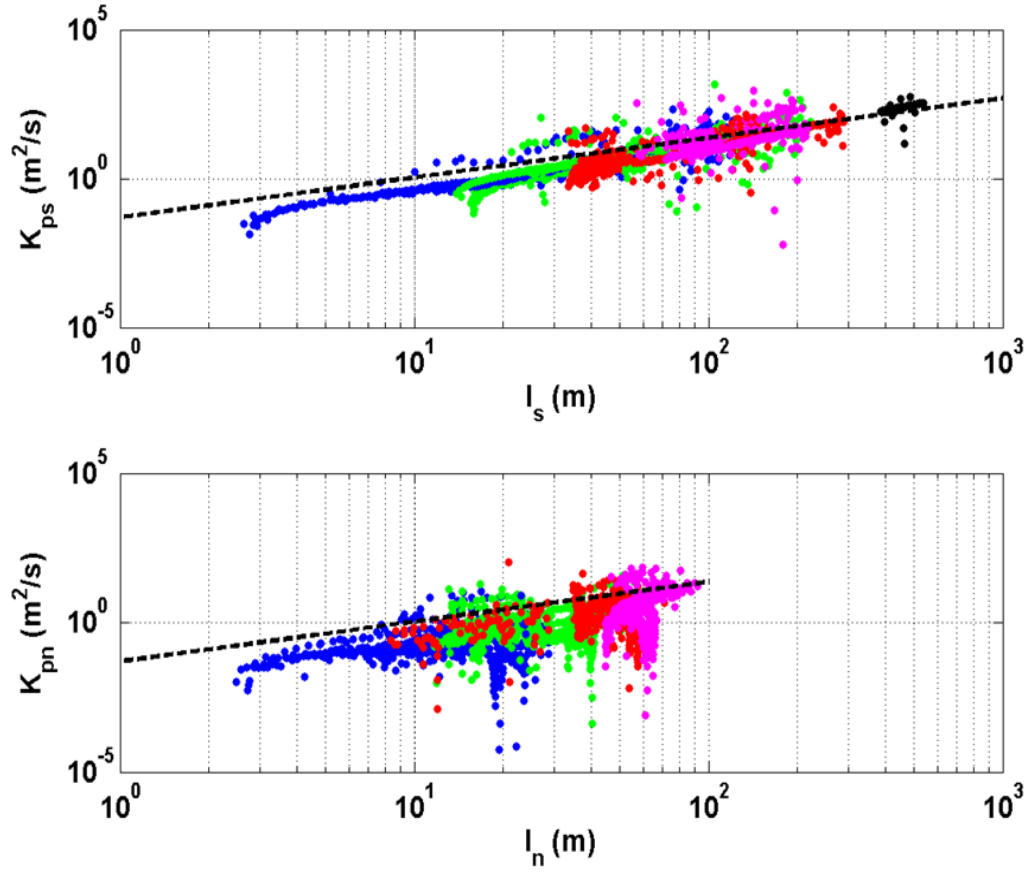
Figure 13.   Northfork (NOF) relative diffusivity, K_{pi}, and pair separation length, 1,
streamwise diffusivity (top panel) and transverse diffusivity (bottom panel)
Colored dots are initial pair separation, $l_{0:}$, $|l_0| < 5n$ (blue), $5 < |l_0| < 25n$ (green),
$25 < |l_0| < 50n$ (red), $50 < |l_0| < 300n$ (magenta), and $300 < |l_0| < 500n$ (black).
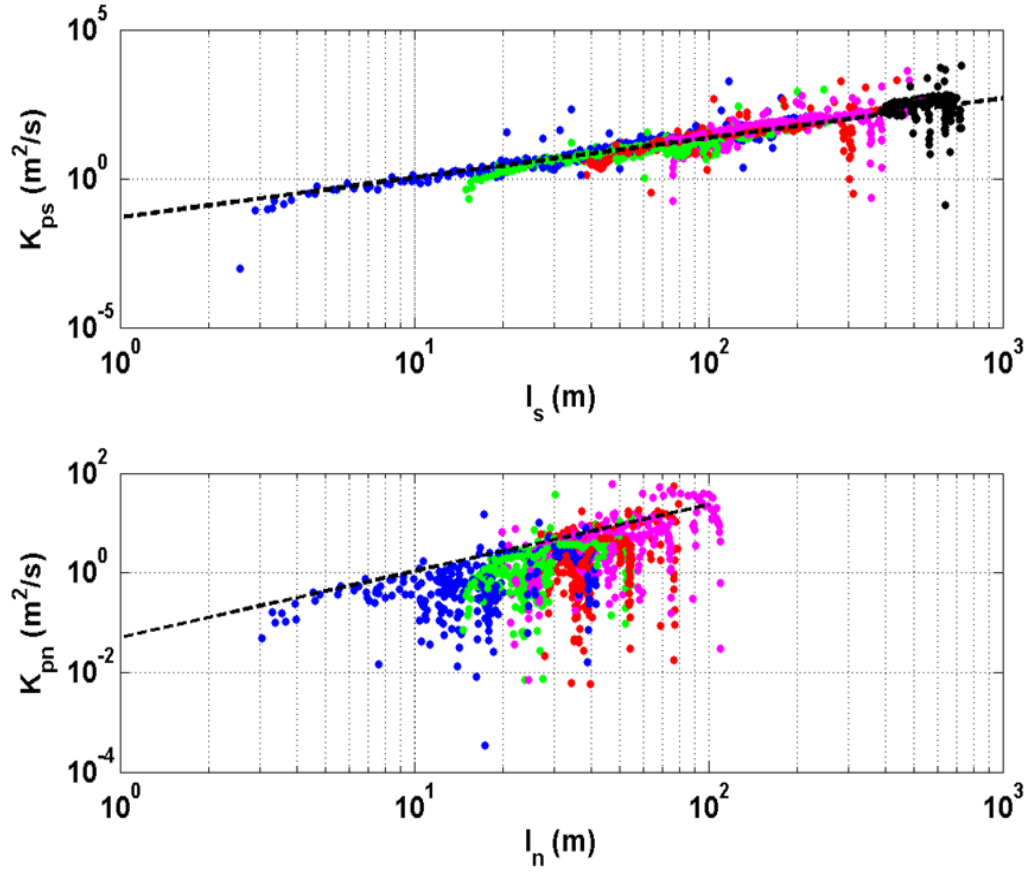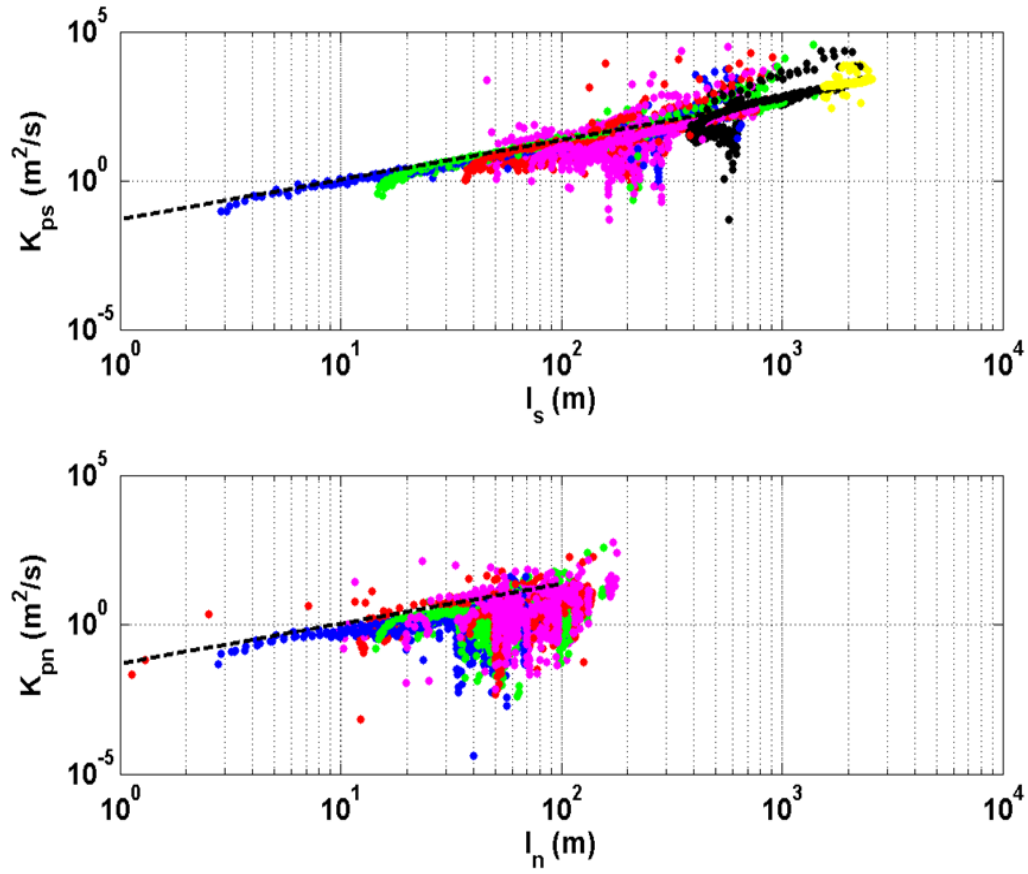Dashed line provide comparisons to Richardson scaling ($l_i^{4/3}$).

Figure 14.   Braided (BRK) relative diffusivity, K_{pi}, and pair separation length, 1,
streamwise diffusivity (top panel) and transverse diffusivity (bottom panel)
Colored dots are initial pair separation, l_0: , $|l_0| < 5\eta$ (blue), $5 < |l_0| < 25\eta$ (green),
$25 < |l_0| < 50\eta$ (red), $50 < |l_0| < 300\eta$ (magenta) and $300 < |l_0| < 500\eta$ (black).
Dashed line provide comparisons to Richardson scaling ($l_i^{4/3}$).

Figure 15.   Upper Skagit (UPS) relative diffusivity, K_{pi}, and pair separation length, 1,
streamwise diffusivity (top panel) and transverse diffusivity (bottom panel)
Colored dots are initial pair separation, $l_{0:}$, $|l_0| < 5n$ (blue), $5 < |l_0| < 25n$ (green),
$25 < |l_0| < 50n$ (red), $50 < |l_0| < 30n$ (magenta), $30 < |l_0| < 50n$ (black) and
$|l_0| > 100n$ (yellow). Dashed line provide comparisons to Richardson scaling
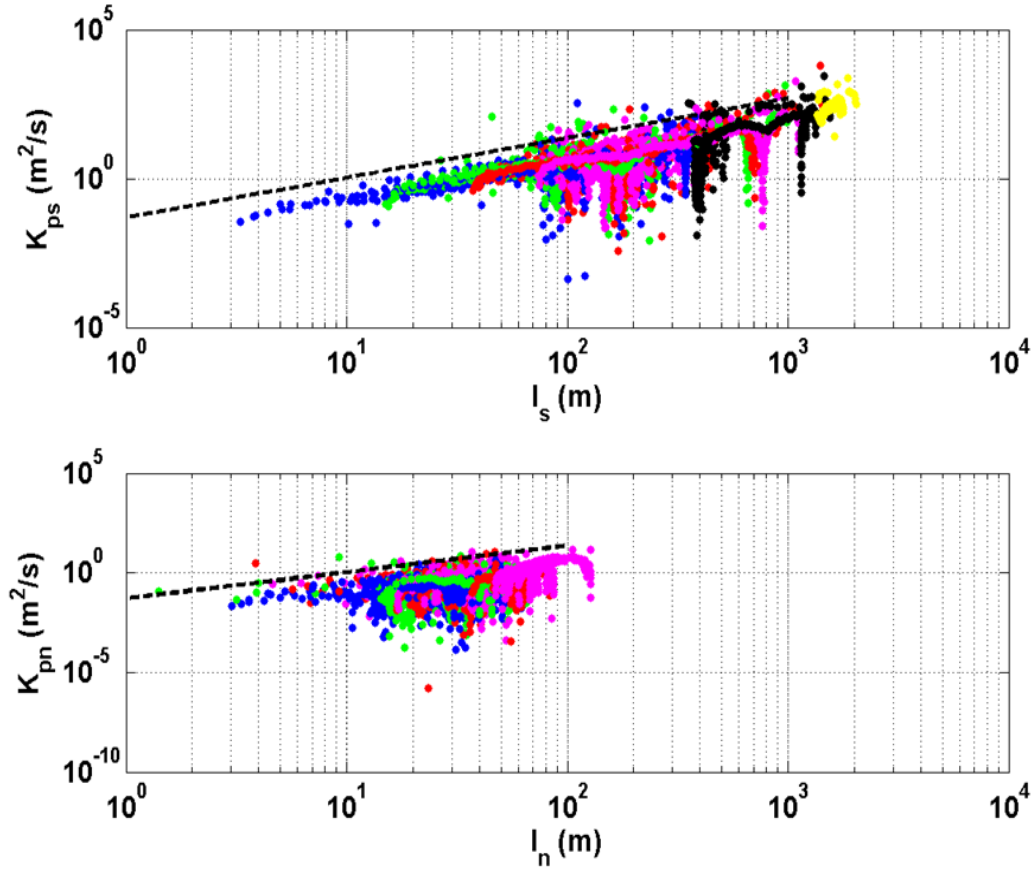$(l_i^{4/3})$.

Figure 16.   Meander (MEK) relative diffusivity, K_{pi}, and pair separation length, 1,
streamwise diffusivity (top panel) and transverse diffusivity (bottom panel)
Colored dots are initial pair separation, $l_{0:}$, $|l_0| < 5n$ (blue), $5 < |l_0| < 25n$ (green),
$25 < |l_0| < 50n$ (red), $50 < |l_0| < 300n$ (magenta), $300 < |l_0| < 500n$ (black) and
$|l_0| > 1000n$ (yellow). Dashed line provide comparisons to Richardson scaling
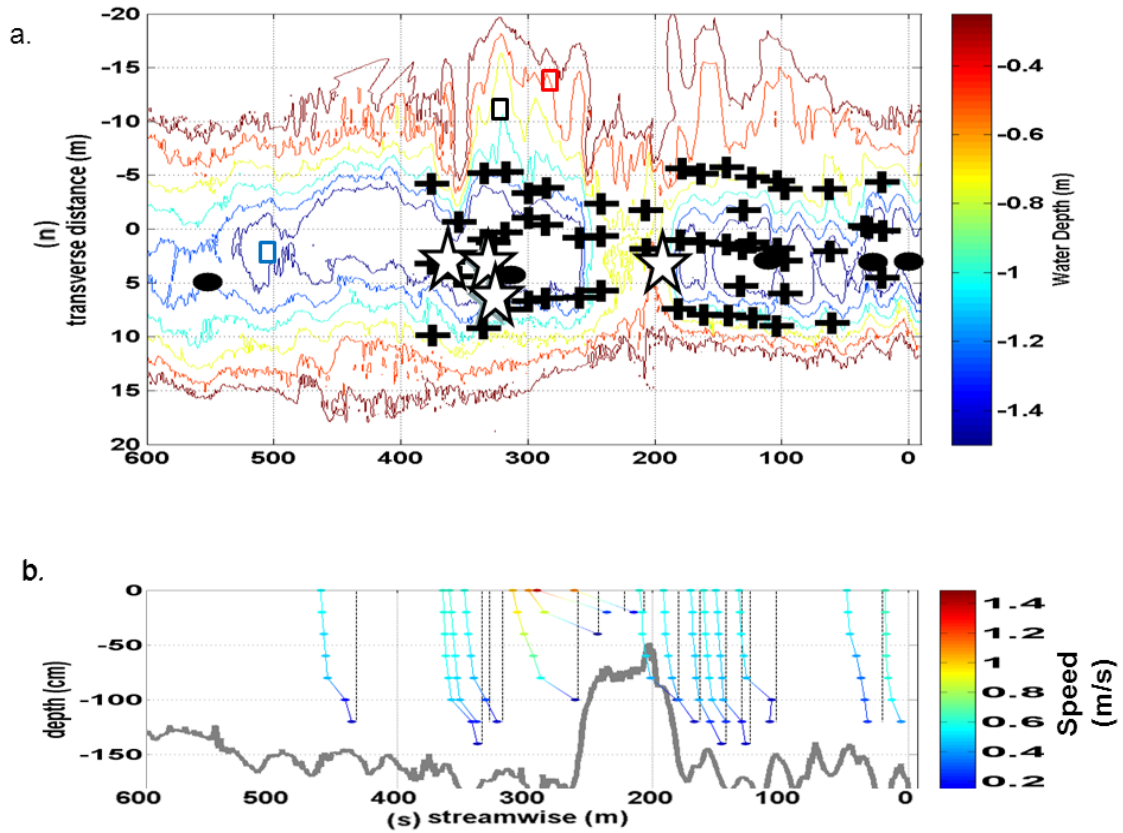$(l_i^{4/3})$.

Figure 17.   a. Plan view of the Kootenai River Study reach, ID, U.S.A. in a local coordinate frame utilizing Legleiter and Kyriadkidis (2007) technique. Channel depth contours (color lines) are based on USGS and Naval Postgraduate School survey. Black dots indicate vertical fluorometer array location, stars are ADV frame locations, "+" are ADCP locations and the colored boxes are the locations of dye exchange comparisons discussed in § IV D. 2. b. b. Is the centerline depth profile (gray line) with mean ADCP vertical velocity profiles (color lines with dots).
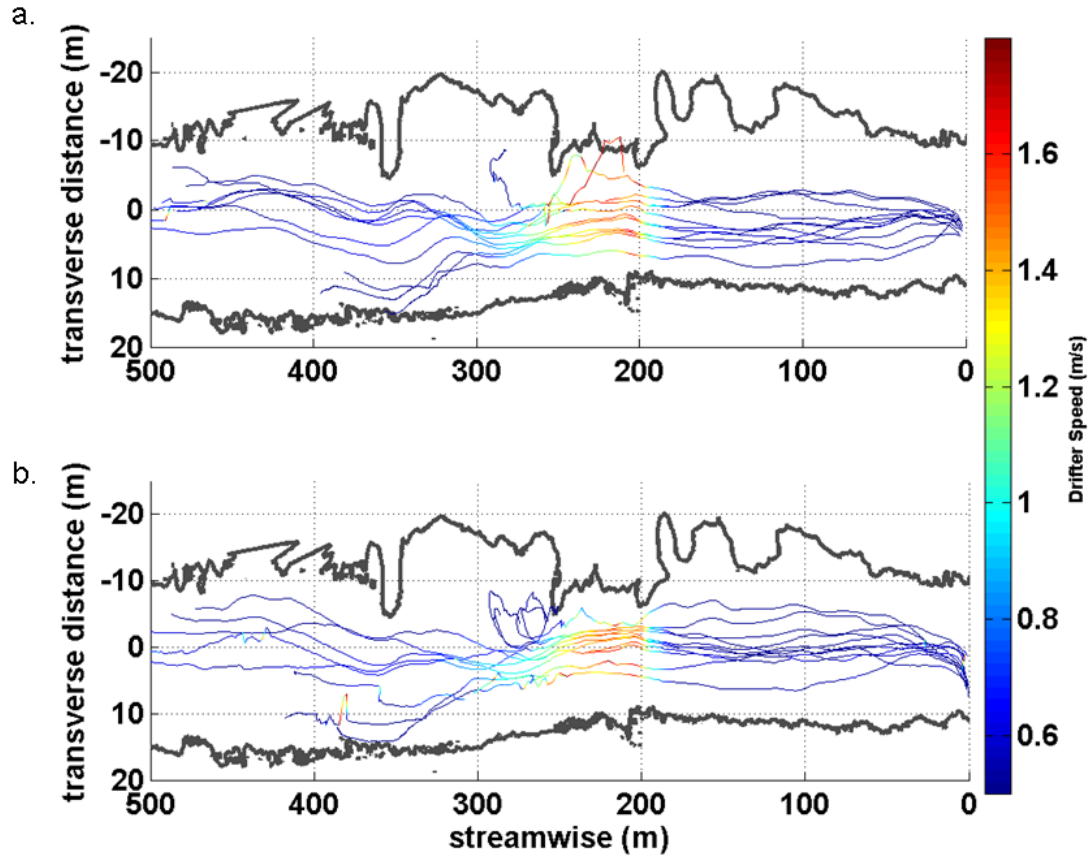
Figure 18.　　　11 GPS Drifter trajectories and speeds, in a channel-fitted local coordinate frame utilizing Legleiter and Kyriadkidis (2007) technique. Color represents drifter speed (colorbar plotted on the right). Two drifter releases are conducted after each concentration test, D1 (a) and D2 (b).
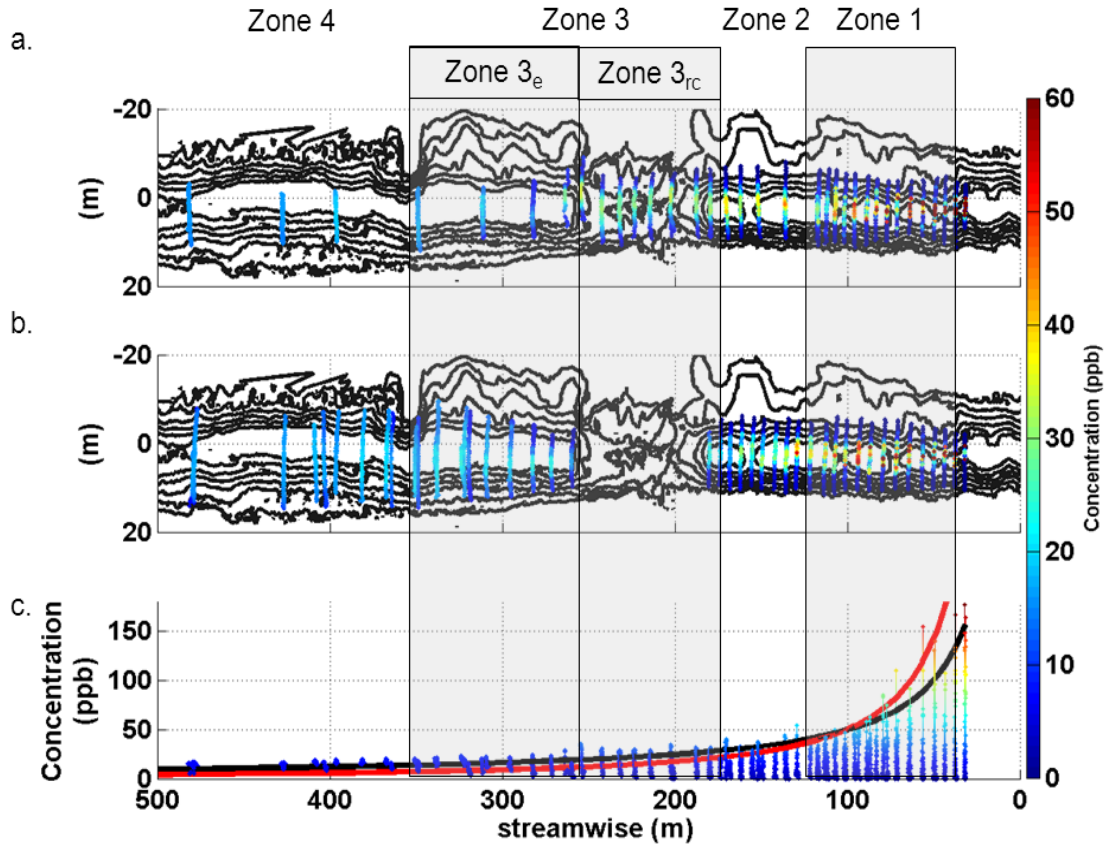
Figure 19. Plan view of surface concentration transects, C(n,s), (color dots) overlaid on river bathymetry (black lines) (T1(a.) and T2 (b.)). Concentration decreases with downstream distance initially as a 3D mixing behavior, (c. red Line) and then behaves similar to a 2D mixing behavior, (black line). Labeled boxes mark four zones along the channel based on plume mixing behavior and channel geometry. Zone 1 (0<s<125 m), where s denotes streamwise distance shown on the x-axis, the plume is mixing in three dimensions (s, n, and vertical, z). Zone 2 (125<s<160 m) begins once complete vertical mixing has occurred. Zone 3 (160<s<355 m) has strong bank and bathymetric irregularities (riffle/constriction and embayment) this zone is subdivided to emphasize transport and mixing effects between distinct flow regimes induced by the channel features: 1) riffle/constriction (Zone 3rc , 160<s<260 m) and 2) embayment (Zone 3e, 260<s<355). Zone 4 s>355.
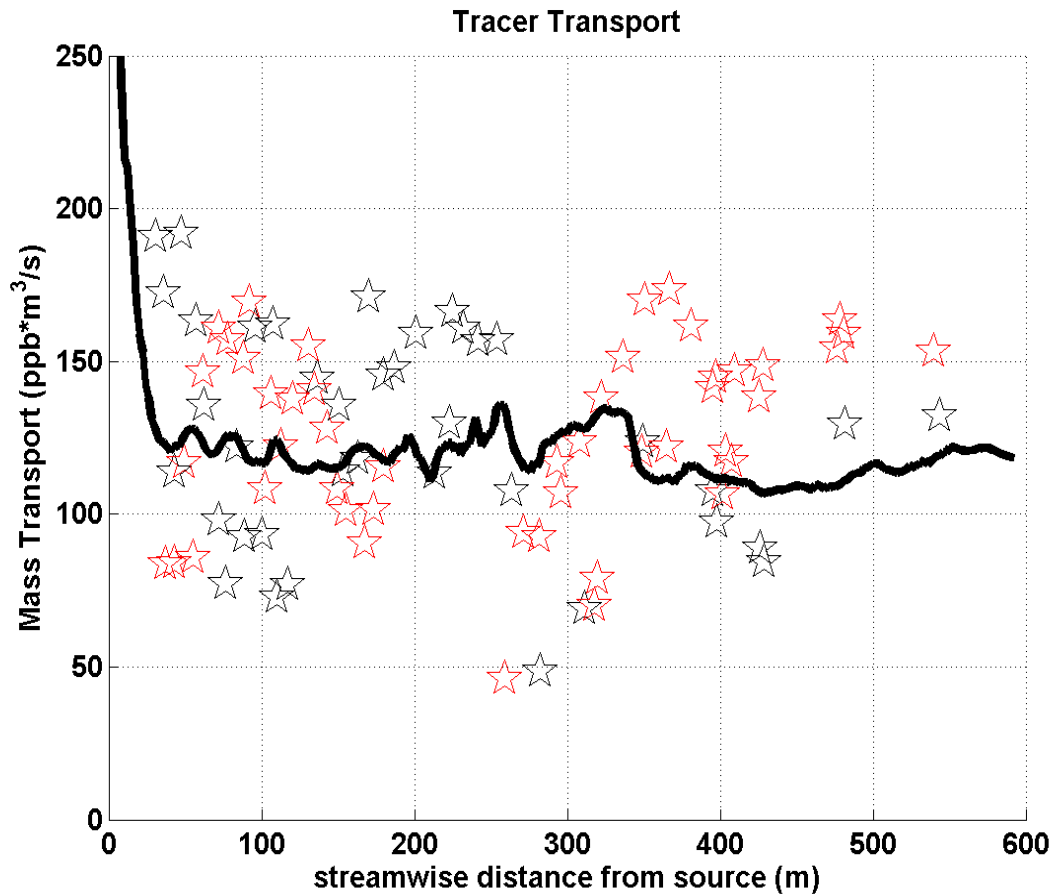
Figure 20.   Concentration streamwise transport M(s), for T1 (black stars), T2 (red stars) and S4 model (black line). Dye releases have a standard deviation of 29% and 23% of a mean value of 120 ppb and 122 ppb for T1 and T2.
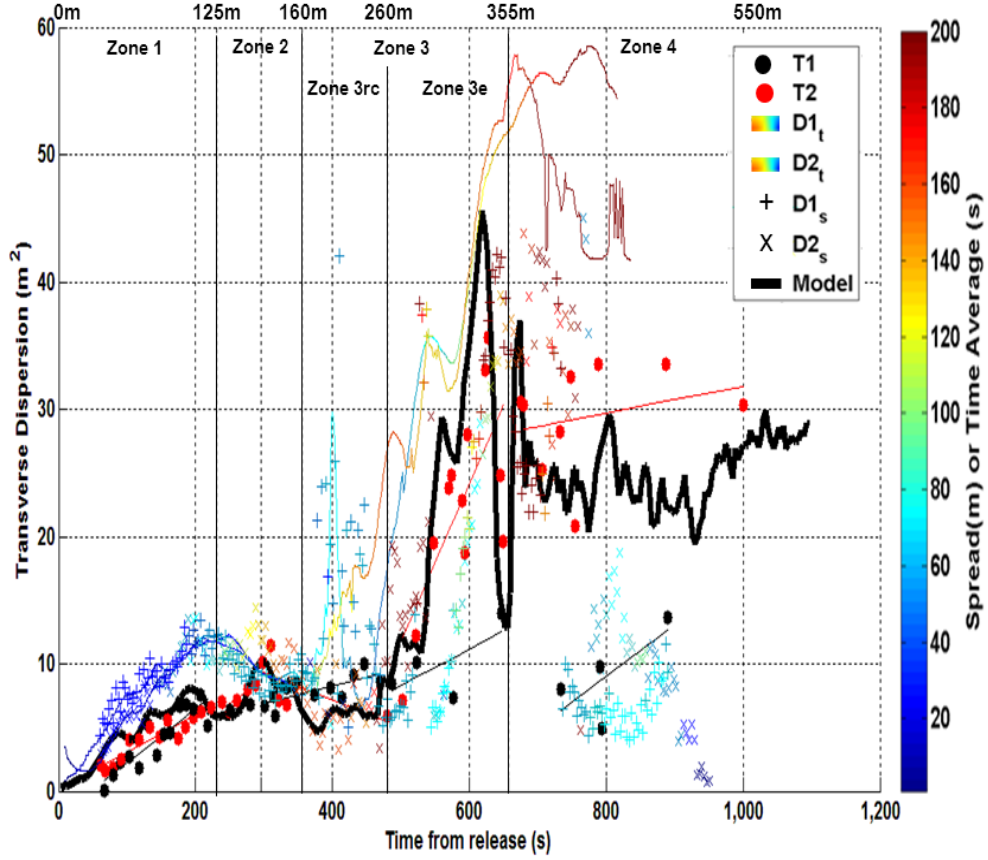
Figure 21. Integrated transverse dye profile dispersion, $\overline{\sigma_h^2}$ (dots), GPS-equipped drifter, instantaneous in time spatial average, $\overline{\sigma_{ht}^2}$ (thin colored lines) and fixed point in streamwise distance, s, temporal average $\overline{\sigma_{ht}^2}$ (colored markers). Spatial zones are labeled and denoted by solid black vertical lines with streamwise distances are plotted above. Linear regression fit in each zone for T1 (thin black lines) and T2 (thin red lines): Pre-riffle $k_n \sim 0.01$ m^2/s with R$^2 \sim 0.92$, Post-riffle $k_n = 0.05$ m^2/s R$^2 = 0.82$ for T2
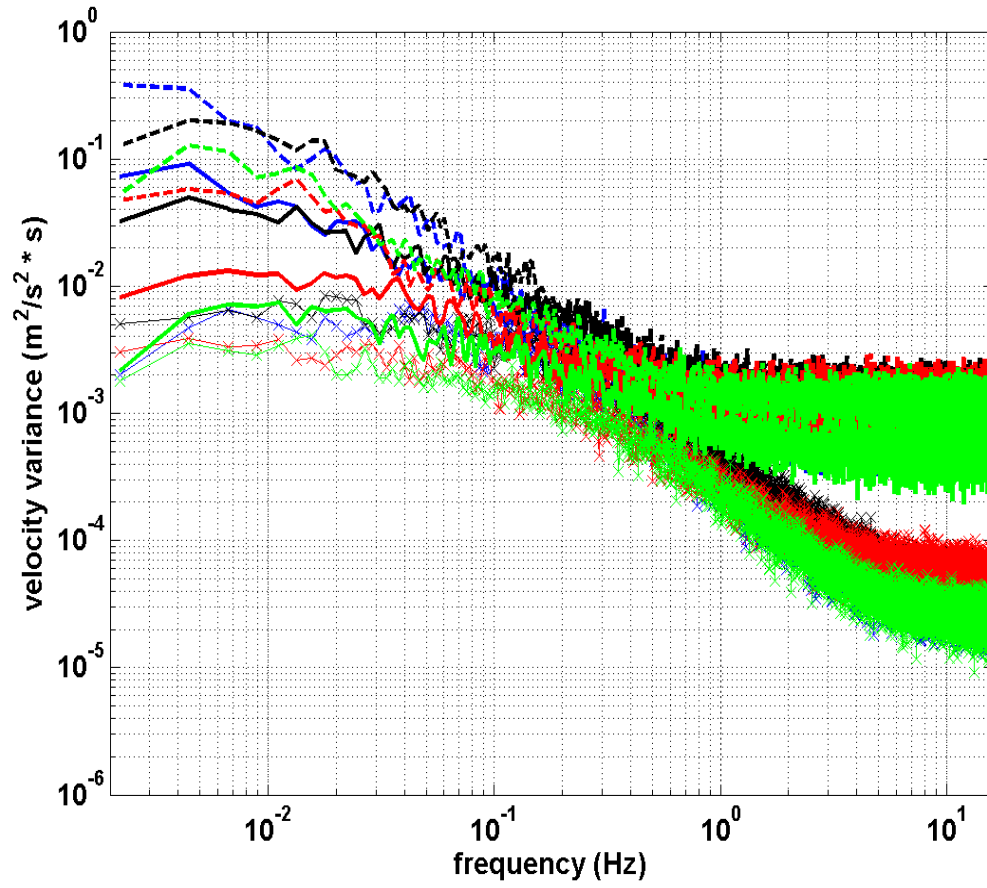
Figure 22.   ADV Velocity Spectra. Streamwise velocity (dashed lines), transverse velocity (solid lines), vertical (thin line "x" marker). Colored lines represent ADV location –green (s=195m), blue (s=327m), black (s=330m), and red (s=361m)).
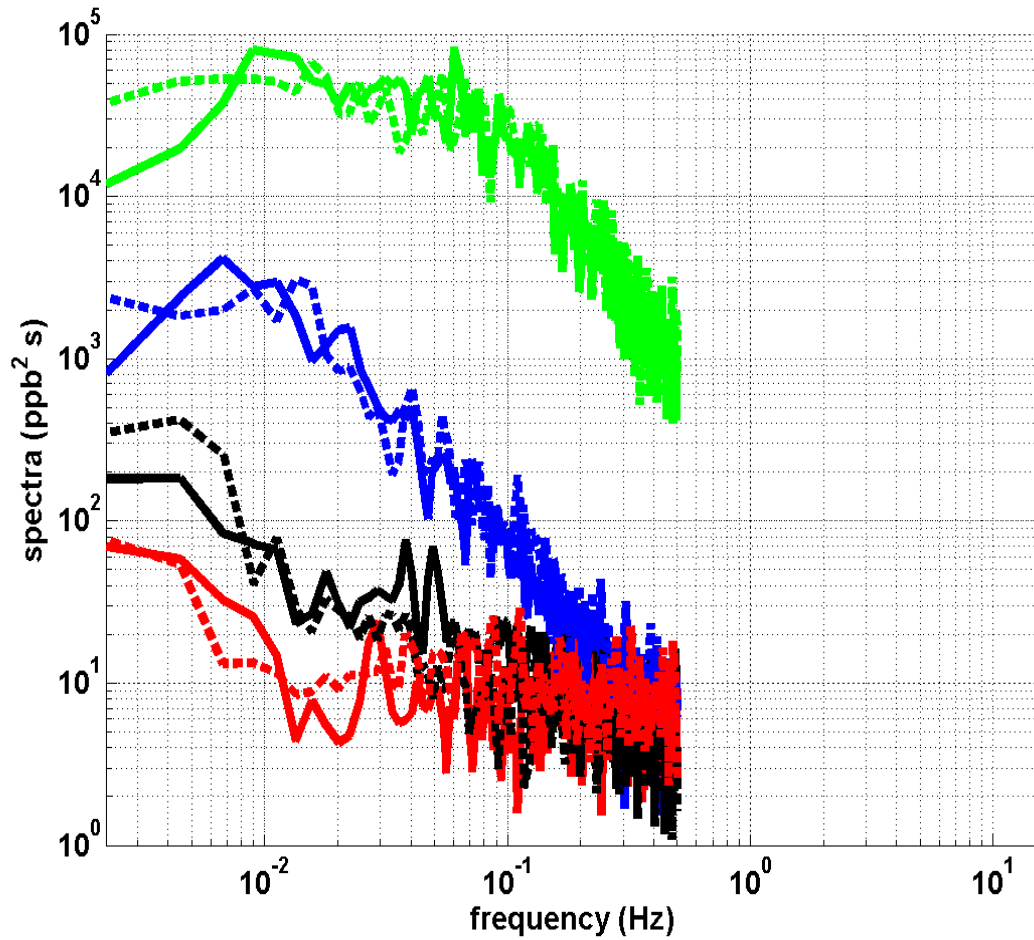
Figure 23.   Surface dye spectra from two constant releases, T1 (solid lines) and T2 (dashed lines). Colored lines represents locations at s=25m (green), s=110m (blue line) and s=313m (black line) and s=550m (red line).
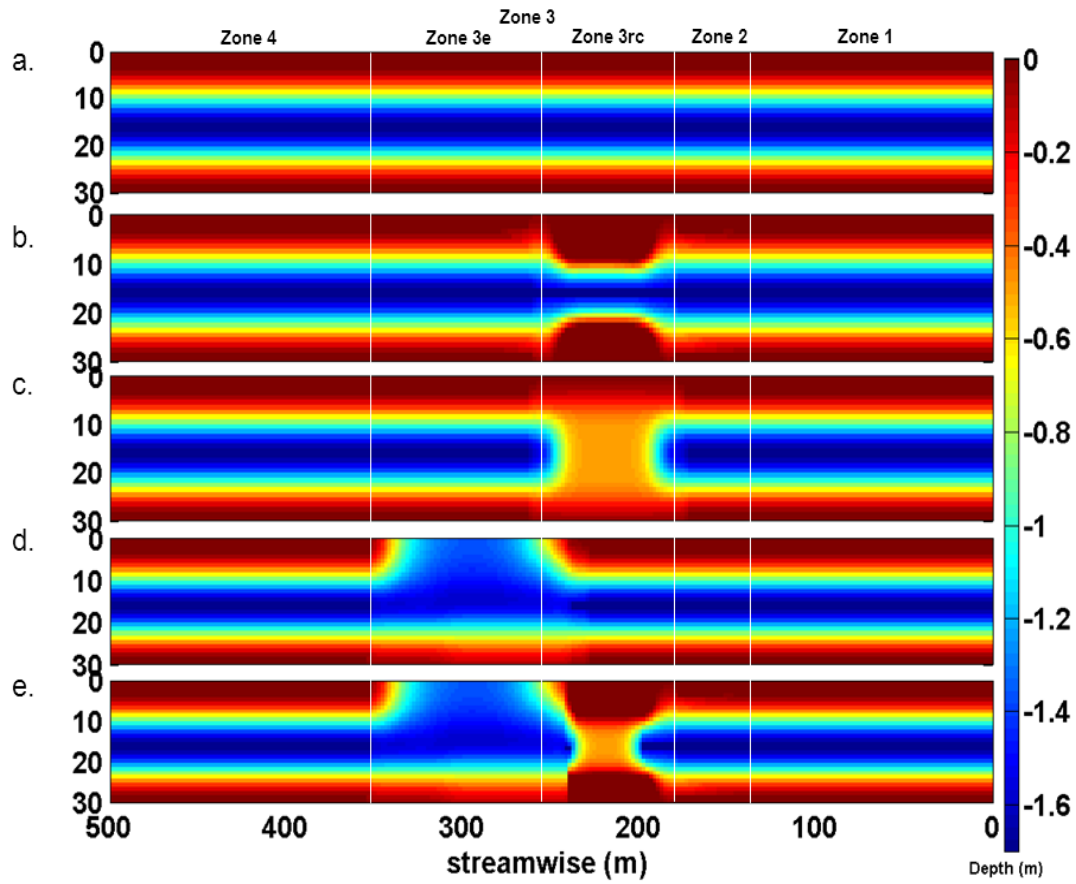
Figure 24.   Idealized bathymetry for a straight channel, S (a), constriction, IC (b), riffle, IR (c), embayment, IE (d) and combined, CP (e). Spatial zones are labeled and denoted by solid white vertical lines.

91

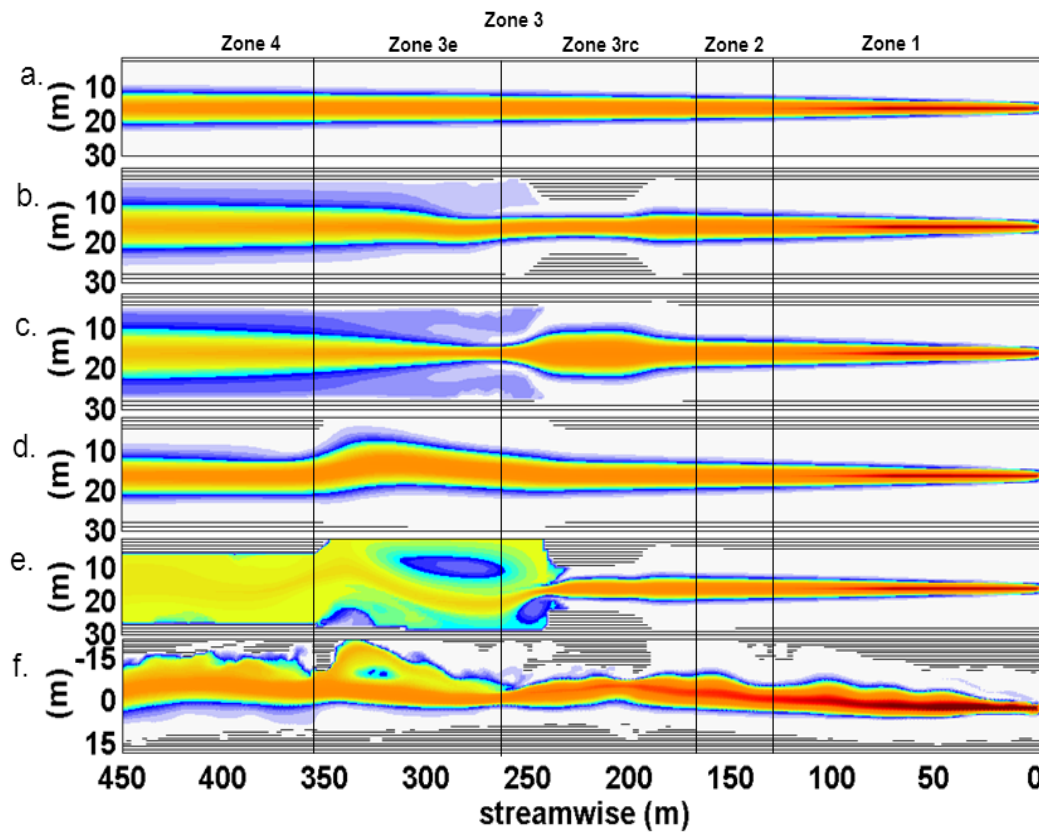Figure 25.   Simulated normalized spatial surface dye distribution where red indicates higher values, blue low values and white denotes concentration values less than 0.1% of the maximum concentration. Straight, S (a), constriction, IC (b), riffle, IR (c), embayment, IE (d), combined, CP (e), and natural channel (f). Spatial zones are labeled and denoted by solid black vertical lines. Shoreline is denoted by gray areas.
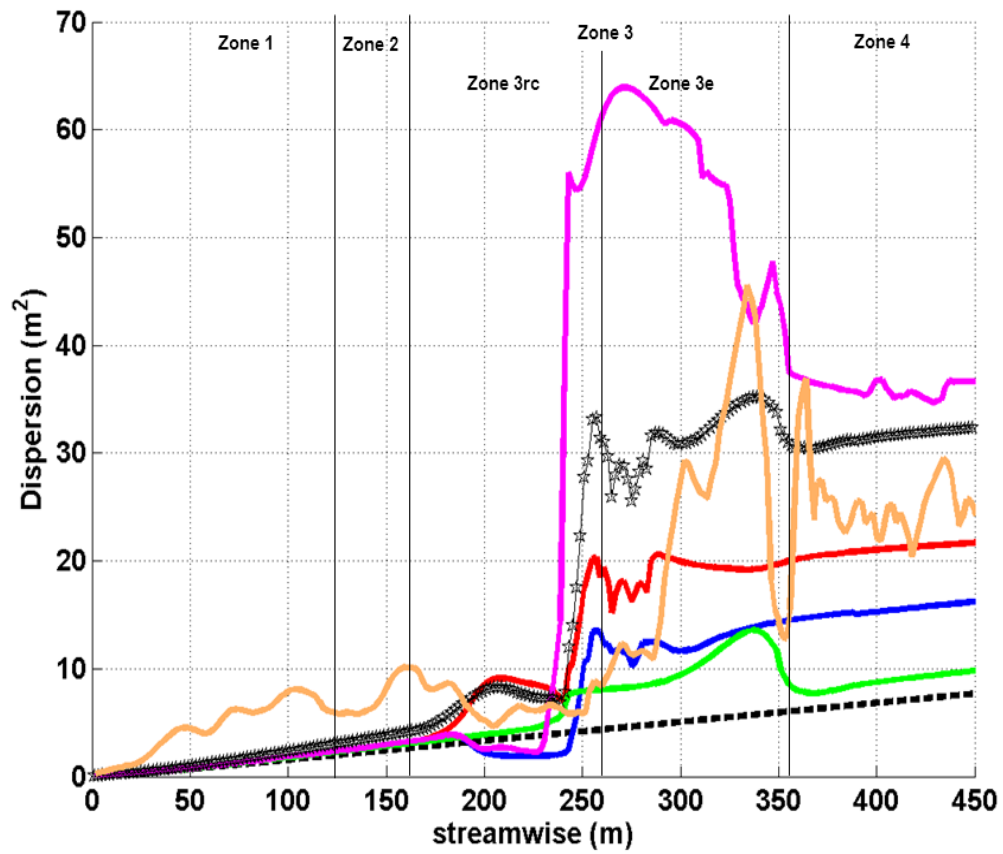
Figure 26.   Simulated Dye dispersion: straight (black dashed line), constriction (blue
            line), riffle (red line), embayment (green line), superposition of all features (black
            line with stars), combined case (magenta line) and natural channel (orange line).
                    Spatial zones are labeled and denoted by solid black vertical lines.

93

Figure 27.   1 min particle trajectories (white arrows),width of arrows indicate speed overlaid on mean vorticity. Constriction, IC (a.), riffle, IR (b.), embayment, IE (c.). Spatial zones are labeled and denoted by solid black vertical lines.

Figure 28. 1 min particle trajectories (white arrows),width of arrows indicate speed overlaid on mean vorticity. combined case, CP (a.) and natural channel (b.). Spatial zones are labeled and denoted by solid black vertical lines.

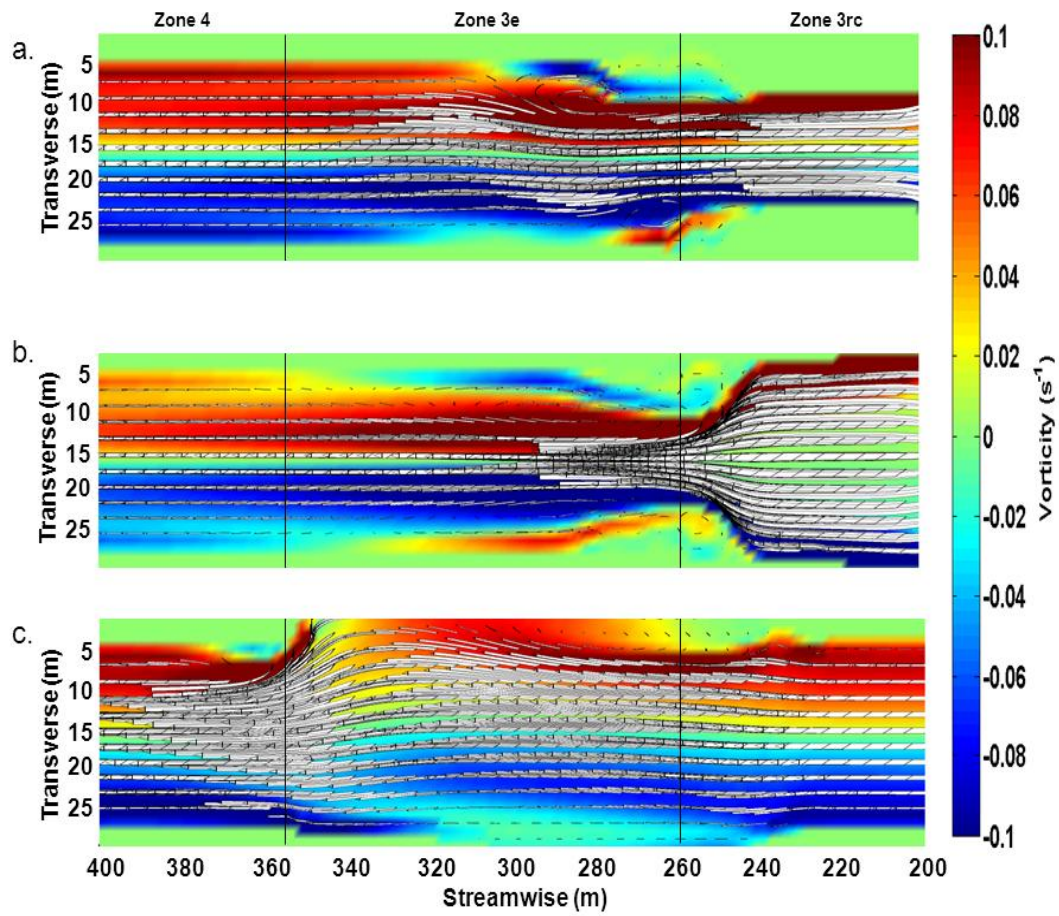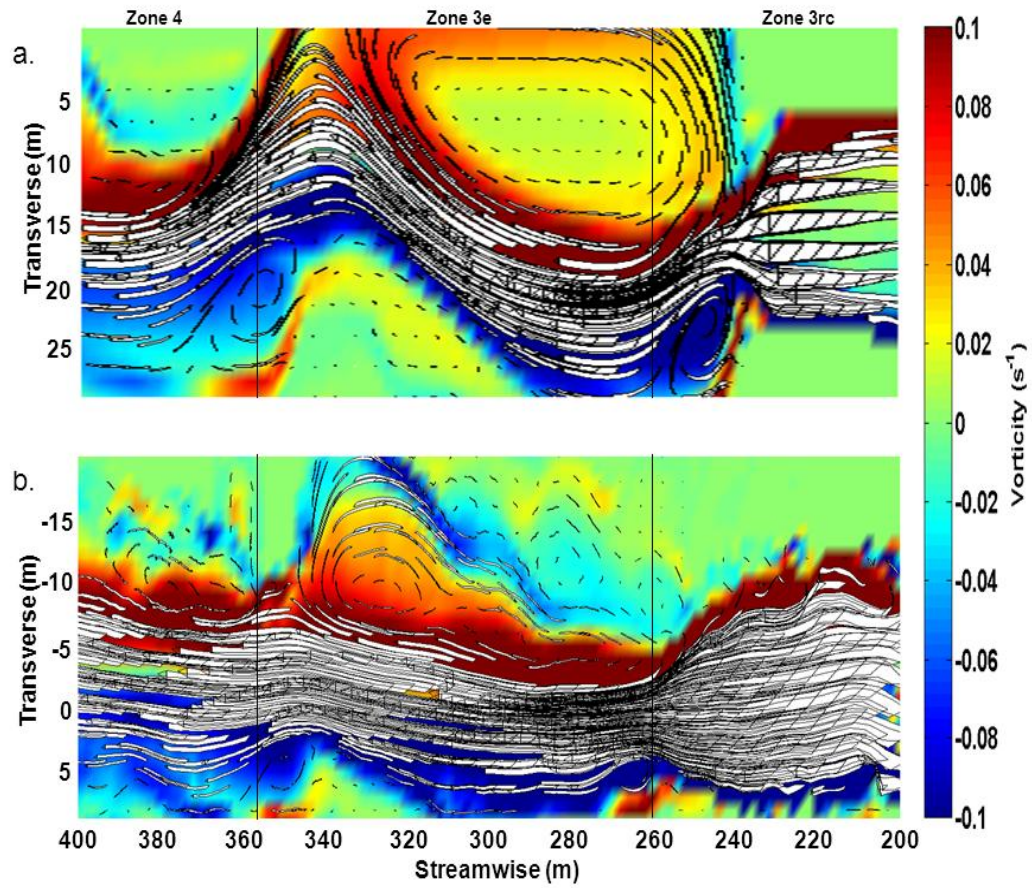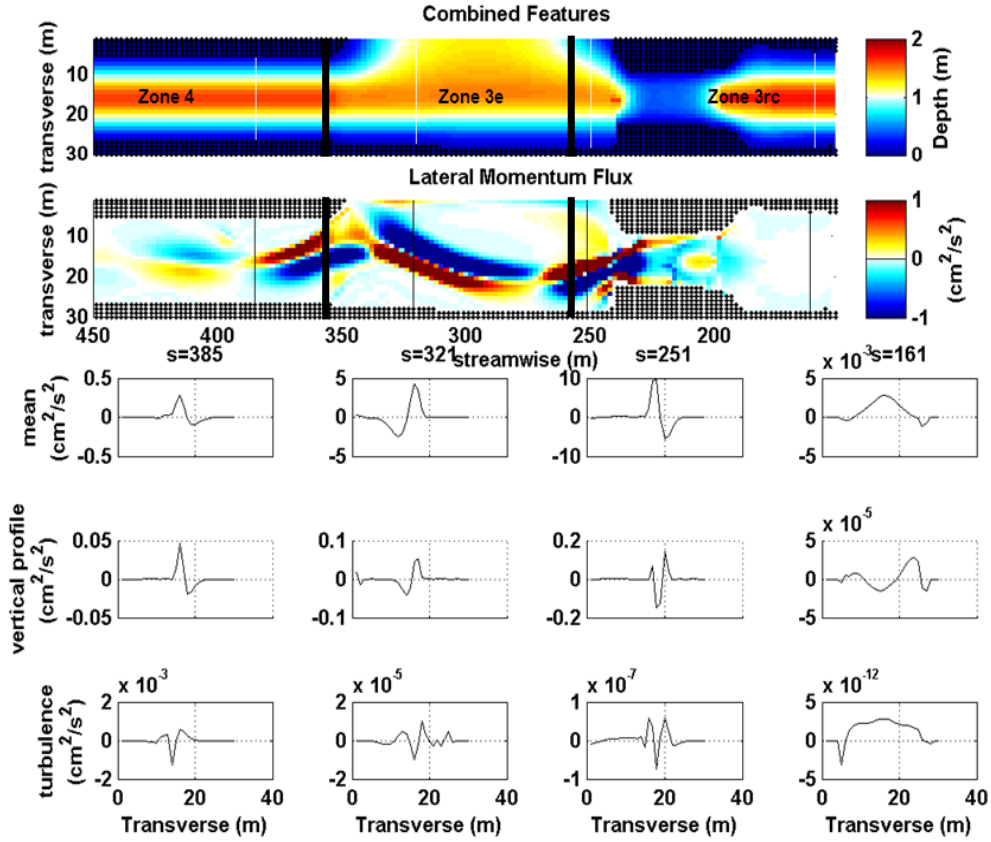Figure 29.   Combined case bathymetry (top panel) and momentum flux gradient (bottom panel) at four transects (white vertical lines top panel and thin black lines bottom panel) correspond to line plots. Line plots locations (columns) are shown from right to left s=161, 251, 321 and 385m of lateral momentum flux components (rows):, $d(h\,\overline{U_{s}}\overline{U_{n}})/dn$ (top row), $d(h\,\overline{(U_{\varsigma}-\overline{U_{s}})(U_{n}-\overline{U_{n}})})/dn$ (middle row) and $d(h\,\overline{\langle U_{\varsigma}'U_{n}'\rangle})/dn$ (bottom row). Note scale differences between line plots. Spatial zones are labeled (top panel) and denoted by solid thick black vertical lines. Shoreline is denoted by black dots.
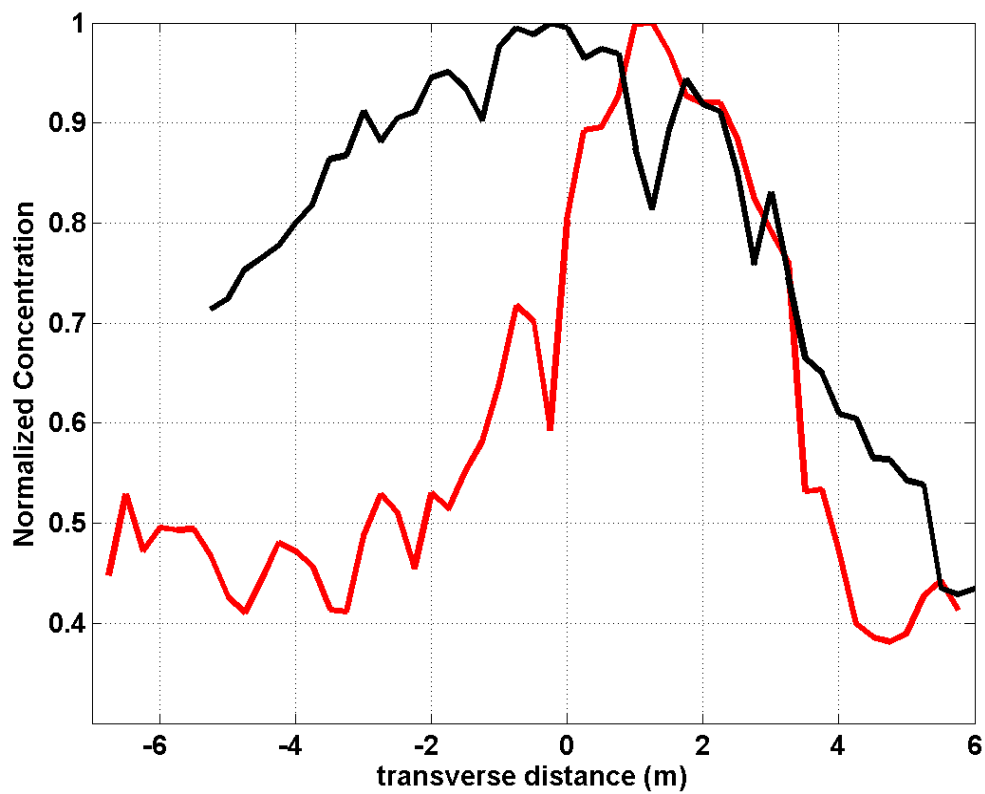
Figure 30.   Colored lines correspond to concentration transects from deployment 1 collected at s=280m (red line) and s=310m (black line). "River right" is negative and "River Left" is positive transverse distance.
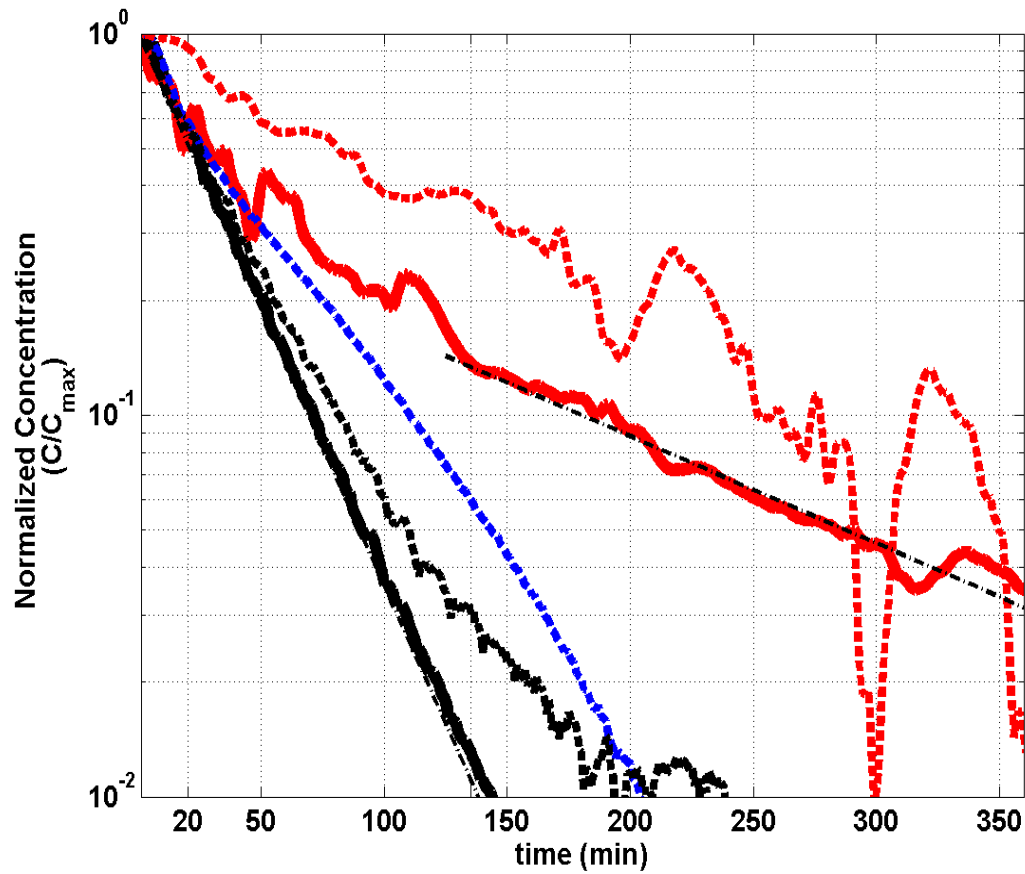
Figure 31.   Concentration exchange for flushing (solid lines) normalized by initial concentration and for filling (dashed lines) normalized by maximum concentration and subtracted from one. Dash-dot black lines are an exponential comparison with a residence time of 30s for primary flushing (fitting solid black line) and 155s for the secondary eddy (fitting solid red line). Colors represent boxes depicted in Figure 1a.
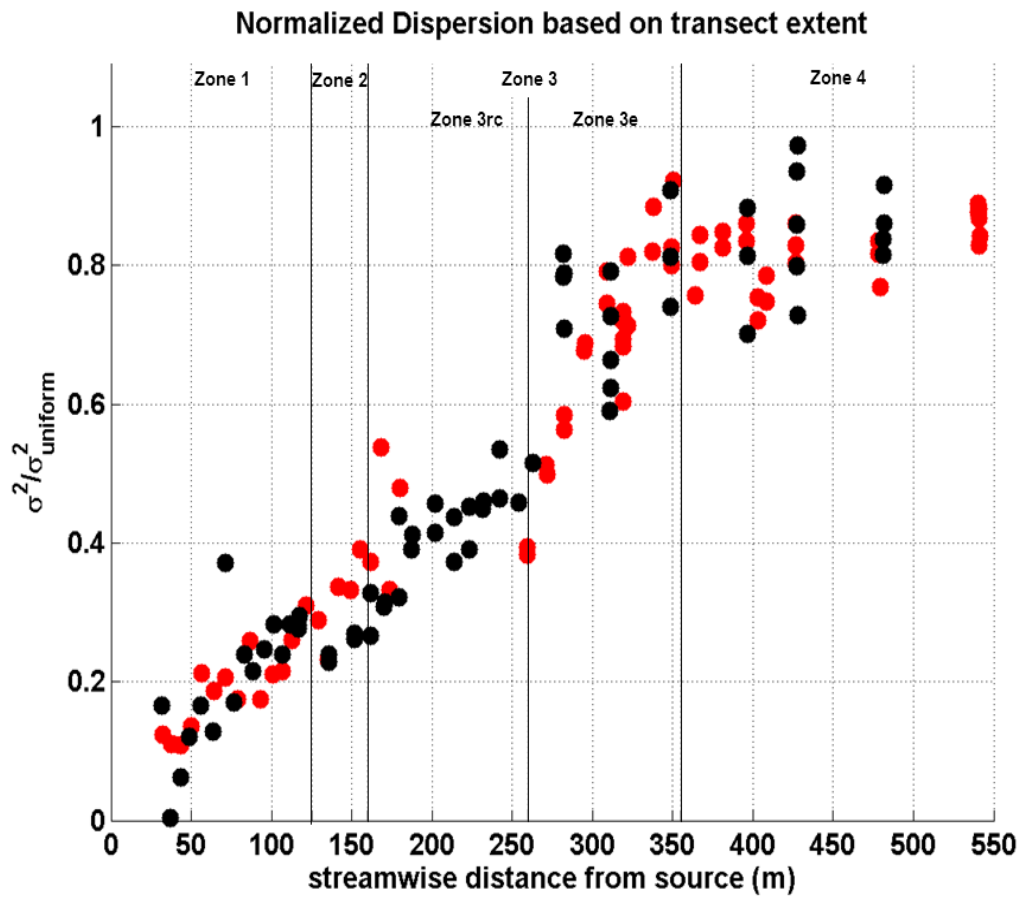
Figure 32.   Normalized Transverse Mixing verse streamwise distance. Tracer Study
measurements T1 (black dots) and T2 (red dots). Spatial zones are labeled and
denoted by solid thick black vertical lines.

THIS PAGE INTENTIONALLY LEFT BLANK

LIST OF REFERENCES

Atkinson, T. C. and P. M. Davis, 2000: Longitudinal dispersion in natural channels: 1. Experimental results from the River Severn, *Britain. Hydrol. Earth System Sci.*, **4,** 345–353.

Batchelor, G. K., 1952: Diffusion in a field of homogeneous turbulence. II. The relative motion of particles. *Proc. Cambridge Philos. Soc.*, **48,** 345–363.

Barton, G. J., R. R. McDonald, J. M. Nelson, and R. L. Dinehart, 2005: Simulation of flow and sediment mobility using a multidimensional flow model for the white sturgeon critical-habitat reach, Kootenai River near Bonners Ferry, Idaho. *U.S. Geological Survey Scientific Investigations Report 2005–5230*, 54 pp.

Barton, G. J., E. H. Moran, and C. Berenbrock, 2004: Surveying cross sections of the Kootenai River between Libby Dam, Montana, and Kootenay Lake, British Columbia, Canada. *U.S. Geological Survey Open-File Report* 2004-1045, 35 pp.

Beltaos, S., 1980: Longitudinal Dispersion in rivers. *Journal of Hydraulics Division*, ASCE **106,** 71–83.

Boxall, J.B., and I. Guymer, 2006: Streamwise mixing in meandering channels: New experimental data set and verification of a predictive technique. *Water Research*, **41,** 341–354.

Brown, J., J. MacMahan, A. Reniers, and E. Thornton, 2009: Surf zone diffusivity on a rip-channeled beach. *Journal of Geophysical Research–Oceans*, **114,** DOI: 10.1029/2008JC005158.

Brown, J., C. Tuggle, J. MacMahan, and A. Reniers, 2011: The use of autonomous vehicles for spatially measuring mean velocity profiles in rivers and estuaries, *submitted Intelligent Service Robotics*.

Clark, D. B., F. Feddersen, and R. T. Guza, 2010: Cross-shore surfzone concentration dispersion in an alongshore current. *Journal of Geophysical Research-Oceans*, **115,** DOI: 10.1029/2009JC005683.

Constantinescu, G., A. Sukhodolov, and A. McCoy, 2009: Mass exchange in a shallow channel flow with a series of groynes: LES study and comparison with laboratory and field experiments. *Environmental Fluid Mechanics*, **9,** 587–615.

Davis, R. E., 1985: Drifter observations of coastal surface currents during CODE – The method and descriptive view. *Journal of Geophysical Research-Oceans*, **90,** 4741–4755.

Davis, P. M., T. C. Atkinson, and T. M. L. Wigley, 2000: Longitudinal dispersion in natural channels: 2. The roles of shear flow dispersion and dead zones in the River Severn, UK. *Hydrology and Earth System Sciences*, **4,** 355–371.

Demuren, A. O., and W. Rodi, 1984: Calculation of turbulence-driven secondary motion in noncircular ducts. *Journal of Fluid Mechanics*, **140,** 189–222.

———, 1986: Calculation of flow and pollutant dispersion in meandering channels. *Journal of Fluid Mechanics*, **172,** 63–92.

Dever, E. P., M. C. Hendershott, and C. D. Winant, 1998: Statistical aspects of surface drifter observations of circulation in the Santa Barbara Channel. *Journal of Geophysical Research-Oceans*, **103,** 24781–24797.

Dow, K. E., P. M. Steffler, and D. Z. Zhu, 2009: Case Study: Intermediate Field Mixing for a Bank Discharge in a Natural River. *Journal of Hydraulic Engineering-ASCE*, **135,** 1–12.

Fischer, H. B., 1968: Dispersion prediction in natural streams. *Journal of Hydraulics Division-ASCE* **94(5),** 927–943.

Fischer, H. B., E. J. List, R. C. Y. Koh, J. Imberger, and N. H. Brooks, 1979: *Mixing in inland and coastal waters*. Academic Press, New York, 302 pp.

Fosness, R. L., and M. L. Williams, 2009: Sediment characteristics and transport in the Kootenai River white sturgeon critical habitat near Bonners Ferry, Idaho. *U.S. Geological Survey Scientific-Investigations Report* 2009-5228, 40 pp.

Geyer, W. R., R. Chant, and R. Houghton, 2008: Tidal and spring-neap variations in horizontal dispersion in a partially mixed estuary. *Journal of Geophysical Research-Oceans*, **113,** DOI:10.1029/2007JC004644

Glover, R. E., 1964: Dispersion of dissolved or suspended materials in flowing streams. *U.S. Geological Survey Prof. Paper* 433-B.

Godfrey, R. G, and B. J. Frederick, 1963: Dispersion in Natural Streams. *U.S. Geological Survey Open-File Report*, Washington, D.C.

Godfrey, R. G, and B. J. Frederick, 1970: Stream dispersion at selected sites. *U.S. Geological Survey Prof. Pape*r 433-K, Washington, D.C.

Gualtieri, C., 2010: RANS-based simulation of transverse turbulent mixing in a 2D geometry. *Environmental Fluid Mechanics*, **10,** 137–156.

Ho, D., P. Schlosser, T. Caplow, 2002: Determination of longitudinal dispersion coefficient and net advection in the tidal Hudson River with a large-scale, high resolution SF6 tracer release experiment. *Environ. Sci. Technol*, **36,** 3234–3241.

Holzer, M., and E. D. Siggia, 1994: Turbulent mixing of a passive scalar. *Physics of Fluids*, **6,** 1820–1837.

LaCasce, J. H., 2008: Statistics from Lagrangian observations. *Progress in Oceanography*, **77,** 1–29.

LaCasce, J. H., and A. Bower, 2000: Relative dispersion in the subsurface North Atlantic. *Journal of Marine Research*, **58,** 863–894.

Lee, H. C., C. Y. Lin, C. H. Lin, S. W. Hsu, and C. T. King, 2011: A Low-Cost Method for Measuring Surface Currents and Modeling Drifting Objects. *IEEE Transactions on Instrumentation and Measurement*, **60,** 980–989.

Leendertse, J. J., 1967: Aspects of a computational model for long-period water-wave propagation. Ph. D. Thesis, RM-5294-RR, Rand Corporation, Santa Monica.

Legleiter, C. J., and P. C. Kyriakidis, 2006: Forward and inverse transformations between cartesian and channel-fitted coordinate systems for meandering rivers. *Mathematical Geology*, **38,** 927–958.

MacMahan, J., J. Brown, and E. B. Thornton, 2009: Low-cost handheld Global Positioning Systems for measuring surf zone currents. *J. Coastal Res*, DOI: 10.2112/08–1000.1.

McQuivey, R. S., and T. N. Keefer, 1974: Simple method for predicting dispersion in streams. *J. Envir. Engrg. Div*, **100(4),** 997–1011.

Microsoft Corporation, 2011: BING Maps. [Available online at http://www.bing.com/maps]

Muste, M., K. Yu, T. Pratt, and D. Abraham, 2004: Practical aspects of ADCP data use for quantification of mean river flow characteristics; Part II: fixed-vessel measurements. *Flow Measurement and Instrumentation*, **15,** 17–28.

Nokes, R. I., 1986: Problems in turbulent dispersion, PhD Thesis, University of Canterbury, Christchurch, New Zealand.

Nordin, C. F., and G. V. Sabol, 1974: Empirical data on longitudinal dispersion in rivers. *U.S. Geological Survey Water Resources Investigation*, 20–74.

Okoye, J. K., 1970: Characteristics of Transverse Mixing in Open-Channel Flows. Rep. KH-R-23, California Institute of Technology, Pasadena, California.

Rhoads, B. L., and A. N. Sukhodolov, 2008: Lateral momentum flux and the spatial evolution of flow within a confluence mixing interface. *Water Resources Research*, **44(8),** 1–17.

Richardson, L. F., 1926: Atmospheric diffusion on a distance-neighbour graph. *Proc. R. Soc. London, Ser. A,* **110,** 709–737.

Rutherford, J.C., 1994: *River Mixing*. Wiley, New York, 362 pp.

Saeki, M., and M. Hori, 2006: Development of an accurate positioning system using low-cost L1 GPS receivers. *Computer-Aided Civil and Infrastructure Engineering*, **21,** 258–267.

Simoes, F. J. M., and S. S. Y. Wang, 1997: Numerical prediction of three-dimensional mixing in a compound open channel. *Journal of Hydraulic Research*, **35,** 619–642.

Spydell, M., F. Feddersen, R. T. Guza, and W. E. Schmidt, 2007: Observing surf-zone dispersion with drifters. *Journal of Physical Oceanography*, **37,** 2920–2939.

Stockdale, R. J., S. J. McLelland, R. Middleton, and T. J. Coulthard, 2008: Measuring river velocities using GPS River Flow Concentrations (GRiFTers). *Earth Surface Processes and Landforms*, **33,** 1315–1322.

Sukhodolov, A. N., and W. S. J. Uijttewaal, 2010a: Assessment of a River Reach for Environmental Fluid Dynamics Studies. *Journal of Hydraulic Engineering-ASCE*, **136,** 880–888.

Swick, W., and J. MacMahan, 2009: The Use of Position-Tracking Drifters in Riverine Environments. *IEEE Oceans09 MTS*. 1–10.

Swick, W., J. MacMahan, A. Reniers, and E. Thornton, 2011: Numerical Model Comparisons of Transverse Mixing in a Natural River *submitted to Water Resources Research.*

Taylor, G. I., 1954: The dispersion of matter in turbulent flow through a pipe. *Proc. R.Soc. London Set. A* **223,** 446–68.

Uittenbogaard, R. E., 1998: Model for eddy diffusivity and viscosity related to sub-grid velocity and bed topography. *Note, WL | Delft Hydraulics*.

Weitbrecht, V., S. A. Socolofsky, and G. H. Jirka, 2008: Experiments on mass exchange between groin fields and main stream in rivers. *Journal of Hydraulic Engineering-ASCE*, **134,** 173–183.

Wilson, J. F., and W. E. Forrest, 1965: Potomac River Time-of-Travel Measurements. *Proceedings, Lamont Geological Observatory Symposium on Diffusion in Oceans and Fresh Waters*. Pallisades, N.Y., 1–18.

Wilson, C., J. B. Boxall, I. Guymer, and N. R. B. Olsen, 2003: Validation of a three-dimensional numerical code in the simulation of pseudo-natural meandering flows. *Journal of Hydraulic Engineering-ASCE*, **129,** 758–768.

Wilson, C., I. Guymer, J. B. Boxall, and N. R. B. Olsen, 2007: Three-dimensional numerical simulation of solute transport in a meandering self-formed river channel. *Journal of Hydraulic Research*, **45,** 610–616.

WL | Delft Hydraulics, Delft3D-FLOW, 2007: *User manual*, **3.14,** 642 pp.

THIS PAGE INTENTIONALLY LEFT BLANK

INITIAL DISTRIBUTION LIST

1.   Defense Technical Information Center
        Ft. Belvoir, Virginia

2.   Dudley Knox Library
        Naval Postgraduate School
        Monterey, California

3.
        Jamie H. MacMahan
        Department of Oceanography, NPS
        Monterey, California

4.   Edward B. Thornton
        Department of Oceanography, NPS
        Monterey, California

5.   Timothy P. Stanton
        Department of Oceanography, NPS
        Monterey, California

6.   Thomas H.C. Herbers
        Department of Oceanography, NPS
        Monterey, California

7.   Qing Wang
        Department of Meteorology, NPS
        Monterey, California

8.   Jeffrey D. Paduan
        Department of Oceanography, NPS
        Monterey, California

9.   Ad Reniers
        RSMAS, University of Miami
        Coral Gables, Florida

10   CNMOC
        Stennis Space Center, Mississippi

11   Oceanographer of Navy
        Washington, D.C.